



ANDER FRANCISCO PEREIRA

**DEVELOPMENT AND BIOLOGICAL APPLICATION OF
A QUANTUM MECHANICALLY DERIVED FORCE
FIELD: THE CASE OF A PLATINUM (II) COMPLEX**

**LAVRAS - MG
2020**

ANDER FRANCISCO PEREIRA

**DEVELOPMENT AND BIOLOGICAL APPLICATION OF A QUANTUM
MECHANICALLY DERIVED FORCE FIELD: THE CASE OF A PLATINUM (II)
COMPLEX**

Dissertação apresentada à Universidade Federal de Lavras, como parte das exigências do Programa de Pós-Graduação em Agroquímica, área de concentração em Química/Bioquímica, para obtenção do título de Mestre.

Professor Dr. Teodorico de Castro Ramalho
Orientador
Pós-doutoranda Dr.^a Ingrid Guarnetti Prandi
Coorientadora

**LAVRAS - MG
2020**

Ficha catalográfica elaborada pelo Sistema de Geração de Ficha Catalográfica da Biblioteca
Universitária da UFLA, com dados informados pelo(a) próprio(a) autor(a).

Pereira, Ander Francisco.

Development and biological application of a quantum
mechanically derived force field : the case of a platinum (ii)
complex / Ander Francisco Pereira. - 2020.
102 p. : il.

Orientador(a): Teodorico de Castro Ramalho.

Coorientador(a): Ingrid Guarnetti Prandi.

Dissertação (mestrado acadêmico) - Universidade Federal de
Lavras, 2020.

Bibliografia.

1. Parametrização de campo de força. 2. Complexo de platina
(II). 3. simulações de Dinâmica Molecular (DM). I. Ramalho,
Teodorico de Castro. II. Prandi, Ingrid Guarnetti. III. Título.

ANDER FRANCISCO PEREIRA

**DEVELOPMENT AND BIOLOGICAL APPLICATION OF A QUANTUM
MECHANICALLY DERIVED FORCE FIELD: THE CASE OF A PLATINUM (II)
COMPLEX**

**DESENVOLVIMENTO E APLICAÇÃO BIOLÓGICA DE UM CAMPO DE
FORÇA DERIVADO QUANTUM MECANICAMENTE: O CASO DE UM
COMPLEXO PLATINUM (II)**

Dissertação apresentada à Universidade Federal de Lavras, como parte das exigências do Programa de Pós-Graduação em Agroquímica, área de concentração em Química/Bioquímica, para obtenção do título de Mestre.

Aprovada em 07 de Fevereiro de 2020.

Prof. Dr. Laurent Emmanuel Dardenne

LNCC

Prof.^a Dr.^a Elaine Fontes Ferreira da Cunha

UFLA

Pós-doutoranda Dr.^a Ingrid Guarnetti Prandi

UFLA/UFPA

Professor Dr. Teodorico de Castro Ramalho
Orientador

Pós-doutoranda Dr.^a Ingrid Guarnetti Prandi
Coorientadora

**LAVRAS - MG
2020**

Aos meus pais, Maria e Benedito, por todo amor, confiança e exemplos de vida.

Dedico

AGRADECIMENTOS

Agradeço primeiramente a Deus, por iluminar a minha vida e abençoar as minhas decisões.

A minha família, por torcer e acreditar em mim.

Aos meus pais, Maria e Benedito, que são a base da minha vida. Obrigado por todo amor, carinho, confiança e ensinamentos. Eu amo muito vocês!

À minha irmã Amanda, pelo carinho e confiança que temos um pelo outro.

Ao meu orientador, grande professor Teodorico, por ter me dado a oportunidade de trabalhar com o grupo desde o início da minha graduação, por todo aprendizado, pelos bons conselhos e também pela amizade.

À minha coorientadora e grande amiga Ingrid, por todo aprendizado e por não ter medido esforços para me ajudar durante a realização desse trabalho.

Ao Alexandre, pelos trabalhos que desenvolvemos juntos, por todo aprendizado e também pela amizade.

Aos demais amigos do Grupo de Química Computacional, pelo companheirismo diário e amizade construída durante esses anos.

A todos os amigos que conheci em Lavras, especialmente o Matheus, Jéssica, Samuel, Ana, Gustavo Gomide, Gustavo Gonçalves e o Richard, pelos votos de confiança, companheirismo e amizade desde 2014. Agradeço também pelas confraternizações e presença nos momentos importantes.

Aos meus amigos de Estiva pela amizade e companheirismo, mesmo distantes.

À Universidade Federal de Lavras, ao Departamento de Química e ao Programa de Pós-Graduação em Agroquímica, pela oportunidade.

O presente trabalho foi realizado com apoio do Conselho Nacional de Desenvolvimento Científico e Tecnológico (CNPq) e da Coordenação de Aperfeiçoamento de Pessoal de Nível Superior – Brasil (CAPES) – Código de Financiamento 001.

Muito obrigado!

RESUMO

Os metais apresentam uma grande diversidade química e biológica, e a sua utilização na medicina foi impulsionada com a descoberta da atividade antitumoral da Cisplatina ($[\text{Pt}(\text{NH}_3)(\text{Cl})]$). Desde então, vários compostos à base de platina (Pt) têm sido desenvolvidos, mas apenas dois deles (Carboplatina e a Oxaliplatina) receberam aprovação para uso mundial pela Administração de Alimentos e Medicamentos (FDA). Nesse contexto, a utilização de ferramentas computacionais desempenha um importante papel no planejamento de novos fármacos e na previsão de suas propriedades. Uma metodologia que permite a simulação de novos fármacos em condições *in vitro*, é a Dinâmica Molecular clássica (DM). Entretanto, adotar um modelo que descreva adequadamente o sistema molecular na simulação é fundamental. Apesar disso, em sistemas contendo metalodrogas e/ou moléculas muito conjugadas os parâmetros já disponíveis na literatura geralmente são escassos ou podem não ser confiáveis. Nesse sentido, um novo conjunto de parâmetros de campo de força AMBER foi desenvolvido e validado, com base nos cálculos da teoria do funcional de densidade (DFT), para um possível complexo anticâncer de platina (II) (*cis*-dicloro(2-aminometilpiridina)platina (II) ligado ao derivado 2-(4'-aminofenil-2'-hidroxifenil)benzotizol (AHBT)). A fim de clarear algumas discordâncias na literatura sobre a existência ou não de uma ligação química coordenada entre o complexo de Pt e o DNA, o modelo desenvolvido foi aplicado em duas simulações de DM: complexo de Pt ligado e não ligado ao DNA. A validação da parametrização mostra que o novo modelo descreve adequadamente as propriedades estruturais do complexo, estando em muito boa concordância com a estrutura de referência quântica. Além disso, os resultados da simulação revelam uma alta afinidade entre o sulco menor do DNA e o complexo metálico estudado. Quando coordenado, o complexo induz mudanças conformacionais na estrutura do DNA. No geral, é esperado que este trabalho contribua significativamente para futuras simulações de DM de complexos de Pt em alvos biológicos, ainda não bem exploradas, principalmente devido aos poucos parâmetros para o metal encontrados na literatura.

Palavras-chave: Parametrização de campo de força; Complexo de platina (II); simulações de Dinâmica Molecular (DM); Ácido desoxirribonucleico (DNA).

ABSTRACT

The metals exhibit a great chemical and biological diversity, and their use in medicine was increased with the discovery of the antitumor activity of cisplatin ($[\text{Pt}(\text{NH}_3)_2(\text{Cl})_2]$). Since then, several Platinum-based (Pt) compounds have been developed, but only two of them (Carboplatin and Oxaliplatin) have received approval for worldwide use by the Food and Drug Administration (FDA). In this context, the use of computational tools plays an important role in the design of new drugs and predicting their properties. One methodology that allows the simulation of new drugs under *in vivo* conditions is the classical Molecular Dynamics (MD). However, adopting a model that adequately describes the molecular system in the simulation is critical. Nevertheless, for the description of metallodrugs and/or very conjugated molecules the parameters already available in the literature are generally scarce or may not be reliable. In this sense, a new set of AMBER force field parameters, based on density functional theory (DFT) calculations, has been developed, validated and applied to a possible anticancer platinum (II) complex (*cis*-dichloro(2-aminomethylpyridine)platinum (II) bonded to 2-(4'-amino2'-hydroxyphenyl)benzothiazole (AHBT)). In order to clarify some disagreements in the literature about the existence or not of a chemical bond between the Pt complex and DNA, the developed model was applied in two MD simulations: Pt complex bonded to the DNA and a non-bonded system. The parameterization validation shows that the new model adequately describes the structural properties of the complex, being in very good agreement with the quantum reference structure. In addition, the simulation results reveal a high affinity between the DNA minor groove and the studied metallic complex. When coordinated, it induces conformational changes in the DNA structure. Overall, we expect this work to contribute significantly to future MD simulations of Pt complexes in biological targets, still not well explored mainly due to the few metal parameters for found in the literature.

Keywords: Force field parameterization; Platinum (II) complex; Molecular Dynamics (DM) simulation; Deoxyribonucleic Acid (DNA).

LISTA DE FIGURAS

PRIMEIRA PARTE

Figura 1 - <i>cis</i> -dicloro(2-aminometilpiridina)platina(II) ligado ao derivado 2-(4'-aminofenil-2'-hidroxifenil)benzotizol (AHBT).	15
Figura 2 - Estrutura dos complexos de rutênio (Ru).	17
Figura 3 - Estrutura da Auranofina.	18
Figura 4 - Estrutura dos complexos [Cu(NN)(ON)]NO ₃ (1) e [Cu(NN)(OO)]NO ₃ (2).	19
Figura 5 - Estruturas dos principais medicamentos à base de platina (Pt) aprovados para o tratamento de cânceres.	20
Figura 6 - Estrutura do composto benzotiazol.	22
Figura 7 - Estrutura do Salicilato de Metila.	22
Figura 8 - Formas biológicas do DNA.	24
Figura 9 - Sulcos do DNA.	25
Figura 10 - Formação do aduto intrafita Pt-DNA (1,2-d(GpG)).	26
Figura 11 - Representação do raio de corte para um sistema periódico 2D.	29

SEGUNDA PARTE

ARTIGO

Figure 1 - Structural projection of the <i>cis</i> -dichloro(2-aminomethylpyridine)platinum (II) bonded to 2-(4'-amino2'-hydroxyphenyl)benzothiazole (AHBT).	44
Figure 2 - Atom names (in red) and atom types (in green).	47
Figure 3 - I) Potential energy surface (PES) obtained from the torsion of the dihedral N12-C22-C13-C14. II) Global minimum corresponding to the first red circle structure in figure 3 I). III) Local minimum corresponding to the second red circle structure in figure 3 I).	53
Figure 4 - RMSD <i>versus</i> time graph calculated for platinum (II) complex in vacuum (T = 300 K).	54
Figure 5 - Bond length <i>versus</i> time graph for bonds involving the metal center of the complex.	55

Figure 6 - Variation of the N12-C22-C13-C14 dihedral (in black) and distribution of the structures obtained from the MD simulation.	56
Figure 7 - Variation of the H24-N23-C25-O26 dihedral and distribution of the structures obtained from the MD simulation.	57
Figure 8 - BLA of the platinum (II) complex models computed from the quantum structure (QM_opt) and of the mean values of the bond lengths along with the MD simulations performed with the developed parameters (New_FF) and GAFF parameters.	58
Figure 9 - Infrared spectrum calculation for platinum (II) complex (blue and green curves represent the quantum structure and the mean structure spectra from vacuum MD simulation, respectively).....	59
Figure 10 - RMSD <i>versus</i> time graph calculated for platinum (II) complex (blue) and DNA (red) during 100 ns of the MD simulation of the non-covalently bonded DNA-complex system.	61
Figure 11 - Hydrogen bonds between the platinum (II) complex and the nucleotides in the minor groove of DNA.....	63
Figure 12 - RMSD <i>versus</i> time graph calculated for platinum (II) complex (blue) and DNA (orange) during 100 ns of the MD simulation of the Platinum-DNA Intrastrand Adducts.....	65

SUPPORTING INFORMATION

Figure S1.1 - Energy of the conformations obtained after the conformational search of the platinum (II) complex.	76
Figure S1.2 - Structural projection of platinum (II) complex optimized with different levels of theory.	76
Figure S1.3 - Part of the complex analyzed by BLA (green).....	77
Figure S2.1 - Atom names (in red) and atom types (in green).	78
Figure S3.1 - Platinum (II) complex in the minor groove of DNA (sequence 5'-CGCGAATTCGCG-3', PDB ID: 1BNA). ¹ Cytosine (C) in blue, Guanine (G) in red, Adenine (A) in light blue, Thymine (T) pink.	88
Figure S3.2 - Platinum (II) complex bonded in the DNA (sequence 5'-CCTCAG*G*CCTCC-3', PDB ID: 2NPW)). ² Cytosine (C) in blue, Guanine (G) in red, Adenine (A) in light blue, Thymine (T) pink.	89

Figure S4.1 - Atom names (in purple) and atom types (in green).....	89
Figure S5.1 - RMSD <i>versus</i> time graph calculated for platinum (II) complex (green) and DNA (blue) during 25 ns of the MD simulation.	92

LISTA DE TABELAS

SEGUNDA PARTE

ARTIGO

Table 1 - Binding free energy components (kcal mol ⁻¹) for complex-DNA system.	64
---	----

SUPPORTING INFORMATION

Table S1.1 - Bond length (Å) and RMSD (Å) values for platinum (II) complex optimized at different levels of theory.....	77
Table S1.2 - Values of BLA (in Angstrom) for the platinum (II) complex computed on the DFT optimized structure and the MD average obtained with the new and the GAFF force fields.	77
Table S2.1 - Atomic charges (RESP) for platinum (II) complex.	86
Table S4.1 - Atomic charges (RESP) for platinum (II) complex bound to DNA.	90

SUMÁRIO

PRIMEIRA PARTE	13
1 INTRODUÇÃO E JUSTIFICATIVA	13
2 REFERENCIAL TEÓRICO	15
2.1 Complexos metálicos como agentes anticâncer	15
2.2 Fármacos à base de platina (Pt) em uso clínico	19
2.3 Derivados benzotiazóis e suas aplicações	22
2.4 Interações de fármacos com o DNA	23
2.5 Química Computacional	27
2.5.1 Dinâmica Molecular Clássica	28
2.5.2 Campo de força	29
2.5.2.1 Parâmetros do campo de força	33
3 OBJETIVOS	34
4 CONCLUSÃO	35
5 REFERÊNCIAS	35
SEGUNDA PARTE - ARTIGO	43
Parameterization, validation and application of a new force field for Pt (II) complexes of 2-(4'-amino-2'-hydroxyphenyl)benzothiazole: exploring new anticancer drugs	41
SUPPORTING INFORMATION	76
ANEXO I – Trabalhos desenvolvidos	94

PRIMEIRA PARTE

1 INTRODUÇÃO E JUSTIFICATIVA

Nos últimos anos, um grande número de publicações na literatura tem abordado as propriedades de complexos metálicos para o tratamento de doenças, principalmente o câncer. O grande interesse pelo estudo e desenvolvimento desses complexos deve-se às características únicas dos metais, que incluem vários modos de coordenação e reatividade, além de apresentarem diferentes estados de oxidação, podendo interagir com um número variado de compostos orgânicos (JOHNSTONE; SUNTHARALINGAM; LIPPARD, 2016; KENNY; MARMION, 2019; KONKANKIT et al., 2018; NDAGI; MHLONGO; SOLIMAN, 2017; SIMPSON et al., 2019).

Nesse contexto, a descoberta das atividades biológicas da Cisplatina ($[\text{Pt}(\text{NH}_3)_2\text{Cl}_2]$), bem como seu uso no tratamento de diversos tipos de câncer, representou um marco na história da Química Inorgânica Medicinal. Apesar disso, alguns anos após sua introdução no mercado farmacêutico, efeitos colaterais como nefrotoxicidade (toxicidade sobre os rins), neurotoxicidade (toxicidade sobre o sistema nervoso central e periférico) e ototoxicidade (toxicidade sobre o ouvido) foram atribuídos ao composto, principalmente devido à falta de seletividade entre as células tumorais e saudáveis (KENNY; MARMION, 2019; RÉBÉ et al., 2020). Desde então, muitos compostos à base de platina (Pt) foram desenvolvidos, e ainda continuam sendo planejados, a fim de contornar esses efeitos indesejáveis (BONDI et al., 2020; DEO et al., 2018; JOHNSTONE; SUNTHARALINGAM; LIPPARD, 2016).

Os mecanismos de ação de quimioterápicos à base de Pt ainda não foram completamente elucidados, mas o DNA é considerado um alvo crítico desses fármacos (DASARI; TCHOUNWOU, 2014; SIMPSON et al., 2019). Sendo assim, informações detalhadas dos modos de interação e das propriedades estruturais de fármacos à base de Pt com o DNA são de clara importância para o avanço na terapia de diversos tipos de câncer.

Para isso, o sistema de interesse pode ser investigado experimentalmente e com o uso de técnicas computacionais, para apoiar as informações obtidas do experimento, e prever àquelas que não podem ser avaliadas com técnicas experimentais disponíveis atualmente. Um método computacional muito utilizado na predição de propriedades estruturais e de parâmetros termodinâmicos de um sistema molecular é a Dinâmica

Molecular Clássica (DM) (DURRANT; MCCAMMON, 2011; LIU et al., 2018). Evidentemente, para que resultados com significado físico possam ser obtidos das simulações de DM, o modelo utilizado para descrever as moléculas que serão simuladas e as interações entre elas precisa ser avaliado. Esse modelo compõe um campo de força, que será descrito mais formalmente na seção 2.5.2.

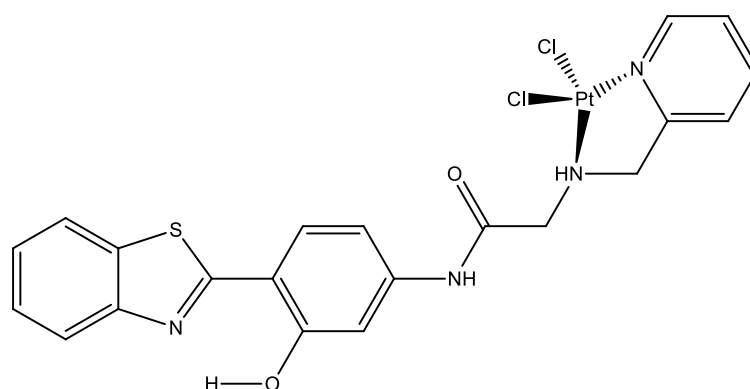
Para pequenas moléculas orgânicas, vários programas automáticos de parametrização como ANTECHAMBER (WANG et al., 2004) e CCGEN (WANG et al., 2006) são frequentemente utilizados para designar parâmetros de campo de força, enquanto que para compostos inorgânicos, especialmente os complexos de Pt, os parâmetros são escassos e muitas vezes não estão presentes em campos de força padrão (LOPES et al., 2006; SCHEEFF; BRIGGS; HOWELL, 1999; YAO; PLASTARAS; MARZILLI, 1994). É importante ressaltar que os campos de força gerais apresentam um número reduzido de tipos atômicos (baseado no número atômico, ligação, e ambiente químico) para descrever um número variado de compostos. Isso, conseqüentemente, resulta em uma descrição menos precisa do sistema parametrizado. Moléculas altamente conjugadas descritas por campos de força gerais podem reproduzir incorretamente seus modos de vibração, resultando em estruturas não físicas (PRANDI et al., 2016)

No presente trabalho, um novo conjunto de parâmetros de campo de força AMBER foi desenvolvido e validado, baseado na teoria do funcional de densidade (DFT), para um complexo de platina (II) (*cis*-dicloro(2-aminometilpiridina)platina (II) ligado ao derivado 2-(4'-amino-2'-hidroxifenil)benzotiazol (AHBT) (Figura 1)). Este complexo foi proposto com base nas propriedades terapêuticas e fotofísicas (MANCINI et al., 2015; ROCHA; RAMALHO, 2016) do ligante AHBT, juntamente com a citotoxicidade do centro metálico (MAVROIDI et al., 2016).

O modelo desenvolvido foi validado comparando resultados de simulação de DM, como análise da alternância dos comprimentos de ligação (do inglês, *Bond Length Alternation*, BLA) e cálculo teórico de infravermelho (IV), com uma referência quântica. Em seguida, o novo conjunto de parâmetros foi utilizado para estudar os modos de interação do complexo com o DNA de modo covalente e não-covalente. Estudos prévios realizados com complexos que compartilham características estruturais com complexo proposto nesse trabalho mostram que: (i) os complexos entram intactos na célula (MAVROIDI et al., 2016; TZANOPOULOU et al., 2010); (ii) eles exibem citotoxicidade contra as células tumorais (CHEN et al., 2015; MAVROIDI et al., 2016).

No entanto, ainda há discordâncias sobre os mecanismos responsáveis pela citotoxicidade desses compostos. Alguns estudos acreditam que os complexos estruturalmente semelhantes à cisplatina se ligam ao N7 das bases guaninas do DNA (CHEN et al., 2015; MAVROIDI et al., 2016; RODRIGUEZ et al., 2018; SCHOBERT; BIRSACK, 2005); enquanto outros apostam na interação não-covalente com o sulco menor do DNA (CHEN et al., 2015; MAVROIDI et al., 2016; MUKHERJEE et al., 2015, 2016; SUNTHARALINGAM et al., 2013).

Figura 1 - *cis*-dicloro(2-aminometilpiridina)platina(II) ligado ao derivado 2-(4'-aminofenil-2'-hidroxifenil)benzotizol (AHBT).



2 REFERENCIAL TEÓRICO

2.1 Complexos metálicos como agentes anticâncer

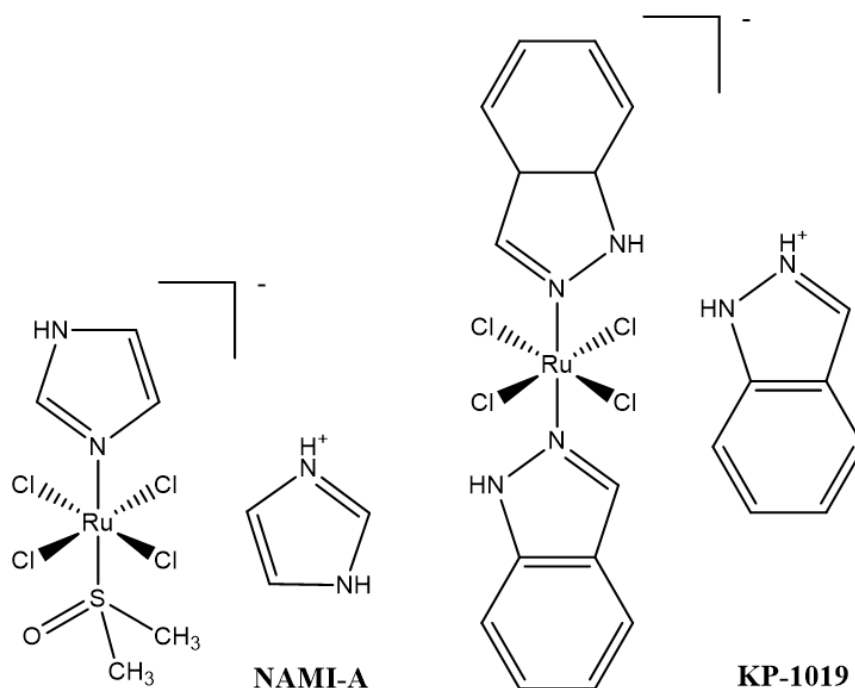
Os metais, particularmente os de transição, são conhecidos por suas características únicas, que incluem uma variedade de números de coordenação, estados de oxidação e arranjos geométricos (ZORODDU et al., 2019). Devido à grande diversidade química e biológica dos metais, vários mecanismos de ação em processos biológicos podem ser observados dependendo dos seus estados de oxidação, o que geralmente não é observado nos compostos orgânicos. A síntese e aplicação de complexos metálicos como anti-inflamatórios, antibacterianos, antirreumáticos e antimaláricos têm sido motivo de muitas pesquisas (MEDICI et al., 2015). Além disso, na medicina nuclear muitos compostos metálicos podem ser utilizados como radiofármacos para o diagnóstico de doenças (PAYOLLA; MASSABNI; ORVIG, 2019).

Dentre as inúmeras aplicações dos metais na medicina, a utilização deles no desenvolvimento de agentes quimioterápicos contra o câncer tem sido uma estratégia promissora. Apesar dos avanços significativos nos últimos anos, o câncer continua sendo uma das principais causas de morte no mundo (SIEGEL; MILLER; JEMAL, 2018). Juntamente com a ressecção cirúrgica (remoção de parte de um tecido ou órgão) e radioterapia, a quimioterapia ainda é a forma predominante de tratamento para a doença. No entanto, os efeitos colaterais tóxicos associados aos agentes quimioterápicos estimulam as pesquisas para o desenvolvimento de novos fármacos. Particularmente, alguns metais como rutênio (Ru), ouro (Au), cobre (Cu) e platina (Pt) tem sido revisados na literatura diante dos seus potenciais para o planejamento de fármacos anticâncer (SIMPSON et al., 2019).

Em condições fisiológicas o Ru pode apresentar vários estados de oxidação (II, III e IV). Os complexos de Ru (III) são cineticamente inertes, mas podem ser reduzidos à Ru (II) quando em contato com microambientes tumorais com baixa concentração de oxigênio, característicos de tumores sólidos (KENNY; MARMION, 2019). Dessa forma, essa propriedade dos complexos de Ru (III) pode ser explorada como uma estratégia para a entrega do fármacos em locais específicos. Entre as vantagens do processo de biotransformação de um determinado fármaco, pode-se citar a redução dos efeitos colaterais, visto que o mesmo permanece íntegro na corrente sanguínea antes do contato com o alvo biológico.

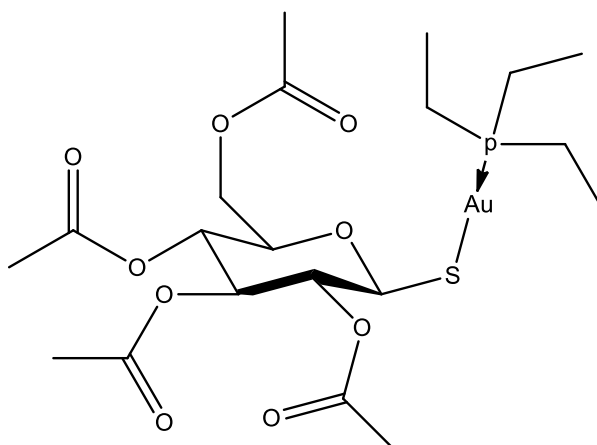
Exemplos de complexos de Ru (III) são o NAMI-A ($\text{ImH}[\text{trans-RuCl}_4(\text{Im})\text{-DMSO}]$, sendo Im=Imidazol) e KP-1019 ($\text{IndH}[\text{trans-RuCl}_4(\text{Ind})_2]$, sendo Ind=Indazol) (Figura 2), que já foram aprovados para realização de testes clínicos (HARTINGER et al., 2008; LEIJEN et al., 2015). O NAMI-A foi considerado um inibidor de células cancerígenas metastáticas. Já o composto KP-1019 mostrou-se mais eficaz contra tumores primários. Ainda não há muita informação sobre o mecanismo de ação desses compostos, mas acredita-se que esses atuam na inibição da enzima DNA polimerase, que é uma das enzimas responsáveis pela síntese de DNA. Em meio ácido, o íon cloreto (Cl^-) do complexo é hidratado, devido à baixa concentração de Cl^- nas células cancerosas. Esse processo de aquação aumenta a labilidade do complexo, tornando-o uma espécie antitumoral mais ativa (CHATLAS; VAN ELDIK; KEPPLER, 1995; PAULA et al., 2000).

Figura 2 - Estrutura dos complexos de rutênio (Ru).



Os compostos à base de Au são utilizados na medicina há séculos (PRICKER, 1996). Em 1985, a aprovação do fármaco Auranofina ([2, 3, 4, 6-tetra-O-acetil-1-tio- β -D-glicopiranosato-trietilfosfinaouro(I)] (Figura 3)) para o tratamento de artrite reumatoide impulsionou ainda mais a busca por novas propriedades desse elemento (QUEIROZ; BATISTA, 1996). Desde então, pesquisas têm evidenciado as potencialidades dos compostos de ouro no tratamento de inflamações, doenças microbianas, tumores, entre outros. O metal possui estados de oxidação que variam de -1 a +5, mas os compostos de Au (I) e (III) têm sido destacados por suas propriedades anticancerígenas (YEO; OOI; TIEKINK, 2018). Complexos de Au (III) se ligam a tiorredoxina redutase (TrxR), uma enzima crucial na redução de espécies reativas de oxigênio (ERO), levando à alteração de processos celulares e, conseqüentemente, à apoptose da célula (DA SILVA MAIA; DEFLON; ABRAM, 2014; PORCHIA et al., 2018).

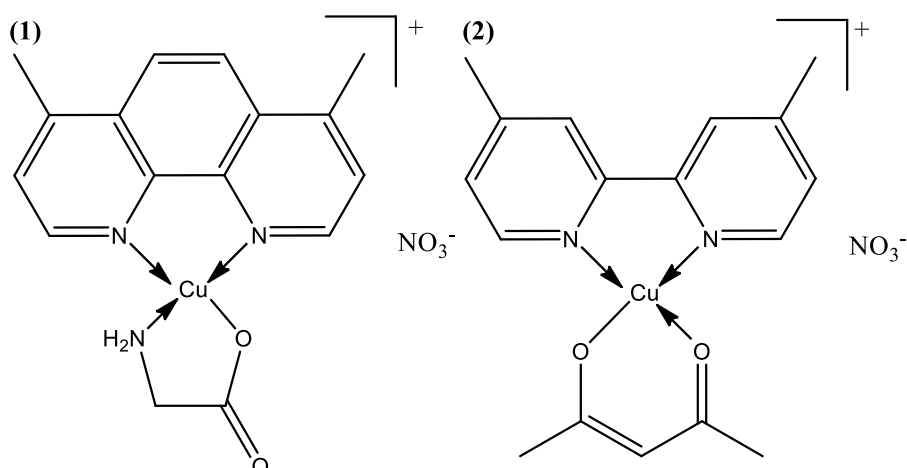
Figura 3 - Estrutura da Auranofina.



O Cu, por sua vez, é um elemento essencial para o funcionamento adequado do corpo humano, pois está envolvido em vários processos biológicos e também é um cofator enzimático. Tais características tornam os complexos de Cu uma alternativa atraente para o planejamento de novos fármacos com efeitos colaterais menos tóxicos (MCGIVERN; AFSHARPOUR; MARMION, 2018).

Entre os complexos de Cu relatados na literatura, os complexos de Cu (II), representados pela fórmula geral $[Cu(NN)(OO)]NO_3$ e $[Cu(NN)(ON)]NO_3$ (em que NN representa a 2,2'-bipiridina substituída; o ligante ON representa um α -aminoácido ou um peptídeo; e OO é utilizado para representar o acetilacetato ou o salicilaldeído) estão em fase de triagem clínica (Figura 4) (MEJIA; RUIZ-AZUARA, 2008). Embora o potencial anticancerígeno dos complexos de Cu já ter sido identificado, os mecanismos de ação dos mesmos ainda não foram totalmente elucidados. Estudos anteriores indicam que a função citotóxica dos complexos envolve a geração de espécies reativas de oxigênio e interações não-covalentes com as bases de DNA, que têm como consequência a sua clivagem e morte celular (GALINDO-MURILLO et al., 2015).

Figura 4 - Estrutura dos complexos $[Cu(NN)(ON)]NO_3$ (1) e $[Cu(NN)(OO)]NO_3$ (2).



Os complexos com atividade anticancerígena apresentados são apenas alguns exemplos diante do grande número de moléculas inorgânicas que têm sido descobertas nos últimos anos. Embora seja observado o grande avanço no desenvolvimento de fármacos à base de metais, os fármacos à base de Pt continuam a desempenhar um papel fundamental no tratamento de vários tipos de câncer. Dados recentes mostram que quase metade dos pacientes que recebem quimioterapia anticâncer são tratados com um fármaco de Pt (ARMSTRONG-GORDON et al., 2018).

2.2 Fármacos à base de platina (Pt) em uso clínico

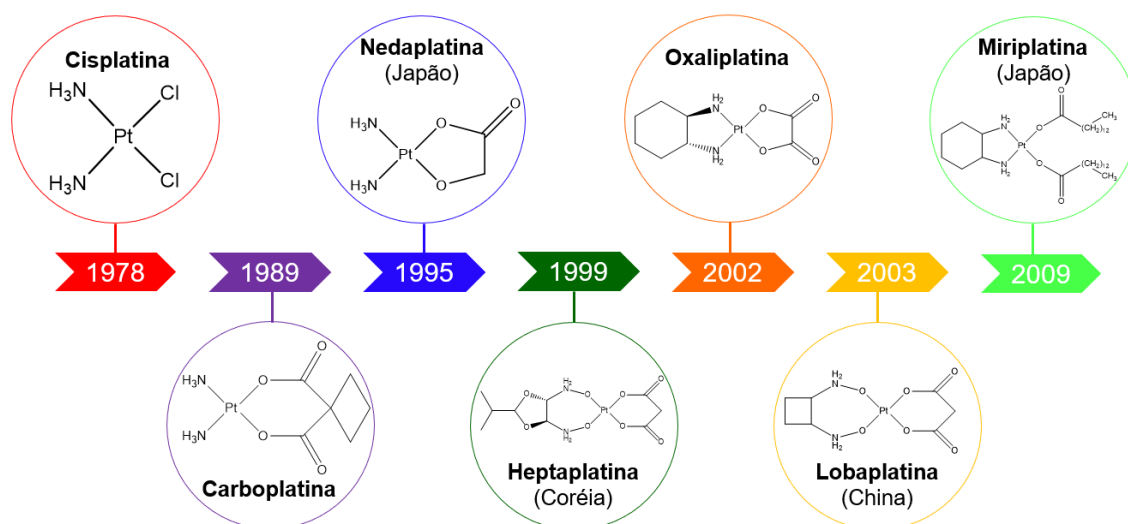
A Cisplatina (*cis*-[PtCl₂(NH₃)₂]) foi o primeiro fármaco à base de Pt aprovado pela FDA (Food and Drug Administration) para o tratamento de neoplasias malignas (KELLAND, 2007). Apesar de ter sido relatada pela primeira vez em 1845, apenas na década de 60, Barnett Rosenberg e colaboradores descobriram as propriedades farmacológicas do composto (ROSENBERG; VAN CAMP; KRIGAS, 1965). Em 1978, a Cisplatina foi aprovada para uso comercial no tratamento de diversos tipos de câncer, dentre eles câncer de bexiga, colo do útero, cabeça, pescoço, testículo, pulmão e ovário. O primeiro caso de utilização da Cisplatina foi no tratamento de um câncer de testículo com sobrevida acima de 95% (HOWLADER et al., 2012).

Após a introdução clínica da Cisplatina no tratamento contra o câncer, milhares de complexos de Pt foram submetidos à triagem pré-clínica, mas poucos complexos foram aprovados para uso clínico (Figura 5) (KENNY; MARMION, 2019). Os outros

compostos à base de Pt desenvolvidos e aprovados para o uso clínico no mundo todo são a Carboplatina (1989) (KELLAND, 2007) e a Oxaliplatina (2002) (GRAHAM; MUHSIN; KIRKPATRICK, 2004). Outros complexos de Pt foram aprovados para uso clínico apenas em algumas nações, como: (i) Nedaplatina (1995) e a Miriplatina (2009), (Japão); e (ii) Heptaplatina (1999) e Lobaplatina (2003), (Coréia e China, respectivamente) (CHEFF; HALL, 2017).

Os fármacos Carboplatina e Nedaplatina são considerados fármacos de segunda geração, uma vez que a única diferença em relação à Cisplatina é a substituição dos ligantes cloro (Cl). Já os fármacos Heptaplatina, Oxaliplatina e Lobaplatina são fármacos de terceira geração, pois tanto os ligantes Cl quanto os ligantes amina (NH_3) são substituídos.

Figura 5 - Estruturas dos principais medicamentos à base de platina aprovados para o tratamento de cânceres.



A Carboplatina, difere-se da Cisplatina pela presença de um ligante dicarboxilato bidentado, que substitui os dois átomos de Cl. A substituição dos ligantes Cl na estrutura da Carboplatina resultou em uma menor reatividade e toxicidade do complexo, quando comparado com a Cisplatina, permitindo que doses mais concentradas fossem prescritas (WHEATE et al., 2010).

A Nedaplatina, outro fármaco de segunda geração, apresentou-se menos nefrotóxica quando comparada com a Cisplatina e a Carboplatina, além de ser muito mais solúvel (10 mg mL^{-1}) que a Cisplatina ($2,5 \text{ mg mL}^{-1}$). Desde sua aprovação, em

1995, a Nedaplatina é utilizada principalmente no tratamento dos cânceres de cabeça, pescoço, esôfago e pulmão (WHEATE et al., 2010).

Os fármacos de terceira geração também apresentam outras características importantes. A Heptaplatina, se destacou em relação aos outros análogos pela baixa nefrotoxicidade e atividade contra linhas celulares de câncer gástrico (KIM et al., 1995). Na Oxaliplatina, a substituição dos ligantes amina por outro ligante bidentado (1,2-diaminocicloexano) foi responsável por contornar a resistência obtida pela Cisplatina, formando diferentes adutos com o DNA. Além disso, outra vantagem inclui a atividade clínica contra o câncer colorretal (BRUNO et al., 2017). A Lobaplatina, apesar de compartilhar algumas características estruturais com a Heptaplatina, atua principalmente no tratamento dos cânceres de mama metastático, pulmão e leucemia mielóide crônica (WELINK et al., 1999). Finalmente, a Miriplatina foi desenvolvida especificamente para o tratamento câncer hepatocelular. Além disso, difere estruturalmente das demais fármacos à base de Pt, pela presença de longas cadeias alquil, o que confere lipofilicidade (TANAKA et al., 2011).

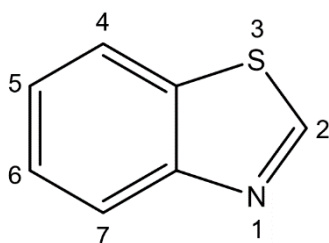
Os dados apresentados mostram que em mais de 40 anos após a introdução da Cisplatina no cenário clínico, apenas dois fármacos à base de Pt foram aprovados para uso mundial e outros quatro para uso em nações específicas. Esses análogos da Cisplatina, de segunda e terceira geração, foram desenvolvidos para contornar a sua toxicidade para tecidos ou órgãos, e também para expandir a atividade contra outros tumores. Infelizmente esses medicamentos ainda causam uma variedade de efeitos colaterais. No entanto, eles ainda permanecem entre os quimioterápicos anticancerígenos mais amplamente utilizados. Dessa forma o desenvolvimento de novos compostos à base de Pt, com atividades melhoradas em relação aos fármacos atuais, é útil e justificado (ARMSTRONG-GORDON et al., 2018; UM et al., 2019).

Esforços têm sido realizados no planejamento de novos compostos à base de Pt que sejam mais seletivos para regiões específicas do tumor, e que possivelmente levam a diminuição dos efeitos colaterais para as células saudáveis. Uma das estratégias consiste em incorporar um ligante transportador adequado na estrutura do complexo, como os derivados benzotiazóis (CHEN et al., 2015; MAVROIDI et al., 2016).

2.3 Derivados benzotiazóis e suas aplicações

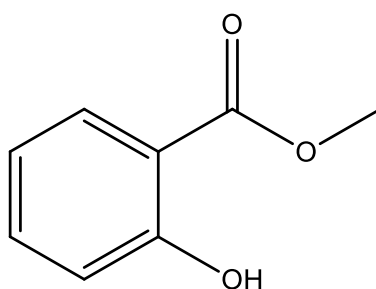
O heterociclo benzotiazol é constituído por um anel de cinco membros, contendo os heteroátomos nitrogênio (N) e enxofre (S) condensado a um anel aromático de seis membros (Figura 6). Tal composto, juntamente com seus derivados, tem atraído considerável atenção devido ao amplo espectro de atividades biológicas, como anti-inflamatório, antimicrobiano, antidiabético, antiviral, anticâncer, analgésico, fungicida, dentre outras (GILL; RAWAL; BARIWAL, 2015; IRFAN et al., 2020; KERI et al., 2015).

Figura 6 - Estrutura do composto benzotiazol.



Particularmente, os compostos da classe dos aminofenilbenzotiazóis vêm mostrando ser extremamente potentes e seletivos contra células cancerosas desde 1996 (CHEN et al., 2015; MAVROIDI et al., 2016; SHI et al., 1996; TZANOPOULOU et al., 2010). Além das propriedades anticâncer, o 2-(4'-amino-2'-hidroxifenil)benzotiazol (AHBT), dessa mesma classe, também é conhecido por apresentar uma intensa emissão de fluorescência devido ao mecanismo de transferência de próton intramolecular no estado excitado (ESIPT). O processo ESIPT foi primeiramente reportado por Weller em 1955 para o salicilato de metila (Figura 7) (WELLER, 1956).

Figura 7 - Estrutura do Salicilato de Metila.



Assim como o salicilato de metila, o AHBT pode apresentar fluorescência pelo processo ESIPT devido à presença de uma ligação de hidrogênio intramolecular entre os grupos doador (-OH) e aceptor (=N-) de ligação de hidrogênio. No estado fundamental, a forma enol (E) é a mais estável. Quando o E é excitado pela absorção de um fóton de luz, a sua forma excitada (E*) fica em equilíbrio dinâmico com a forma ceto excitada (C*). Esse processo fotoinduzido ocorre em um curto intervalo de tempo, na escala de femto à picosegundos (YANG; ZHAO; LI, 2016). Seguindo o processo fotoinduzido, o produto ESIPT (forma C*) retorna ao seu estado fundamental emitindo radiação. Posteriormente, ocorre uma transferência de próton reversa, produzindo a forma E original.

O mecanismo apresentado é uma possível via pela qual compostos com ligação de hidrogênio intramolecular, assim como o AHBT, são promissores para o desenvolvimento de sondas espectroscópicas fluorescentes, que podem ser utilizadas na detecção de doenças (MANCINI et al., 2015; ROCHA; RAMALHO, 2016; SEDGWICK et al., 2018). Essa é apenas mais uma grande aplicação para a classe dos aminofenilbenzotiazóis.

2.4 Interações de fármacos com o DNA

O ácido desoxirribonucleico (DNA) é um composto orgânico responsável por armazenar e transmitir a informação genética da célula. A estrutura do DNA é composta por duas longas cadeias de nucleotídeos, que são ordenados de modo a formar um espiral conhecido como dupla hélice. Cada nucleotídeo consiste na associação de três moléculas: uma base nitrogenada (Citosina (C), Timina (T), Adenina (A) ou Guanina (G)), um açúcar (desoxirribose) e um grupo fosfato. As bases C e T são denominadas de pirimidinas, que se associam em pares por meio de ligações de hidrogênio intermoleculares com as bases purinas G e A, respectivamente. No entanto, o empilhamento das bases hidrofóbicas é um dos principais contribuintes para a estabilidade da dupla hélice do DNA (FENG et al., 2019).

As principais formas que o DNA costuma adotar são a A-DNA, B-DNA e Z-DNA (Figura 8). A forma predominante de cada uma dessas conformações depende das condições do ambiente. No interior da célula, a forma B-DNA é a mais comum. Essa forma possui o sulco principal mais largo que o sulco secundário, embora as profundidades sejam praticamente idênticas. É conhecido que em condições de

desidratação, a forma B-DNA tende a assumir a forma A-DNA. A forma A-DNA é estruturalmente semelhante à forma B-DNA, porém é mais rígida e compacta. Isso permite que a estrutura tenha um sulco principal estreito e profundo, embora o sulco secundário seja mais largo e raso. Já a forma Z-DNA é estruturalmente diferente das formas A e B. Sua estrutura é mais alongada e composta por um único sulco, análogo ao sulco menor da B-DNA, resultando em um arranjo com forma de zigue-zague (KELLETT et al., 2019). Estudos ainda têm sido realizados para determinar o seu envolvimento em processos biológicos (VONGSUTILERS; GANNETT, 2018).

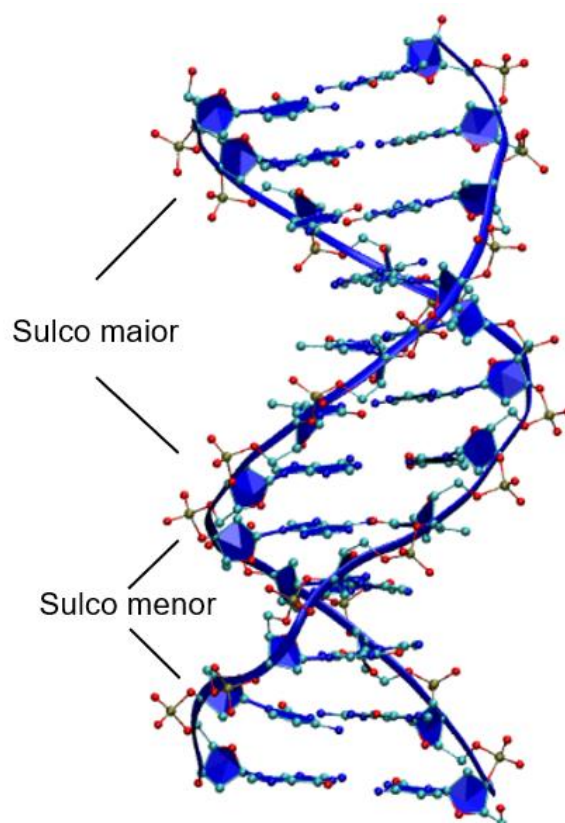
Figura 8 - Formas biológicas do DNA.



FONTE: KELLETT et al., (2019).

Diante do reconhecimento das principais formas do DNA, também é de suma importância entender suas propriedades mecânicas e biofísicas na presença de potenciais fármacos. Isso, conseqüentemente, pode levar ao desenvolvimento de novos fármacos que buscam atingir o DNA para curar/tratar uma determinada doença. É conhecido que os compostos podem interagir com o DNA de forma específica (intercalação e a interação com os sulcos maior e menor (Figura 9)) e inespecífica (ligação eletrostática) (ALMAQWASHI et al., 2016).

Figura 9 - Sulcos do DNA.



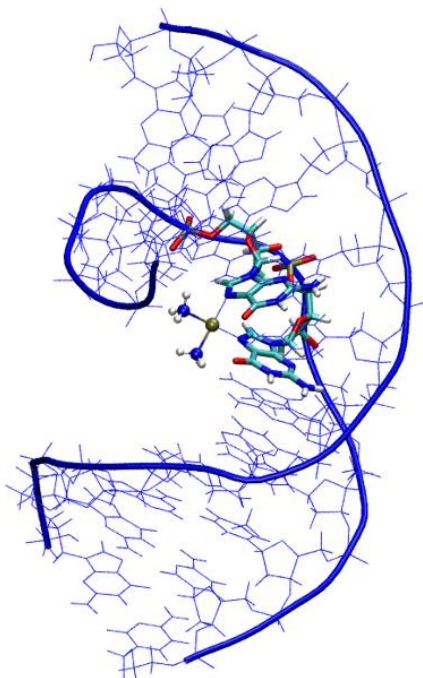
A intercalação ocorre quando uma molécula aromática é inserida entre dois pares de bases nitrogenadas. A primeira evidência estrutural desse tipo de interação foi relatada há mais de 40 anos com um complexo de Pt contendo ligantes heterocíclicos (BOND et al., 1975). Para que esse tipo de interação ocorra é necessário que a dupla hélice seja parcialmente desenrolada, criando uma cavidade de tamanho suficiente para acomodar a molécula, que pode ser estabilizada por interações do tipo π - π e ligações de hidrogênio (ALOTAIBI; MOMEN, 2019).

Em relação à interação com os sulcos do DNA, há evidências experimentais e teóricas que a interação não-covalente ocorre principalmente com o sulco menor do DNA, em especial na região rica em adenina (A) e timina (T) (JALILI; MADDAH, 2017; KAMAL et al., 2010; MAVROIDI et al., 2016). Uma das principais causas que levam a preferência por essa região é o formato do sulco. Apesar de estreito, possui uma profundidade que favorece o encaixe das moléculas por meio das interações não-covalentes, como ligações de hidrogênio intermoleculares. Essa região do DNA é rica em grupos aceptores de ligações de hidrogênio, o que pode intensificar ainda mais a interação de moléculas com grupos doadores de ligação de hidrogênio. As interações

não-covalentes são reversíveis, mas induzem deformações estruturais no DNA e podem levar à separação das fitas da dupla hélice (JAIN et al., 2018; SIRAJUDDIN; ALI; BADSHAH, 2013).

Já a interação covalente ocorre principalmente no sulco maior do DNA. Após a formação do aduto, os mecanismos de reparo são ativados a fim de remover essas “lesões”. Caso a remoção não seja completa, o aduto formado induzirá a morte celular. Um exemplo típico de composto que forma aduto com o DNA é a Cisplatina (BERGAMO; DYSON; SAVA, 2018). Estudos de Ressonância Magnética Nuclear (RMN) de ^{195}Pt , mostram que o fármaco Cisplatina forma primeiramente adutos monofuncionais com o DNA (BANCROFT; LEPRE; LIPPARD, 1990). Os adutos bifuncionais (cada átomo de Pt faz duas ligações com o DNA) podem ser formados tanto entre as bases de mesma fita de DNA (intrafita), quanto em fitas diferentes (interfita) (AHMAD, 2017). Há várias possibilidades para formação dos adutos bifuncionais, mas a forma predominante ocorre pela ligação intrafita do átomo de Pt aos átomos de N7 duas bases guaninas consecutivas (Figura 10) (DE CÓZAR et al., 2016).

Figura 10 - Formação do aduto intrafita Pt-DNA (1,2-d(GpG)). Os átomos da Cisplatina estão representados como esferas e os nucleotídeos de guanina como tubos.



A forma inespecífica de interação com o DNA pode ocorrer principalmente com grupos fosfatos da sua estrutura que são ricos em elétrons e favorecem a aproximação

de cátions (como íons metálicos livres ou complexos). Recentemente ROSA et al., (2019) observaram a grande estabilidade das interações entre átomos de hidrogênio de um complexo trinuclear de Pt com os átomos de oxigênio dos grupos fosfatos de DNA.

Dependendo das características dos complexos de Pt, como a natureza dos grupos de saída, dos ligantes transportadores, e também a sua geometria, os modos de interação com o DNA podem variar, sejam eles específicos ou inespecíficos (DASARI; TCHOUNWOU, 2014). Logo, entender os possíveis modos de interação de complexos de Pt com o DNA é crucial para o planejamento de novos complexos mais ativos contra as células tumorais. Nesse contexto, a química computacional se destaca como uma importante ferramenta no design molecular preditivo de novos compostos (BRAUN et al., 2019; COLE et al., 2019).

2.5 Química Computacional

Nas últimas décadas, a utilização de computadores para estudar o comportamento de sistemas moleculares vem ganhando espaço devido ao grande desenvolvimento tecnológico na área de informática. Com o aumento no poder computacional torna viável a execução de cálculos anteriormente inacessíveis. Isso, aliado ao desenvolvimento de métodos computacionais mais acurados, permite uma melhor descrição e compreensão das propriedades ao nível atômico/molecular e eletrônico, que são difíceis ou impossíveis de se obter experimentalmente (KIRCHMAIR et al., 2015). Por meio de técnicas computacionais é possível prever a existência ou não de espécies moleculares em condições reais.

Certamente, a predição das inúmeras propriedades moleculares obtidas com uso de técnicas computacionais depende dos métodos utilizados, sejam eles quânticos ou clássicos. Os cálculos quânticos, que são baseados na equação de Schrödinger, permitem a obtenção de informações sobre a estrutura eletrônica das moléculas. No entanto, esses cálculos limitam-se na descrição de sistemas moleculares menores e exigem uma maior demanda computacional quando comparados com os cálculos baseados na Mecânica Molecular (MM).

Os cálculos MM não tratam os elétrons de forma explícita, são menos demorados e permitem o tratamento de sistemas mais complexos. Esses cálculos são descritos de acordo com a Mecânica Clássica e apresentam-se como uma boa alternativa na determinação de propriedades estruturais e parâmetros termodinâmicos de um

sistema molecular. Um exemplo é a simulação por Dinâmica Molecular Clássica (DM), que se mostra uma das técnicas computacionais mais empregadas para o entendimento e previsão das propriedades, estrutura e função de macromoléculas biológicas (NAIR; MINERS, 2014).

2.5.1 Dinâmica Molecular Clássica

A simulação por Dinâmica Molecular (DM) é uma abordagem computacional que se fundamenta na mecânica clássica e fornece informações sobre o movimento e a interação de átomos e moléculas no tempo. As moléculas que compõem o sistema são tratadas como uma coleção de partículas unidas por forças harmônicas ou elásticas. Sendo assim, não é possível observar formação e ruptura de ligações, interações entre os orbitais, transferência de carga ou qualquer outro efeito eletrônico (BRAUN et al., 2019; DE VIVO et al., 2016; NAIR; MINERS, 2014).

Para realizar os cálculos de DM, necessita-se resolver as Equações de movimento de Newton (1 e 2), a fim de encontrar o conjunto de posições e interações entre os átomos em cada intervalo de tempo, que é preestabelecido (FRENKEL; SMIT, 2001).

$$\vec{F}_i = m_i \vec{a}_i(t) \quad (1)$$

$$\vec{F}_i = - \frac{\partial V_{TOT}(r_1, r_2, \dots, r_n)}{\partial r_i} \quad (2)$$

Em que \vec{F}_i representa a força atuando na partícula i , m_i é a massa atômica; \vec{a}_i é a aceleração; t é o tempo; r_i é a posição do átomo e V_{TOT} é o potencial total dependente da posição da partícula que será discutido de forma mais detalhada na próxima seção.

As Equações 1 e 2 são resolvidas simultaneamente, resultando em um conjunto de equações de movimento para cada partícula do sistema. No entanto, as Equações de Newton não podem ser descritas analiticamente devido à interação de inúmeras partículas. Na prática, a resolução das equações deve ser realizada através da integração numérica. Esse tipo de resolução torna-se possível com a utilização de algoritmos específicos, nos quais a integração é feita em pequenos intervalos de tempo. Inicialmente, a força que atua em cada uma das partículas, em uma condição inicial e no

tempo t , é obtida pela contribuição das interações com as demais partículas do sistema. Como consequência, obtêm-se a aceleração de cada partícula. Dessa forma, sabendo as coordenadas espaciais de cada partícula, bem como suas velocidades no tempo t , torna-se possível calcular as novas posições e velocidades no tempo $t + \Delta t$. Esse cálculo é realizado consecutivamente assumindo que a força permanece constante no intervalo de tempo Δt . Os algoritmos mais utilizados para a integração dessas equações são o Verlet (VERLET, 1967) e Leap-Frog (HOCKNEY, 1970).

O algoritmo de Verlet utiliza as posições e acelerações das partículas em função de um tempo t . As novas posições são determinadas como $r(t + \Delta t)$ e as posições do passo anterior como $r(t - \Delta t)$. Essas duas equações podem ser obtidas por meio da expansão em série de Taylor, nos instantes posterior e anterior a t (Equações 3 e 4 respectivamente).

$$r(t + \Delta t) \cong r(t) + v(t)\Delta t + \frac{1}{2} a(t)\Delta t^2 + \dots \quad (3)$$

$$r(t - \Delta t) \cong r(t) - v(t)\Delta t + \frac{1}{2} a(t)\Delta t^2 - \dots \quad (4)$$

Somando e rearranjando as Equações 3 e 4 é possível determinar novas posições atômicas, após o tempo de simulação programado, conforme a Equação 5.

$$r(t + \Delta t) \cong 2r(t) - r(t - \Delta t) + a(t)\Delta t^2 \quad (5)$$

Uma das desvantagens do algoritmo de Verlet é a incapacidade de calcular a velocidade do sistema de forma explícita. Com isso, a partir do algoritmo de Verlet várias modificações foram realizadas até que o algoritmo de Leap-Frog fosse desenvolvido, sendo possível calcular explicitamente a velocidade. Mas, apesar da velocidade ser calculada explicitamente, a desvantagem desse algoritmo é que as posições e velocidades estão sempre dessincronizadas por $\frac{1}{2}\Delta t$, não sendo possível a obtenção de ambas as grandezas físicas num mesmo instante de tempo. Desta forma, a velocidade do sistema pode ser calculada pela Equação 6.

$$v\left(t + \frac{1}{2}\Delta t\right) \cong v\left(t - \frac{1}{2}\Delta t\right) + \Delta t a(t) \quad (6)$$

Posteriormente, as posições das partículas são calculadas por meio da Equação 7.

$$r(t + \Delta t) \cong r(t) + \Delta t v \left(t + \frac{1}{2} \Delta t \right) \quad (7)$$

Normalmente, a fim de reproduzir a maioria dos experimentos realizados em laboratório, as propriedades termodinâmicas das simulações de DM são extraídas após o equilíbrio do sistema sob temperatura e pressão constantes (BRAUN et al., 2019). Isso geralmente é possível pela utilização de algoritmos conhecidos como termostatos e barostatos, que atuam mantendo os valores médios de temperatura e pressão próximos aos valores estabelecidos no início da simulação.

Para que as equações 1 e 2 sejam resolvidas, as posições e velocidades dos átomos que compõe o sistema também precisam ser definidas. As coordenadas atômicas são definidas antes de iniciar a simulação, e as velocidades iniciais podem ser obtidas pela distribuição gaussiana de Maxwell-Boltzmann, após a minimização de energia do sistema na temperatura desejada (KARPLUS; PETSKO, 1990). O processo de minimização busca encontrar sobre a superfície potencial o mínimo de energia local mais próximo e deve ser realizado para evitar os maus contatos entre os átomos.

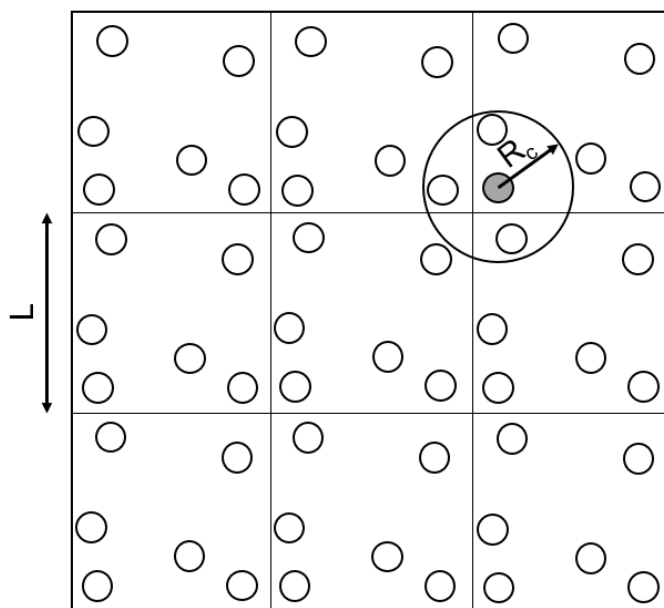
Em alguns casos, um sistema contendo N partículas pode ser simulado isoladamente, ou seja, no vácuo. Contudo, na maioria das vezes, é de interesse determinar as propriedades macroscópicas do sistema, necessitando incluir o efeito do solvente no mesmo. Desse modo, para que o cálculo se torne computacionalmente viável, condições periódicas de contorno devem ser usadas. Então, as partículas são colocadas em uma caixa, que é replicada de forma idêntica infinitamente. Quando uma partícula deixa a caixa original, essa é substituída por outra partícula (em posição oposta na caixa) que tenha a mesma velocidade, permitindo que o sistema continue com o mesmo número de partículas inicialmente estabelecido (HINCHLIFFE, 2005).

A caixa de simulação deve ser escolhida considerando o sistema que será simulado, bem como o custo computacional para executar a simulação. Na maioria das vezes, o soluto e o solvente são colocados em uma caixa cúbica. Esse tipo de caixa é comumente utilizado para solutos que se aproximam do formato esférico. Para solutos com formatos não esféricos, como o DNA, geralmente utiliza-se uma caixa octaédrica truncada (WASSENAAR; MARK, 2006). Devido às diferentes dimensões 3D do DNA,

a utilização de uma caixa cúbica exigiria uma maior demanda computacional. Entretanto, uma caixa com formato retangular também não seria uma boa opção, uma vez que a rotação do DNA levaria à interação com as imagens periódicas.

Por outro lado, uma partícula inserida na caixa de simulação pode interagir consigo mesma por meio de sua imagem, ou interagir mais de uma vez com a partícula vizinha. Para que essas condições sejam evitadas, um raio de corte (R_c) da ordem de $L/2$ ($R_c \leq L/2$, onde L é o menor comprimento da caixa de simulação) deve ser aplicado, principalmente para as interações de curto alcance, uma vez que o potencial de Lennard-Jones se decompõe rapidamente com o aumento da distância entre as partículas. A representação de um raio de corte esférico é dada na (Figura 11). Como pode ser observado na figura, o sistema simulado consiste de um subconjunto dentro de um sistema infinito de pequenos conjuntos idênticos (HINCHLIFFE, 2005).

Figura 11 - Representação do raio de corte para um sistema periódico 2D.



Para as interações eletrostáticas de longo alcance, a imposição de um raio de corte compromete os resultados das simulações, pois ocorre uma descontinuidade entre as forças, uma vez que o potencial eletrostático não decai rapidamente com a distância. Um modelo amplamente utilizado para tratar as interações coulombianas é a soma de Ewald (EWALD, 1921). Esse modelo considera que a interação de uma determinada partícula do sistema ocorre com todas as outras e com todas as caixas replicadas infinitamente.

2.5.2 Campo de força

A função de energia potencial de um sistema molecular é calculada por um potencial total (V_{TOT}), que descreve as forças atuantes sobre cada átomo devido às contribuições dos átomos ligados e não ligados. Geralmente, as interações ligadas são descritas pelos potenciais de estiramento (V_S), angular (V_A) e diédrico (V_D); enquanto que as interações não ligadas podem ser representadas pelos potenciais de Lennard-Jones (V_{LJ}) e de Coulomb (V_C), de acordo com a Equação 8.

$$V_{Total} = V_S + V_A + V_D + V_{LJ} + V_C \quad (8)$$

Os potenciais harmônicos V_S e V_A , referem-se aos valores de energia de estiramentos e deformações angulares, respectivamente, em relação aos valores de equilíbrio. Tais potenciais obedecem à lei de Hooke e podem ser representados pelas Equações 9 e 10.

$$V_S = \sum_{\text{ligação}} k_b (b - b_0)^2 \quad (9)$$

$$V_A = \sum_{\text{ângulo}} k_\theta (\theta - \theta_0)^2 \quad (10)$$

Em que b e θ são os comprimentos e ângulos de ligação, respectivamente; b_0 e θ_0 correspondem aos valores de equilíbrio; k_b e k_θ são as constantes de força.

De modo geral, os valores de k_b são altos, indicando que uma grande quantidade de energia é necessária para esticar ou comprimir uma ligação química (MONTICELLI; TIELEMAN, 2013).

O V_D representa o potencial de energia das moléculas do sistema para uma torção. O valor de energia torcional é usualmente representado por uma por uma função cosseno, como na Equação 11.

$$V_D = \frac{1}{2} \sum_{\text{diédros}} k_\phi [\cos(n\phi - \delta) + 1] \quad (11)$$

Em que k_ϕ corresponde à constante que define a altura da barreira de rotação; n é o número de mínimos; ϕ é o ângulo diedro e δ é o ângulo de fase.

O V_{LJ} e o V_C estão relacionados às interações de van der Waals e eletrostáticas, respectivamente. Esses potenciais podem ser representados pelas Equações 12 e 13.

$$V_{LJ} = \sum_{Lennard-Jones} 4\epsilon_{ij} \left[\frac{\sigma^{12}}{r_{ij}^{12}} - \frac{\sigma^6}{r_{ij}^6} \right] \quad (12)$$

$$V_C = \sum_{Coulomb} \left[\frac{q_i q_j}{4\pi\epsilon_0 r_{ij}} \right] \quad (13)$$

Em que r_{ij} representa a distância entre os átomos i e j ; ϵ corresponde à profundidade do poço de potencial; σ é a distância em que V_{LJ} é zero; q_i e q_j correspondem à carga pontual de cada átomo e ϵ_0 é a permissividade no vácuo.

Ao conjunto dos potenciais e dos parâmetros descritos anteriormente, dá-se o nome de campo de força (do inglês, Force Field (FF)). As funções potenciais anteriormente descritas são representações de um campo de força típico (como AMBER) (CASE et al., 2010), mas termos adicionais podem ser incluídos para representar o potencial total. Como exemplo, pode-se citar potenciais para descrever as interações entre multipolos fixos, entre sítios polarizáveis e, menos frequentemente, potenciais explícitos para ligações de hidrogênio. Esses potenciais adicionais são frequentemente observados em campos de força polarizáveis, como o AMOEBA (PONDER et al., 2010).

2.5.2.1 Parâmetros do campo de força

Como mostrado nas Equações 9, 10 e 11, para descrever as ligações e as interações angulares de um sistema molecular, necessita-se dos valores de equilíbrio e das constantes de força para todas as ligações, ângulos e diedros. Tais valores podem ser obtidos dos campos de força AMBER (WANG et al., 2004), CHARMM (WANG et al., 2006), (JORGENSEN; MAXWELL; TIRADO-RIVES, 1996), OPLS (JORGENSEN; MAXWELL; TIRADO-RIVES, 1996) e GROMOS (OOSTENBRINK et al., 2004), que são comumente utilizados na simulação de biomoléculas. Além disso, os valores de

equilíbrio também podem ser obtidos de cálculos teóricos e dados experimentais (como as estruturas de raio-X e Ressonância Magnética Nuclear (RMN)).

A utilização dos campos de força gerais para descrever diferentes ligantes como inibidores, substratos, cofatores e pequenas moléculas com potencial farmacológico nem sempre é suficiente para a obtenção de resultados precisos. Uma simulação de DM, contendo moléculas altamente conjugadas descritas com parâmetros dos campos de força gerais, poderá reproduzir incorretamente seus modos de vibração, resultando em estruturas não físicas (PRANDI et al., 2016).

Embora estejam disponíveis na literatura outras formas de se obter as constantes de força e os valores de equilíbrio, como as ferramentas automáticas de parametrização (NORRBY; LILJEFORS, 1998; SEMINARIO, 1996; STROET et al., 2018; WANG et al., 2006), os parâmetros são escassos, pois dificilmente incorporam a modelagem de centros metálicos. Dados experimentais (obtidos, por exemplo de espectros de infravermelho (IV) e Raman) também podem ser utilizados para obtenção das constantes de força. No entanto, geralmente os experimentos são realizados em fase condensada e as energias associadas as deformações do sistema podem ter contribuições vibracionais e entrópicas (NORRBY; BRANDT, 2001). Então, esses dados devem ser corrigidos para descrever as frequências vibracionais do sistema molecular.

Em sistemas contendo metais de transição, a falta de parâmetros para descrever esses elementos consiste em uma das maiores limitações em aplicar a técnica de DM. Ao contrário dos elementos do bloco *s* e *p*, os metais de transição possuem orbitais *d* e *f* em sua camada de valência, que estão envolvidos na formação e quebra de ligações. Além disso, esses elementos possuem uma variedade estados de oxidação de números de coordenação, podendo formar sistemas altamente carregados, que devem ser descritos com precisão nas simulações. Dessa forma, os cálculos quânticos *ab initio* constituem a principal forma de se obter parâmetros (GONZÁLEZ, 2011; LI; MERZ JR, 2017).

3 OBJETIVOS

Este trabalho foi realizado com os seguintes objetivos: 1) Desenvolver um novo conjunto de parâmetros de campo de força AMBER, com base nos cálculos da teoria do funcional de densidade (DFT), para um complexo de platina (II) (*cis*-dicloro(2-piridilmetil)aminoplatina (II) ligado ao derivado 2-(4'-amino2'-hidroxifenil)benzotiazol

(AHBT)); 2) Validar os parâmetros comparando resultados de simulação de Dinâmica Molecular (DM) com uma referência quântica; 3) Aplicar o conjunto de parâmetros desenvolvidos em simulações de DM, a fim de avaliar os modos de interação do complexo com o DNA de forma covalente e não-covalente.

4 CONCLUSÃO

De acordo com a revisão da literatura, pode-se dizer que os complexos metálicos desempenham um importante papel na medicina, especialmente no planejamento de potenciais agentes terapêuticos para o tratamento do câncer. Entretanto, os dados mais recentes mostram que os únicos fármacos à base de metal aprovados para uso clínico têm como constituinte principal a Pt. No que diz respeito ao planejamento de novos compostos de Pt, mas com atividades melhoradas frente aos fármacos atuais, as simulações no computador, especialmente as simulações de DM, são ferramentas valiosas para entender o sistema em nível molecular. Logo, em decorrência da falta de parâmetros ou imprecisão dos mesmos na descrição de sistemas contendo metalodrogas ou moléculas altamente conjugadas, novos parâmetros precisam ser desenvolvidos.

5 REFERÊNCIAS

- AHMAD, S. Kinetic aspects of platinum anticancer agents. **Polyhedron**, v. 138, p. 109–124, 2017.
- ALMAQWASHI, A. A. et al. Mechanisms of small molecule–DNA interactions probed by single-molecule force spectroscopy. **Nucleic acids research**, v. 44, n. 9, p. 3971–3988, 2016.
- ALOTAIBI, S. H.; MOMEN, A. A. Anticancer Drugs' Deoxyribonucleic Acid (DNA) Interactions. In: **Biophysical Chemistry**. IntechOpen, 2019.
- ARMSTRONG-GORDON, E. et al. Patterns of platinum drug use in an acute care setting: a retrospective study. **Journal of cancer research and clinical oncology**, v. 144, n. 8, p. 1561–1568, 2018.
- BANCROFT, D. P.; LEPRE, C. A.; LIPPARD, S. J. Platinum-195 NMR kinetic and mechanistic studies of cis- and trans-diamminedichloroplatinum (II) binding to DNA. **Journal of the American Chemical Society**, v. 112, n. 19, p. 6860–6871, 1990.
- BERGAMO, A.; DYSON, P. J.; SAVA, G. The mechanism of tumour cell death by metal-based anticancer drugs is not only a matter of DNA interactions. **Coordination Chemistry Reviews**, v. 360, p. 17–33, 2018.

BOND, P. J. et al. X-ray fiber diffraction evidence for neighbor exclusion binding of a platinum metallointercalation reagent to DNA. **Proceedings of the National Academy of Sciences**, v. 72, n. 12, p. 4825–4829, 1975.

BONDI, R. et al. DNA interaction of a fluorescent, cytotoxic pyridinimino platinum (II) complex. **Journal of inorganic biochemistry**, v. 202, p. 110874, 2020.

BRAUN, E. et al. Best practices for foundations in molecular simulations. **Living journal of computational molecular science**, v. 1, n. 1, 2019.

BRUNO, P. M. et al. A subset of platinum-containing chemotherapeutic agents kills cells by inducing ribosome biogenesis stress. **Nature medicine**, v. 23, n. 4, p. 461, 2017.

CASE, D. A. et al. AMBER 12; University of California: San Francisco, 2012. **There is no corresponding record for this reference**, p. 1–826, 2010.

CHATLAS, J.; VAN ELDIK, R.; KEPPLER, B. K. Spontaneous aquation reactions of a promising tumor inhibitor trans-imidazolium-tetrachlorobis (imidazole) ruthenium (III), trans-HIm [RuCl₄ (Im)₂]. **Inorganica chimica acta**, v. 233, n. 1–2, p. 59–63, 1995.

CHEFF, D. M.; HALL, M. D. A Drug of Such Damned Nature. 1 Challenges and Opportunities in Translational Platinum Drug Research: Miniperspective. **Journal of medicinal chemistry**, v. 60, n. 11, p. 4517–4532, 2017.

CHEN, Z. et al. Fluorescence imaging of a new monofunctional platinum (II) complex containing a thioflavin-T (ThT)-based fluorophore. **New Journal of Chemistry**, v. 39, n. 3, p. 1592–1596, 2015.

COLE, D. J. et al. **The future of force fields in computer-aided drug design**. Future Science, , 2019.

DA SILVA MAIA, P. I.; DEFLON, V. M.; ABRAM, U. Gold (III) complexes in medicinal chemistry. **Future medicinal chemistry**, v. 6, n. 13, p. 1515–1536, 2014.

DASARI, S.; TCHOUNWOU, P. B. Cisplatin in cancer therapy: molecular mechanisms of action. **European journal of pharmacology**, v. 740, p. 364–378, 2014.

DE CÓZAR, A. et al. New insights into the reactivity of cisplatin with free and restrained nucleophiles: Microsolvation effects and base selectivity in cisplatin–dna interactions. **ChemPhysChem**, v. 17, n. 23, p. 3932–3947, 2016.

DE VIVO, M. et al. Role of molecular dynamics and related methods in drug discovery. **Journal of medicinal chemistry**, v. 59, n. 9, p. 4035–4061, 2016.

DEO, K. M. et al. Platinum coordination compounds with potent anticancer activity. **Coordination Chemistry Reviews**, v. 375, p. 148–163, 2018.

DURRANT, J. D.; MCCAMMON, J. A. Molecular dynamics simulations and drug

discovery. **BMC biology**, v. 9, n. 1, p. 71, 2011.

EWALD, P. P. The calculation of optical and electrostatic grid potential. **Ann. Phys.**, v. 64, n. 3, p. 253–287, 1921.

FENG, B. et al. Hydrophobic catalysis and a potential biological role of DNA unstacking induced by environment effects. **Proceedings of the National Academy of Sciences**, v. 116, n. 35, p. 17169–17174, 2019.

FRENKEL, D.; SMIT, B. **Understanding molecular simulation: from algorithms to applications**. Elsevier, v. 1, 2001.

GALINDO-MURILLO, R. et al. Intercalation processes of copper complexes in DNA. **Nucleic acids research**, v. 43, n. 11, p. 5364–5376, 2015.

GILL, R. K.; RAWAL, R. K.; BARIWAL, J. Recent advances in the chemistry and biology of benzothiazoles. **Archiv der Pharmazie**, v. 348, n. 3, p. 155–178, 2015.

GONZÁLEZ, M. A. Force fields and molecular dynamics simulations. **École thématique de la Société Française de la Neutronique**, v. 12, p. 169–200, 2011.

GRAHAM, J.; MUHSIN, M.; KIRKPATRICK, P. **Oxaliplatin**. Nature Publishing Group, 2004.

HARTINGER, C. G. et al. KP1019, a new redox-active anticancer agent—Preclinical development and results of a clinical phase I study in tumor patients. **Chemistry & biodiversity**, v. 5, n. 10, p. 2140–2155, 2008.

HINCHLIFFE, A. **Molecular modelling for beginners**. John Wiley & Sons, 2005.

HOCKNEY, R. W. **POTENTIAL CALCULATION AND SOME APPLICATIONS**. Langley Research Center, Hampton, v. 9, p. 136, 1970.

HOWLADER, N. et al. **SEER Cancer Statistics Review, 1975–2009**. Bethesda, MD: National Cancer Institute; 2012.

IRFAN, A. et al. Benzothiazole derivatives as anticancer agents. **Journal of Enzyme Inhibition and Medicinal Chemistry**, v. 35, n. 1, p. 265–279, 2020.

JAIN, S. et al. Anticancer Potential of Thiazole Derivatives: A Retrospective Review. **Mini reviews in medicinal chemistry**, v. 18, n. 8, p. 640–655, 2018.

JALILI, S.; MADDAH, M. Molecular dynamics simulation of the sliding of distamycin anticancer drug along DNA: interactions and sequence selectivity. **Journal of the Iranian Chemical Society**, v. 14, n. 3, p. 531–540, 2017.

JOHNSTONE, T. C.; SUNTHARALINGAM, K.; LIPPARD, S. J. The next generation of platinum drugs: targeted Pt (II) agents, nanoparticle delivery, and Pt (IV) prodrugs. **Chemical reviews**, v. 116, n. 5, p. 3436–3486, 2016.

JORGENSEN, W. L.; MAXWELL, D. S.; TIRADO-RIVES, J. Development and testing of the OPLS all-atom force field on conformational energetics and properties of organic liquids. **Journal of the American Chemical Society**, v. 118, n. 45, p. 11225–11236, 1996.

KAMAL, A. et al. Synthesis, DNA-binding ability and anticancer activity of benzothiazole/benzoxazole–pyrrolo [2, 1-c][1, 4] benzodiazepine conjugates. **Bioorganic & medicinal chemistry**, v. 18, n. 13, p. 4747–4761, 2010.

KARPLUS, M.; PETSKO, G. A. Molecular dynamics simulations in biology. **Nature**, v. 347, n. 6294, p. 631, 1990.

KELLAND, L. The resurgence of platinum-based cancer chemotherapy. **Nature Reviews Cancer**, v. 7, n. 8, p. 573, 2007.

KELLETT, A. et al. Molecular methods for assessment of non-covalent metallodrug–DNA interactions. **Chemical Society Reviews**, v. 48, n. 4, p. 971–988, 2019.

KENNY, R. G.; MARMION, C. J. Toward Multi-Targeted Platinum and Ruthenium Drugs—A New Paradigm in Cancer Drug Treatment Regimens? **Chemical reviews**, v. 119, n. 2, p. 1058–1137, 2019.

KERI, R. S. et al. A comprehensive review in current developments of benzothiazole-based molecules in medicinal chemistry. **European journal of medicinal chemistry**, v. 89, p. 207–251, 2015.

KIM, D.-K. et al. Antitumor activity of cis-malonato [(4R, 5R)-4, 5-bis (aminomethyl)-2-isopropyl-1, 3-dioxolane]platinum (II), a new platinum analogue, as an anticancer agent. **Cancer chemotherapy and pharmacology**, v. 35, n. 5, p. 441–445, 1995.

KIRCHMAIR, J. et al. Predicting drug metabolism: experiment and/or computation? **Nature reviews Drug discovery**, v. 14, n. 6, p. 387, 2015.

KONKANKIT, C. C. et al. Anticancer activity of complexes of the third row transition metals, rhenium, osmium, and iridium. **Dalton Transactions**, v. 47, n. 30, p. 9934–9974, 2018.

LEIJEN, S. et al. Phase I/II study with ruthenium compound NAMI-A and gemcitabine in patients with non-small cell lung cancer after first line therapy. **Investigational new drugs**, v. 33, n. 1, p. 201–214, 2015.

LI, P.; MERZ JR, K. M. Metal ion modeling using classical mechanics. **Chemical reviews**, v. 117, n. 3, p. 1564–1686, 2017.

LIU, X. et al. Molecular dynamics simulations and novel drug discovery. **Expert opinion on drug discovery**, v. 13, n. 1, p. 23–37, 2018.

LOPES, J. F. et al. Monte Carlo simulation of cisplatin molecule in aqueous solution. **The Journal of Physical Chemistry B**, v. 110, n. 24, p. 12047–12054, 2006.

MANCINI, D. T. et al. Excited-State Proton Transfer Can Tune the Color of Protein Fluorescent Markers. **ChemPhysChem**, v. 16, n. 16, p. 3444–3449, 2015.

MAVROIDI, B. et al. Palladium (II) and platinum (II) complexes of derivatives of 2-(4'-aminophenyl) benzothiazole as potential anticancer agents. **Inorganica Chimica Acta**, v. 444, p. 63–75, 2016.

MCGIVERN, T. J. P.; AFSHARPOUR, S.; MARMION, C. J. Copper complexes as artificial dna metallonucleases: from sigman's reagent to next generation anti-cancer agent? **Inorganica Chimica Acta**, v. 472, p. 12–39, 2018.

MEDICI, S. et al. Noble metals in medicine: Latest advances. **Coordination Chemistry Reviews**, v. 284, p. 329–350, 2015.

MEJIA, C.; RUIZ-AZUARA, L. Casiopeinas IIgly and IIIa induce apoptosis in medulloblastoma cells. **Pathology & Oncology Research**, v. 14, n. 4, p. 467–472, 2008.

MONTICELLI, L.; TIELEMAN, D. P. Force fields for classical molecular dynamics. In: **Biomolecular simulations**. Springer, 2013. p. 197–213.

MUKHERJEE, S. et al. In vitro model reaction of sulfur containing bio-relevant ligands with Pt (II) complex: kinetics, mechanism, bioactivity and computational studies. **RSC Advances**, v. 5, n. 94, p. 76987–76999, 2015.

MUKHERJEE, S. et al. An experimental and theoretical approach on the kinetics and mechanism for the formation of a four-membered (S, S) chelated Pt (II) complex. **RSC Advances**, v. 6, n. 22, p. 18288–18299, 2016.

NAIR, P. C.; MINERS, J. O. Molecular dynamics simulations: from structure function relationships to drug discovery. **In silico pharmacology**, v. 2, n. 1, p. 4, 2014.

NDAGI, U.; MHLONGO, N.; SOLIMAN, M. E. Metal complexes in cancer therapy—an update from drug design perspective. **Drug design, development and therapy**, v. 11, p. 599, 2017.

NORRBY, P.-O.; BRANDT, P. Deriving force field parameters for coordination complexes. **Coordination Chemistry Reviews**, v. 212, n. 1, p. 79–109, 2001.

NORRBY, P.; LILJEFORS, T. Automated molecular mechanics parameterization with simultaneous utilization of experimental and quantum mechanical data. **Journal of computational chemistry**, v. 19, n. 10, p. 1146–1166, 1998.

OOSTENBRINK, C. et al. A biomolecular force field based on the free enthalpy of hydration and solvation: the GROMOS force-field parameter sets 53A5 and 53A6. **Journal of computational chemistry**, v. 25, n. 13, p. 1656–1676, 2004.

PAULA, Q. A. DE et al. EPR and electrochemistry of [NH₄] trans-[RuCl₄ (DMSO)(L)] complexes (L= DMSO, py). X-ray molecular structure of [pyH][RuCl₄ (DMSO)(py)]. **Journal of the Brazilian Chemical Society**, v. 11, n. 5, p. 530–536, 2000.

PAYOLLA, F. B.; MASSABNI, A. C.; ORVIG, C. Radiopharmaceuticals for diagnosis in nuclear medicine: a short review. **Eclética Química Journal**, v. 44, n. 3, p. 11–19, 2019.

PONDER, J. W. et al. Current status of the AMOEBA polarizable force field. **The journal of physical chemistry B**, v. 114, n. 8, p. 2549–2564, 2010.

PORCHIA, M. et al. New insights in Au-NHCs complexes as anticancer agents. **European journal of medicinal chemistry**, 2018.

PRANDI, I. G. et al. Combining classical molecular dynamics and quantum mechanical methods for the description of electronic excitations: The case of carotenoids. **Journal of computational chemistry**, v. 37, n. 11, p. 981–991, 2016.

PRICKER, S. P. Medical uses of gold compounds: past, present and future. **Gold bulletin**, v. 29, n. 2, p. 53–60, 1996.

QUEIROZ, S. L.; BATISTA, A. A. Complexos fosfínicos e suas aplicações na medicina. **Química Nova**, p. 651–659, 1996.

RÉBÉ, C. et al. Platinum Derivatives Effects on Anticancer Immune Response. **Biomolecules**, v. 10, n. 1, p. 13, 2020.

ROCHA, E. P.; RAMALHO, T. C. Probing the ESIPT process in 2-amino-1, 4-naphthoquinone: thermodynamics properties, solvent effect and chemometric analysis. **Theoretical Chemistry Accounts**, v. 135, n. 2, p. 39, 2016.

RODRIGUEZ, R. et al. **Visual detection of platinated dna lesions from a clickable cisplatin probe used as diagnostic tool or to identify synergistic treatments**. Google Patents, , 13 dez. 2018.

ROSA, N. M. P. et al. TriplatinNC and Biomolecules: building models based on non-covalent interactions. **Frontiers in Chemistry**, v. 7, p. 307, 2019.

ROSENBERG, B.; VAN CAMP, L.; KRIGAS, T. Inhibition of cell division in Escherichia coli by electrolysis products from a platinum electrode. **Nature**, v. 205, n. 4972, p. 698, 1965.

SCHEEFF, E. D.; BRIGGS, J. M.; HOWELL, S. B. Molecular modeling of the intrastrand guanine-guanine DNA adducts produced by cisplatin and oxaliplatin. **Molecular Pharmacology**, v. 56, n. 3, p. 633–643, 1999.

SCHOBERT, R.; BIERSACK, B. cis-Dichloroplatinum (II) complexes with aminomethylnicotinate and-isonicotinate ligands. **Inorganica chimica acta**, v. 358, n. 12, p. 3369–3376, 2005.

SEDGWICK, A. C. et al. Excited-state intramolecular proton-transfer (ESIPT) based fluorescence sensors and imaging agents. **Chemical Society Reviews**, v. 47, n. 23, p. 8842–8880, 2018.

SEMINARIO, J. M. Calculation of intramolecular force fields from second-derivative tensors. **International journal of quantum chemistry**, v. 60, n. 7, p. 1271–1277, 1996.

SHI, D.-F. et al. Antitumor benzothiazoles. 3. Synthesis of 2-(4-aminophenyl) benzothiazoles and evaluation of their activities against breast cancer cell lines in vitro and in vivo. **Journal of medicinal chemistry**, v. 39, n. 17, p. 3375–3384, 1996.

SIEGEL, R. L.; MILLER, K. D.; JEMAL, A. Cancer statistics, 2018. **CA: a cancer journal for clinicians**, v. 68, n. 1, p. 7–30, jan. 2018.

SIMPSON, P. V et al. Metal-based antitumor compounds: beyond cisplatin. **Future medicinal chemistry**, v. 11, n. 2, p. 119–135, 2019.

SIRAJUDDIN, M.; ALI, S.; BADSHAH, A. Drug–DNA interactions and their study by UV–Visible, fluorescence spectroscopies and cyclic voltametry. **Journal of Photochemistry and Photobiology B: Biology**, v. 124, p. 1–19, 2013.

STROET, M. et al. Automated Topology Builder Version 3.0: Prediction of Solvation Free Enthalpies in Water and Hexane. **Journal of chemical theory and computation**, v. 14, n. 11, p. 5834–5845, 2018.

SUNTHARALINGAM, K. et al. A platinum complex that binds non-covalently to DNA and induces cell death via a different mechanism than cisplatin. **Metallomics**, v. 5, n. 5, p. 514–523, 2013.

TANAKA, K. et al. Development of Miriplatin, a Novel Antitumor Platinum for Hepatocellular Carcinoma. **R&D Report, Sumitomo Kagaku**, v. 2011, 2011.

TZANOPOULOU, S. et al. Evaluation of Re and ^{99m}Tc complexes of 2-(4'-aminophenyl) benzothiazole as potential breast cancer radiopharmaceuticals. **Journal of medicinal chemistry**, v. 53, n. 12, p. 4633–4641, 2010.

UM, I. S. et al. Platinum drugs in the Australian cancer chemotherapy healthcare setting: Is it worthwhile for chemists to continue to develop platinum? **Inorganica Chimica Acta**, v. 492, p. 177–181, 2019.

VERLET, L. Computer" experiments" on classical fluids. I. Thermodynamical properties of Lennard-Jones molecules. **Physical review**, v. 159, n. 1, p. 98, 1967.

VONGSUTILERS, V.; GANNETT, P. M. C8-Guanine modifications: Effect on Z-DNA formation and its role in cancer. **Organic & biomolecular chemistry**, v. 16, n. 13, p. 2198–2209, 2018.

WANG, J. et al. Development and testing of a general amber force field. **Journal of computational chemistry**, v. 25, n. 9, p. 1157–1174, 2004.

WANG, J. et al. Automatic atom type and bond type perception in molecular mechanical calculations. **Journal of molecular graphics and modelling**, v. 25, n. 2, p. 247–260, 2006.

WASSENAAR, T. A.; MARK, A. E. The effect of box shape on the dynamic properties of proteins simulated under periodic boundary conditions. **Journal of computational chemistry**, v. 27, n. 3, p. 316–325, 2006.

WELINK, J. et al. Pharmacokinetics and pharmacodynamics of lobaplatin (D-19466) in patients with advanced solid tumors, including patients with impaired renal or liver function. **Clinical cancer research**, v. 5, n. 9, p. 2349–2358, 1999.

WELLER, A. Innermolekularer protonenübergang im angeregten zustand. **Zeitschrift für Elektrochemie, Berichte der Bunsengesellschaft für physikalische Chemie**, v. 60, n. 9-10, p. 1144–1147, 1956.

WHEATE, N. J. et al. The status of platinum anticancer drugs in the clinic and in clinical trials. **Dalton transactions**, v. 39, n. 35, p. 8113–8127, 2010.

YANG, Y.; ZHAO, J.; LI, Y. Theoretical study of the ESIPT process for a new natural product quercetin. **Scientific reports**, v. 6, p. 32152, 2016.

YAO, S.; PLASTARAS, J. P.; MARZILLI, L. G. A molecular mechanics AMBER-type force field for modeling platinum complexes of guanine derivatives. **Inorganic chemistry**, v. 33, n. 26, p. 6061–6077, 1994.

YEO, C.; OOI, K.; TIEKINK, E. Gold-based medicine: A paradigm shift in anti-cancer therapy? **Molecules**, v. 23, n. 6, p. 1410, 2018.

ZORODDU, M. A. et al. The essential metals for humans: a brief overview. **Journal of inorganic biochemistry**, v. 195, p. 120-129, 2019.

SEGUNDA PARTE - ARTIGO

Parameterization, validation and application of
a new force field for Pt (II) complexes of 2-(4'-
amino-2'-hydroxyphenyl)benzothiazole:
exploring new anticancer drugs

Ander F. Pereira^{1}, Ingrid G. Prandi^{1,2*}, Teodorico de C. Ramalho^{1,3*}*

¹Laboratory of Molecular Modelling, Department of Chemistry, Federal University of Lavras, Lavras/MG, 37200000, Brazil.

²Faculdade de Física-ICEN, Universidade Federal do Pará, C.P. 479, 66075-110 Belém, PA, Brazil.

³Department of Chemistry, Faculty of Science, University of Hradec Kralove, Hradec Kralove, Czech Republic.

Corresponding Author:

Ander F. Pereira, e-mail: ander.francisco@hotmail.com, Tel: +55 35 999655673

Ingrid G. Prandi, e-mail: ingrid.prandi@gmail.com, Tel: +39 38 85759266

Teodorico de C. Ramalho, e-mail: teo@ufla.br, Tel: +55 35 38291155

Abstract

Understanding the ways of interaction of a drug with a biological target is crucial for the planning of new prototypes. One methodology that allows the simulation of new drugs under *in vivo* conditions is the classical molecular dynamics (MD). However, molecular dynamics simulations in systems containing metallodrugs and/or very conjugated molecules are challenging due to the lack amount of parameters to describe them properly. Under these conditions, unfortunately, many molecular scientists opt to use a general force field for the ligand, obtaining, in some cases, non-reliable results. In this sense, we developed and validated a new set of AMBER force field parameters, based on density functional theory (DFT) calculations, for a possible anticancer platinum (II) complex: *cis*-dichloro(2-aminomethylpyridine)platinum (II) bonded to 2-(4'-amino-2'-hydroxyphenyl)benzothiazole (AHBT). In order to clarify some disagreements in the literature about the existence or not of a chemical bond between the Pt complex and DNA, the developed model was applied in two MD simulations: of the Pt complex bonded with the DNA and a non-bonded system. The parameterization validation shows that the new model adequately describes the structural properties of the complex, being in very good agreement with the quantum structure. In addition, the simulation results reveal a high affinity between the DNA minor groove and the studied metallic complex. When coordinated, it induces conformational changes in the DNA structure. Overall, we expect this work to contribute significantly to future MD simulations of Pt complexes in biological targets, still not well explored mainly due to the few parameters for the metal found in the literature.

Introduction

The serendipitous discovery of the anticancer properties of the *cis*-dichlorodiammineplatinum (II) (Cisplatin) compound by Rosenberg et al. in the '60s¹ represented a milestone in the history of Inorganic Medicinal Chemistry. The first successful case of the use of this compound against cancer cells was the treatment of testicular cancer, achieving a survival rate of 95%.² Unfortunately, following the approval of Cisplatin in the pharmaceutical market for global use in 1978, many serious side effects were attributed to the compound mainly due to the lack of selectivity between tumors and healthy cells.³

Since then, thousands of metal compounds have been synthesized to bypass the toxic effects of Cisplatin in the organism, most of them are platinum-based drugs. Thus, it is known that to design more effective new drugs it is fundamental to study the interaction of the compound with possible biological targets. The scientific community most accepted mechanism of action of Cisplatin is the covalent attachments of the platinum cation to the guanine bases nitrogen of the deoxyribonucleic acid, which are the most nucleophilic atoms of DNA.⁴ However, the interaction of other platinum complexes with phosphate groups, as the intercalation and interaction with major and minor grooves of the DNA, may also be responsible for the cytotoxic effects.^{5,6}

In this context, the Molecular Dynamics (MD) simulation reveals to be a very promising computational method in the determination of structural properties and thermodynamic parameters of molecular systems.⁷ One of the greatest challenges in using this technique to study the interaction modes of a ligand with its biological target is to find an appropriate force field model for MD simulations.⁸ Although some automatic parameterization tools are available in the literature, it should be kept in mind that the parameters are scarce (especially for metal centers) and can not be reliable.⁹⁻¹¹ In addition, highly conjugated molecules described by general force fields may incorrectly reproduce its conformations and vibration modes, resulting in non-physical structures.¹²

In 1994, Yao et al. developed, by statistical analysis, a force field for the Cisplatin molecule, inferring the stretching and angle parameters,¹³ which were refined later by Scheeff and colleagues.¹⁴ After these works, a new methodology of parameterization for platinum coordination compounds was developed based on quantum dynamics (QD) simulations.¹⁵ In the literature is also possible to find some

other strategies of parameterization for OPLA-SS2¹⁶ and POSSIM¹⁷ force fields.¹⁸ However, the lack of parameters to describe platinum complexes in MD simulations remains a major challenge especially because, in many cases, the parameters cannot be transferable from one force field format to another.

In the present work, we have developed and validated a new set of intramolecular AMBER force field parameters, based on density functional theory (DFT) calculations, for a platinum (II) complex (*cis*-dichloro(2-aminomethylpyridine)platinum (II) bonded to 2-(4'-amino-2'-hydroxyphenyl)benzothiazole (AHBT)) derivative (Figure 1). We propose this complex based on the photophysical^{19,20} and the therapeutic properties of AHBT together with the cytotoxicity of the metal center.²¹

The developed model was validated comparing MD simulations and theoretical infrared (IR) calculations results to a QM reference. Subsequently, the new set of parameters was used to study the modes of the complex interaction with the DNA in a covalent and non-covalent way. Previous *in vitro* studies performed in complexes with very similar structural characteristics to the proposed complex in this work have shown that: (i) the complexes enter into cells intact;^{21,22} (ii) the complexes exhibit cytotoxicity against tumor cells.^{21,23} However, there are still disagreements about the mechanisms responsible for the cytotoxicity of the compound. Some studies believe that the complex binds to the N7 of the guanine bases of DNA^{21,23–25}; while others are betting on non-covalent interaction with a minor groove of DNA.^{5,21,23,26,27}

We believe that the new set of parameters developed can be used in future MD simulations of platinum (II) complexes with biological targets, which is little explored due to the lack of specific parameters for this metal.

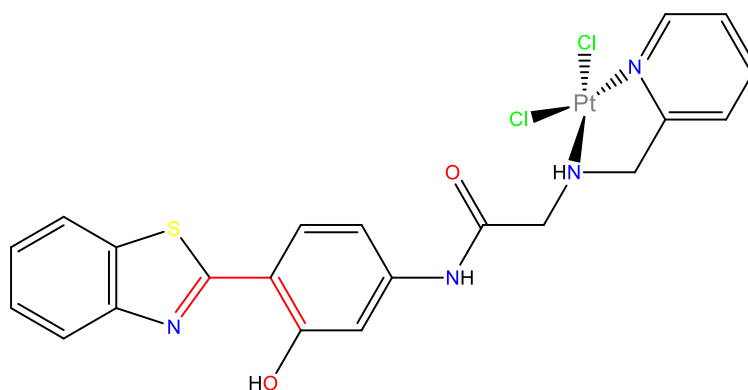


Figure 1. Structural projection of the *cis*-dichloro(2-aminomethylpyridine)platinum (II) bonded to 2-(4'-amino-2'-hydroxyphenyl)benzothiazole (AHBT).

QM calculations

The platinum (II) compound of this study is a large conjugated complex with some free rotation points. It is of paramount importance that before starting the parameterization of a molecule, the global minimum structure be adopted as reference. From the lowest energy conformation, the equilibrium values and force constants - necessary to describe bonded terms like stretching, angular and dihedral modes, are obtained. Therefore, in the absence of a well-defined reference starting geometry, the resulting conformations from the molecular dynamics (MD) simulation will not match the real geometries and may present non-physical results. Secondly, if it is necessary to perform highly geometry-dependent property calculations from the extracted MD snapshots (such as electronic properties through quantum calculations) and these geometries are non-physical, the error propagation may lead to unrealistic final results.

Thus, in order to do a screening to find the complex conformation with the global minimum energy, a conformational search with the theory level PM6 was carried out in the Spartan '14 V1.1.4 software.²⁸ From this conformational search, eight local minimum conformations were obtained (Supporting Information, Section S1 (Figure S1.1)). Then, the lowest energy conformation was adopted for a more precise analysis of the dihedral highlighted in red (Figure 1) by means of a relaxed Potential Energy Surface (PES) scan. The PES calculations were performed with the Gaussian software.²⁹

The torsion of this dihedral leads to both planar and non-planar conformations, which may contribute to different levels of interactions with the DNA. More precisely, the interplay between planar molecules and the DNA grooves, may occur easily either by intercalation or interaction if compared with a non-planar molecule. In order to further investigate the stability of the complex conformations, the rotation of the dihedral highlighted in red (Figure 1) was performed. This scan was performed in vacuum by a 36 steps torsion of 10° each. The B3LYP functional was adopted and the basis set LANL2DZ ECP (effective core potential) was employed for the platinum atom and Def2-TZVPP,³⁰ for the other atoms. The level of theory used to describe the platinum (II) complex was chosen considering the low computational time to perform the calculations as well as the good accuracy in the results, already reported in the literature.³¹⁻³⁴ In addition, a previous study of optimization of this complex with more accurate calculation methods does not yield significantly better results (Supporting Information, Section S1 (Figure S1.2)).

Atom types in the parameters file

Most general force fields are made up of a limited set of atomic parameters, which allows the simulation of secondary compounds or molecules that are not significantly affected by structural deformations. However, the accuracy of these parameters decreases when they are used for critical descriptions in which the properties of interest do not resemble the properties of the compounds that were parameterized directly.

The automatic tools, available in websites, are usually able to model molecules of interest with more accuracy than the general force fields.^{9-11,35} Despite of the simplicity of the automatic tools, such methodologies are not applicable to describe all types of molecules, either because of lack of parameters or accuracy in results. It is important to stress the fact that an MD simulation involving highly conjugated molecules, for example, described by these non-specific parameters, may incorrectly reproduce their vibration modes, resulting in non-physical structures.¹² In our case, the ligand of the complex is, indeed, a molecule that contains a conjugated chain. In addition, there are not sufficient parameters in the literature to describe the coordination center of the *cis*-dichloro(2-aminomethylpyridine)platinum (II) bonded to 2-(4'-aminophenyl-2'-hydroxyphenyl)benzothiazole derivative. Therefore, for a precise model, it is necessary to develop our own set of parameters.

The first step to develop parameters that accurately describe the structural properties of the cited complex is to identify and label each atom of the structure as atom types (Figure 2). Since in MD simulations the electrons are directly neglected, this procedure is extremely important to obtain unique parameters for each interaction described by the force field and to recover some of the electronic effect lost in a classic simulation. In a more chemical view, if the atoms of the model were distinguished only by their atomic number, i.e., without taking into account their chemical environment, there would be a precision reduction of the structural and vibrational characteristics of the system. This discussion shows the importance of adopting different types of atomic particles for the same element, so that the intrinsic properties of chemically different atoms can be explored.

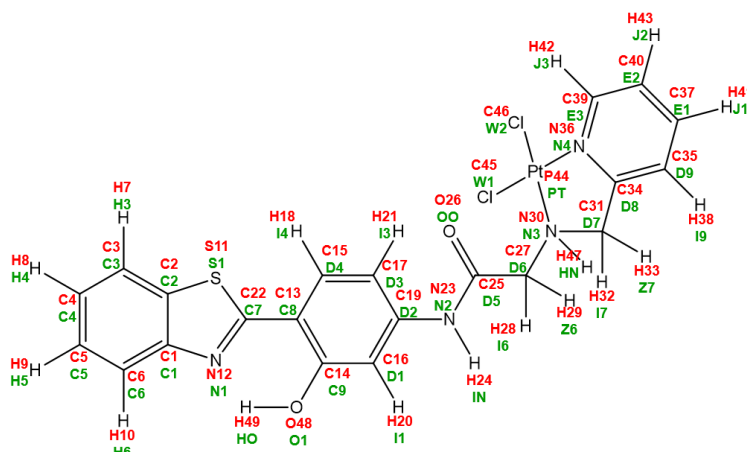


Figure 2. Atom names (in red) and atom types (in green).

The atoms types have been assigned with the assistance of VMD software.³⁶ Since the AMBER simulation package allows atoms to be identified with only two characters, letters and numbers were used in order to increase the number of types of each element of the structure.

Development of AMBER force field parameters

After the conformational search, the structure with the global energy minimum was adopted for the development of the parameters. AMBER total potential function (V_{total}), which describes the molecular system, is defined by means of the sum of bonded (bond, angles and dihedrals) and non-bonded (Coulomb and Lennard-Jones) terms, as is described by Equation 1.

$$\begin{aligned}
 V_{total} &= V_{bond} + V_{angle} + V_{dihe} + V_{Coulomb} + V_{Lennard-Jones} \\
 &= \sum_{bonds} k_b (b - b_0)^2 + \sum_{angles} k_\theta (\theta - \theta_0)^2 \\
 &+ \sum_{dihedrals} k_\phi [\cos(n\phi - \delta) + 1] + \sum_{Coulomb} \left[\frac{q_i q_j}{4\pi\epsilon_0 r_{ij}} \right] \\
 &+ \sum_{Lennard-Jones} 4\epsilon_{ij} \left[\frac{\sigma_{ij}^{12}}{r_{ij}^{12}} - \frac{\sigma_{ij}^6}{r_{ij}^6} \right] \quad (1)
 \end{aligned}$$

Where k_b and k_θ are the force constants to restore the bond lengths and angle to the equilibrium values; k_ϕ is the force constant that defines the height of the dihedral

rotation barrier; b_0 and θ_0 are the equilibrium values; n is the number of the minimums; ϕ is the dihedral angle; δ is the phase angle; r_{ij} is the distance between the atoms i and j ; ϵ is the depth of the potential well; σ is the distance at which the Lennard-Jones Potential ($V_{Lennard-Jones}$) is zero; q_i and q_j are the point charge of each atom and ϵ_0 is the permittivity in vacuum.

The values of the force constants for the bonded terms were obtained from the global minimum geometry by the diagonalization of the Hessian matrix, using the plugin called Paratool³⁷ available in the VMD software.³⁶ In this procedure, the eigenvalues were extracted from the quantum calculation of the Hessian matrix, obtaining the force constants for different internal coordinates (ICs). The Paratool plugin calculates the parameters by converting all values of the Hessian matrix, calculated in internal coordinates, into kcal mol⁻¹, Å and degrees.

The Coulomb interaction parameters were obtained by non-polarizable RESP (Restrained Electrostatic Potential) atomic charges.³⁸ Finally, the Lennard-Jones parameters for all atoms but the platinum were assigned according to GAFF values.³⁹ In the AMBER, the differentiation between intra and intermolecular parameters for charges and van der Waals is not foreseen. So, in order not to change the well-established intermolecular parameters, we could not modify the intramolecular parameters. For the platinum atom, the values of σ and ϵ found by Lopes and collaborators (2006) were attributed.⁴⁰ For the calculations of the Hessian matrix and the atomic charges, we adopted the same functional and basis set used in the optimization calculations. The final parameters set identified by the types in Figure 2 can be found in the Supporting Information, Section S2.

Validation of the force fields

After obtaining the set of parameters, an MD simulation was performed in order to validate the proposed force field. Firstly, the complex was minimized classically and then simulated in vacuum with a time-step of 1 fs using the AMBER11 simulation package.⁴¹ The total simulation time was 20 ns at room temperature, $T = 300$ K, using the Langevin thermostat and Berendsen barostat. For the analysis performed, only the last 10 ns of the simulation were considered, in order to ensure the equilibration of the compound.

Case of study: MD simulations of the platinum (II) complex with DNA

After the development and the validation of the parameters for the *cis*-dichloro(2-aminomethylpyridine)platinum (II) bonded to 2-(4'-aminophenyl-2'-hydroxyphenyl)benzothiazole derivative, two MD simulation were performed. The first simulation was performed with a non-covalent interaction between the complex and the DNA fragment. The second simulation was performed with the complex coordinated to the nitrogen atoms (N7) of the guanine bases of the oligonucleotide. With this methodology, we were able to evaluate the contradictions in the literature about the modes of binding of the complex in the DNA structure, as already mentioned in the introduction of this work.

For the simulation of the unbound complex, the sequence B-DNA 5'-CGCGAATTCGCG-3' (PDB ID: 1BNA)⁴² was adopted. This native sequence has already been co-crystallized with drug molecules in the minor groove of DNA (adenine (A) and thymine (T) rich region)⁴³⁻⁴⁵ and extensively used in *in silico* studies.^{5,27,46} In addition, studies indicate that platinum (II) complexes^{26,27} and benzothiazole derivatives⁴⁷⁻⁴⁹ also showed high affinity for this same region of DNA. It is known that the preference for the minor groove of DNA is mainly due to: (i) the electrostatic and van der Waals interactions being more favorable than in the major groove;⁵⁰ (ii) because it is a narrower region than the rich region in cytosine (C) and guanine (G).⁴⁹ Consequently, the presence of drugs with anticancer potential in the minor groove of DNA may inhibit its replication and transcription process. Therefore, based on these previous studies, the complex of this study was simulated in the minor groove of the 5'-CGCGAATTCGCG-3' sequence to describe non-covalent interactions with the biomacromolecule, and also to determine the structural properties and binding free energy of system.

The reason why the simulation of the bonded complex to the guanine bases of the DNA was performed is the great similarity of its metallic center with Cisplatin. The metallic coordination of the platinum-based drugs to guanine bases of DNA is already a clear mechanism in the literature.⁵¹ In this sense, the second system was performed with the platinum atom of the complex coordinated to the nitrogen atoms of the guanine bases of the oligonucleotide (sequence 5'-CCTCAG*G*CCTCC-3', PDB ID: 2NPW⁵² - Supporting Information, Section S3 (Figure S3.2)). For this, the crystallized cisplatin ligands were replaced by the proposed complex ligand. For this simulation, it was

necessary to develop few other parameters of bonds, angles, dihedrals and charges of the platinum center coordinated to those nitrogen atoms. Since the complex is coordinated with DNA, it is reasonable that the charges are described with a level of theory compatible with the description of the environment. So, in this case, the charges for the complex, except the platinum atom, were calculated with HF/6-31G*.⁵³ The HF/def-SV(P) method was used to describe the platinum atom. The same methodology previously described for the development parameters of bonds, angles, dihedrals for the complex was employed to derive the missing parameters. This parameters set can be found in the Supporting Information, Section S4.

Both MD simulations were performed under the same initial conditions with the Amber 11 software package. Complex plus DNA fragment were added in an octahedral box truncated with the explicit solvation model (water TIP3P). Because of the 3D different dimensions of the DNA, the usual cubic box would require a greater computational demand. However, the use of a rectangular box would also not be a good choice, since the rotation of the DNA would lead to interaction with its neighboring periodic images. Therefore, the use of a truncated octahedral box is recommended for simulating non-spherical systems. Twenty-two and twenty sodium ions were used to neutralize the first and the second systems, respectively. The added sodium ions were modelled with the ff99SB force field.⁵⁴ The parmbsc1 force field was used to model the DNA fragment.⁵³ The preparation of both systems for the MD simulation was performed in three steps. Initially, the systems were minimized constraining the complex and the DNA fragment with a constant force of 500 kcal mol⁻¹. Then, both systems were minimized without restrictions. Subsequently, the systems were heated from 0 K to 310 K through three 100 ps MD in constant volume, using the force constants of 20, 10 and 5 kcal mol⁻¹, consecutively, to restrain the positions of the complex and the DNA. Finally, the systems was simulated at a temperature of 310 K and 1 bar pressure (ensemble NPT) using the Langevin thermostat and the Berendsen barostat implemented in Amber 11.⁴¹ A cutoff of 10 Å was used for van der Waals interactions. Long-range electrostatic interactions were modelled with the Particle Mesh Ewald approach (PME).⁵⁵ The first and the second MD simulation were considered equilibrated after 75 ns and 10 ns, respectively.

MM/PBSA calculations

The binding free energy (ΔG_{bind}) of the non-covalently bonded system was estimated with the molecular mechanics Poisson–Boltzmann surface area (MM/PBSA)⁵⁶ method implemented in AMBER 11.⁴¹ The value of ΔG_{bind} is obtained by the difference between the free energy of the system ($G_{DNA+complex}$) and the free energy of the DNA (G_{DNA}) plus the free energy of the platinum (II) complex ($G_{complex}$), as described in Equation 2.

$$\Delta G_{bind} = G_{DNA+complex} - (G_{DNA} + G_{complex}) \quad (2)$$

The free energy values associated with each term of Equation 2 are calculated by the contribution of the molecular mechanical energy in the gas-phase (E_{MM}), solvation free energy (G_{sol}) and entropic contribution ($T\Delta S_{MM}$), where T is the temperature and S_{MM} is the entropy of the molecule.

$$G = (E_{MM}) + (G_{sol}) - T\Delta S_{solute} \quad (3)$$

The value of E_{MM} includes the sum of the internal energies (E_{int} , which is the energy associated to bond stretching, angular and torsional deformations), electrostatic (E_{elec}) and van der Waals energy (E_{vdw}). The G_{sol} is calculated by polar solvation free energy (G_{PB}), using the Poisson–Boltzmann (PB) equation, plus the non-polar term (G_{SA}), estimated by solvent accessible surface area (SASA). The S_{solute} was estimated by normal-mode analysis of the vibrational frequencies from a set of snapshots taken from the MD simulations.

$$G = (E_{int} + E_{elec} + E_{vdw}) + (G_{PB} + G_{SA}) - T\Delta S_{solute} \quad (4)$$

The approach single trajectory protocol (STP) was adopted for the calculation of the binding free energy. In STP a single trajectory is used to calculate the free energy of receptor (R), ligand (L) and complex (RL). Previous studies show that the STP approach generally provides more accurate results than the multiple trajectory protocol (MTP) approach, where three independent trajectories are required for calculations, one for RL and one for each L and R.⁵⁷

All calculations were performed from the last 4 ns of simulation. In 2010, Hou et al.⁵⁸ found that there is no gain in results in using MD simulations longer than this if the system is well equilibrated. For the calculations of the first two terms in Equation 2, 500 snapshots from MD simulations were selected (1 frame every 16). On the other hand, in order to reduce the computational demand, 100 snapshots (1 frame every 80) were used to estimate the $T\Delta S$ parameter via normal-mode calculations (nmode).⁵⁹ The values of the exterior dielectric constants and of the solute were 80 and 4,⁶⁰ respectively. The G_{PB} , G_{SA} and terms were calculated with the MMPBSA.py script⁶¹ in AmberTools.⁴¹ To estimate G_{SA} , a value of $0.00542 \text{ kcal}\text{\AA}^{-2}$ for surface tension and $0.92 \text{ kcal mol}^{-1}$ for the offset were adopted.⁶² A probe radius of 1.4 \AA was used to define the dielectric boundary between solute and solvent.

Results

Conformer Search

As previously discussed, even before starting the molecule parametrization, it is of great importance to ensure that the starting geometry is a minimum point of the potential energy surface (PES). With that in mind, it is expected that the parameters developed from this geometry will be able to realistically describe the structural properties of the molecular system, as well as its interactions. The energy graph of the eight conformations obtained from the conformational search can be found in the Supporting Information, Section S1 (Figure S1.1). The minimum energy geometry (conformation 1) was adopted for additional analysis of the PES profile with the torsion of the dihedral N12-C22-C13-C14 and the results can be found in Figure 3.

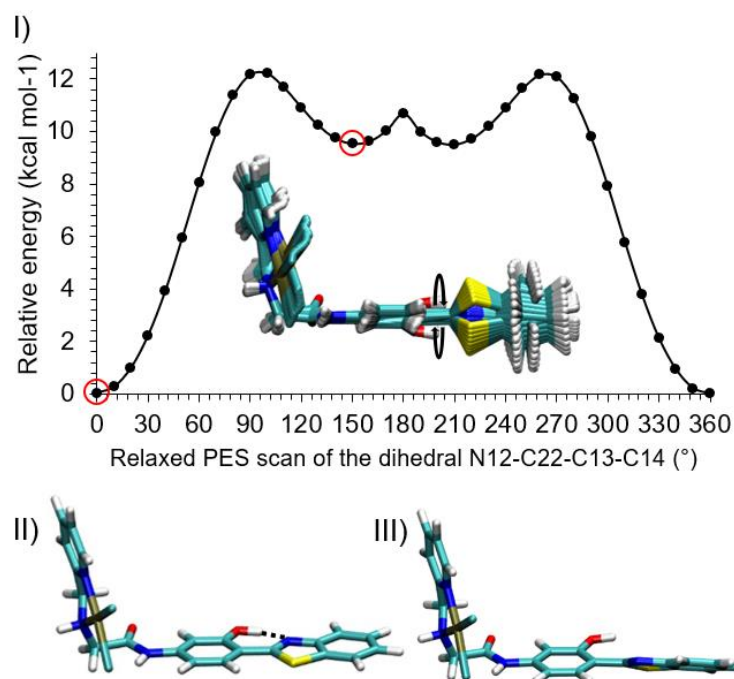


Figure 3. I) Potential energy surface (PES) obtained from the torsion of the dihedral N12-C22-C13-C14. II) Global minimum corresponding to the first red circle structure in figure 3 I). III) Local minimum corresponding to the second red circle structure in figure 3 I).

According to Figure 3, it is possible to observe that, in the global minimum structure (Figure 3 II), the hydrogen H49 remains oriented towards the N12 nitrogen. This conformation is possibly being favored by an intramolecular hydrogen bond. In addition, two other minimum conformations are obtained when the hydrogen H49 is close to the sulfur atom S11. Therefore, because of the lowest energy and the high torsion barrier of about 12 kcal mol⁻¹, it is expected that, in an equilibrated MD simulation, the conformation, in which the hydrogen is oriented towards the nitrogen N12 will be much more populated than a conformation with the H towards the sulfur atom S11.

MD of the complex in vacuum: validation of the force field parameters.

To validate the parameters set developed herein, the RMSD (root mean square deviation) was calculated as a time-dependent variable of the complex in vacuum simulation. The structure obtained after the energy minimization of the system was

adopted as a reference for the RMSD analysis. The RMSD graph over the last 10 ns of simulation is shown in Figure 4.

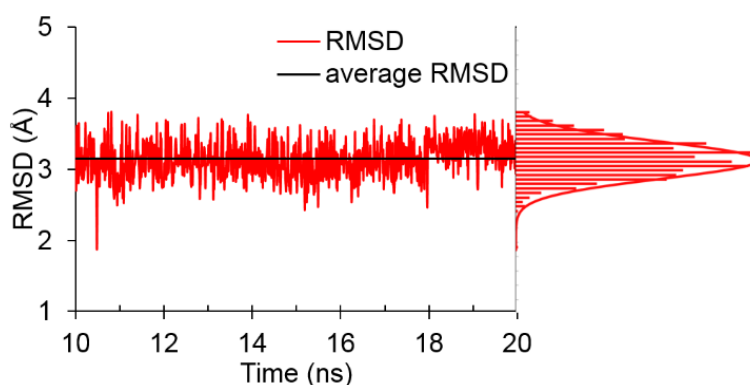


Figure 4. RMSD *versus* time graph calculated for platinum (II) complex in vacuum (T = 300 K).

Analyzing the plot in Figure 4, it is possible to notice that the structure oscillated around 1 Å during the entire simulation time. It is important to remember that the complex was simulated in vacuum, with the absence of molecules that could restrict its flexibility. This feature leads us to conclude that the complex has acquired a good conformational stability, with a Gaussian distribution, indicating that the model developed in this work allows the obtention of physical conformations throughout the simulation.

It was then of interest to specifically analyze the behavior of the complex metal center during the MD simulation, since, according to previous work, this region of the molecule contributes to its cytotoxicity against cancer cells.²¹ Figure 5 shows the variation of the length of the bonds involving the platinum atom during the last 10 ns of simulation.

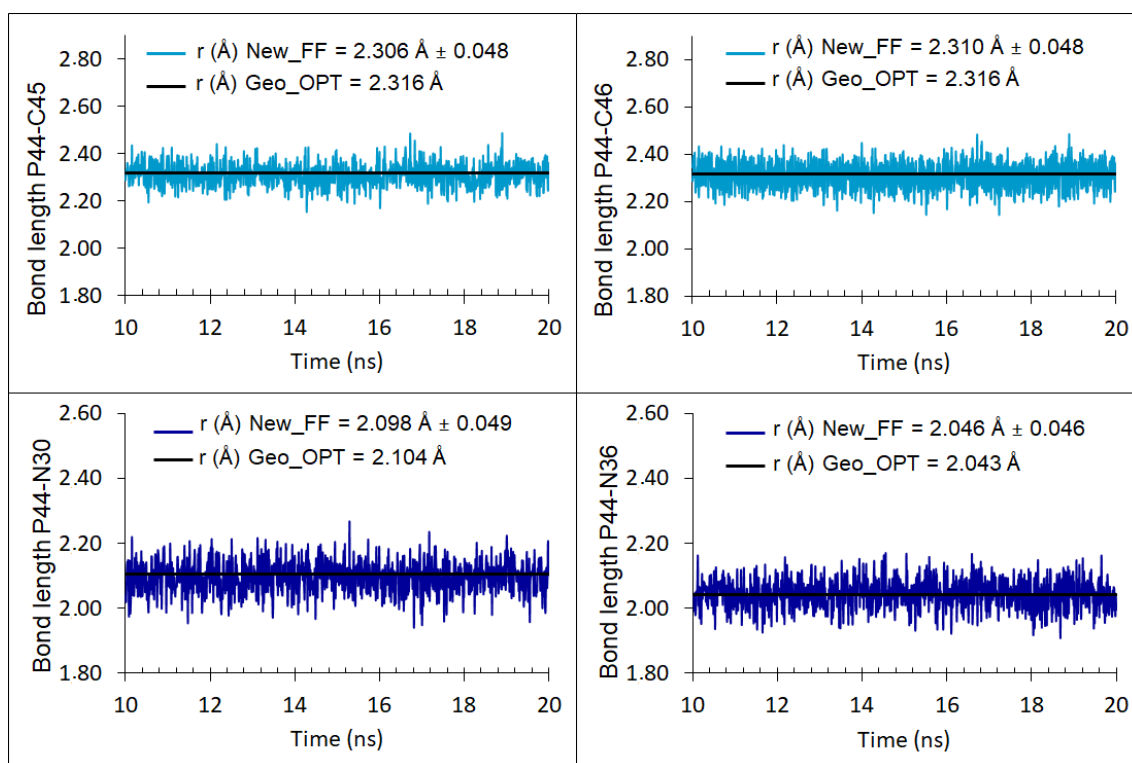


Figure 5. Bond length *versus* time graph for bonds involving the metal center of the complex.

By observing Figure 5, it is possible to notice in all cases that the deformations in the lengths of the bonds were minimal and compatible with their normal modes vibrations in time. The average values of the bonds involving the metallic center agree very well with the values of the lengths of the reference quantum structure, with slight fluctuations. Thus, it is possible to say that the set of parameters developed in this work is indeed able to describe in a satisfactory way the bonds that involve the metallic center.

As mentioned earlier, some of the dihedrals present in the complex structure are likely to rotate. The purpose of a MD simulation is to sample all the possible physical conformations in controlled conditions, which a molecule may exist. The minimum structure obtained after a conformational search of the dihedral N12-C22-C13-C14 shows that the hydrogen H49 remains directed to the N12 nitrogen; as discussed before, this conformation is possibly being favored by a strong intramolecular hydrogen bond. However, another minimum conformation can be obtained with an increase in energy of less than 10 kcal mol⁻¹. Thus, in a sufficiently long simulation, it is expected that both conformations would be populated in the trajectory. Clearly, the stability of each conformation would determine the most frequent population. Figure 6 shows that the

two minimum conformations predicted in previous calculations indeed appeared in the MD simulation.

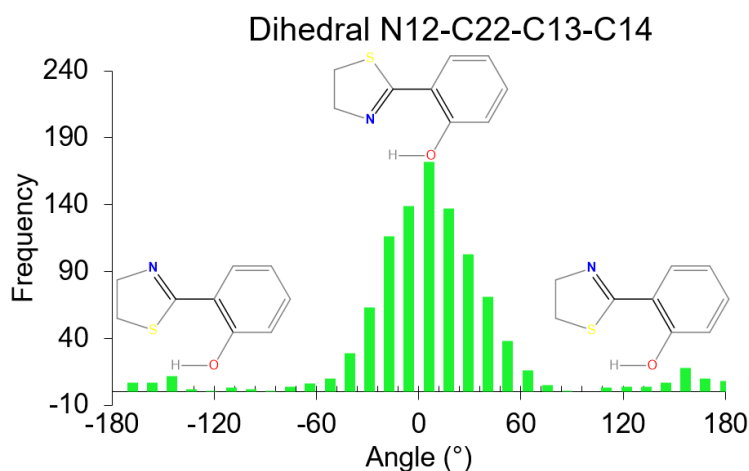


Figure 6. Variation of the N12-C22-C13-C14 dihedral (in black) and distribution of the structures obtained from the MD simulation.

As can be seen in Figure 6, the frequency in which the lowest energy structure appears during the simulation is greater than the frequency in which the second minimum conformation is populated. This leads us to conclude that the parameters developed herein, in addition to sampling all the possible MD conformations for this dihedral, also show that the largest amount of conformations is in agreement with the geometry obtained by quantum methods. Similarly, the dihedral H24-N23-C25-O26 also assumed two possible conformations during the simulation, as can be seen in Figure 7. Clearly, for this dihedral, *s-trans* conformations are predominant compared to *s-cis* conformations. Despite this, it is believed that the *s-cis* conformation is also favored due to the positions of the hydrogen IN and oxygen O26, which allows an intramolecular hydrogen bond. Again, the analysis of the structural properties of the geometries obtained from the MD simulation reveals the effectiveness of the parameter set.

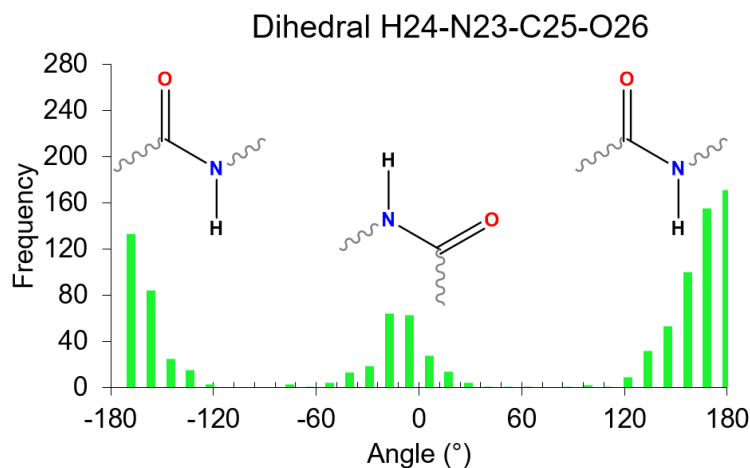


Figure 7. Variation of the H24-N23-C25-O26 dihedral and distribution of the structures obtained from the MD simulation.

BLA

Bond Length Alternation (BLA) is a geometric parameter and it is obtained by calculating the difference between the average lengths of single and double bonds along the linear π -conjugated backbone. For an ideally conjugated system, the single and double bonds have the same values and the BLA is zero. Although it is only a molecular geometric parameter, BLA exerts a strong influence on the electronic structure⁶³ and it is a good way to understand if the new model is able to recover the electronic properties (reflected on the obtained geometries) that are usually lost in classical MD simulations.

Thus, in order to obtain a better structural understanding of the conjugation degree of the AHBT ligand of the complex, the BLA analysis was performed. The ligand region considered for BLA analysis is highlighted in Figure S1.3 (Supporting Information, Section S1). Firstly, the average BLA value of the geometries extracted from the last 10 ns of MD simulation and of the reference quantum geometry were calculated. Thus, it was possible to evaluate if the set of parameters involving the AHBT ligand was also accurately described. According to Figure 8, it was possible to see that the mean value of BLA for the simulated complex with the new force field is in agreement with the BLA value of the structure optimized with quantum methods. So, again we prove the quality of the developed force field. In addition to adequately describing the metallic center of the complex, as shown above, the new set of parameters also yields very satisfactory results for the binding parameters of the AHBT ligand. Subsequently, only for comparison purposes and to confirm the quality of the

model developed against a widely used model in the literature, a second MD simulation was performed using the parameters of a non-specific force field (*General Amber Force Field* – GAFF).³⁹ GAFF is a general force field widespread in the literature developed to model organic molecules. However, it has a limited number of atom types, and its use in MD simulations to describe the structural and vibrational properties of a specific system may not be sufficient.¹² MD simulation with GAFF parameters was performed under the same conditions described in the previous section (*Validation of the force fields*), and the frames of the last 10 ns of the equilibrated simulation were adopted for the calculation of the average BLA value.

In Figure 8, the mean value of BLA for the simulated complex with GAFF parameters is lower, showing that, with this defused description, the degree of conjugation of the complex is superestimated. Thus, if calculations of electronic excitations were made from the conformations extracted from the MD simulation with the GAFF parameters, probably the excitation energy would be underestimated, being able to reveal structures whose physical sense does not exist. On the other hand, it is expected that the simulations performed with the developed force field can precisely describe these properties, since the results show that the new model is able to properly describe the geometries of the complex along the time.

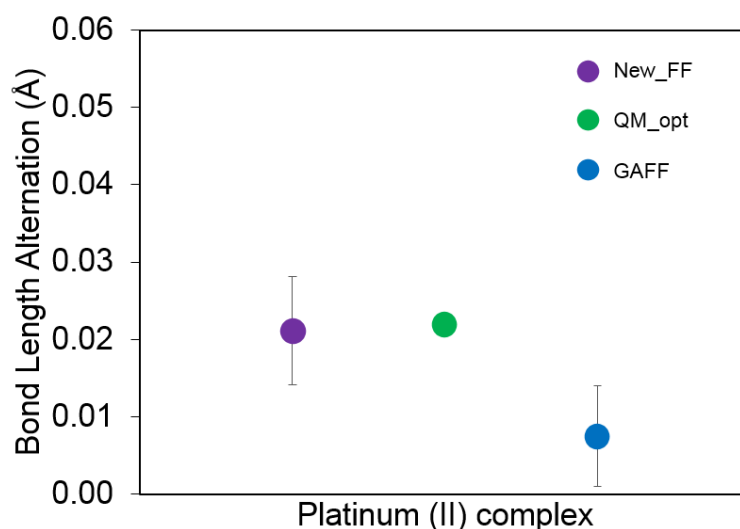


Figure 8. BLA of the platinum (II) complex models computed from the quantum structure (QM_opt) and of the mean values of the bond lengths along with the MD simulations performed with the developed parameters (New_FF) and GAFF parameters.

Infrared spectra

In addition to the previous analyzes that mainly tested the set of the equilibrium constants, to prove the quality of the developed force-constants, an infrared (IR) spectrum of the mean structure of the vacuum MD simulation was calculated and compared with the IR spectrum of the quantum structure. Figure 9 shows the overlap of the two IR spectra.

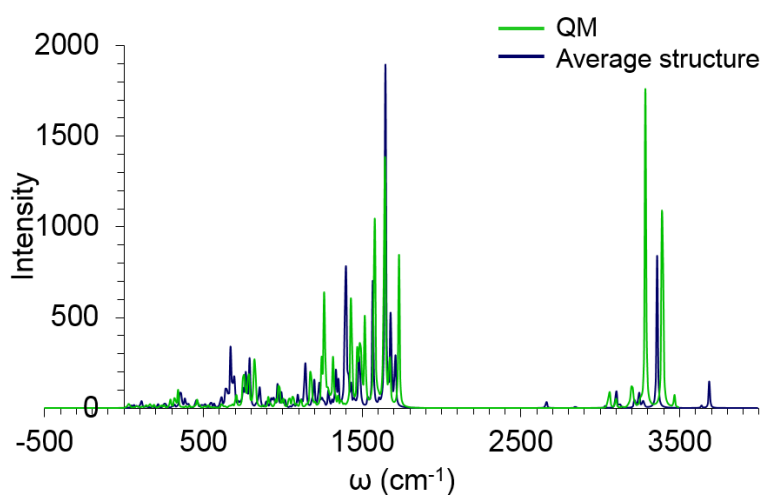


Figure 9. Infrared spectrum calculation for platinum (II) complex (blue and green curves represent the quantum structure and the mean structure spectra from vacuum MD simulation, respectively).

According to Figure 9 it is possible to notice a very good agreement between the spectra, especially the peaks with frequency values below 1700 cm^{-1} , which are mainly correlated with the conjugated modes of the ligands. According to previously published experimental data, the peak for the Pt-N stretching is $478 - 505\text{ cm}^{-1}$.²¹ Another study shows that the symmetrical and asymmetric stretching of the Pt-Cl bond in the Cisplatin is characterized by low intensity peaks located at 342 cm^{-1} and 353 cm^{-1} , respectively.⁶⁴ For the complex in question, in the region between $300-400\text{ cm}^{-1}$ it is possible to clearly find some cited peaks, which can be attributed to the Pt-Cl stretching. The other low intensity peaks can be attributed to the stretching C-H bond and N-H of the amine. Later, it is possible to observe a large overlap of other important peaks between our model and the QM reference. Such peaks may be related to the stretchings C-C, C-N, C-O, C-S, C=C, C=N, C=O bonds and to the bendings of the C-H, N-H and O-H bonds.⁶⁵

The peak around 1700 cm^{-1} can be attributed to the C=O stretching of the amide functional group. Subsequently, from 2600 cm^{-1} there are the characteristic peaks of symmetrical and asymmetrical stretching of C-H, N-H and O-H bonds. In the quantum structure spectrum, two high intensity peaks located around 3300 cm^{-1} and 3400 cm^{-1} can be derived from the O-H and N-H linkages of the amide, respectively. As shown early, hydroxyl hydrogen is directed to the nitrogen atom of the benzothiazole ring. Therefore, the O-H bond becomes more polarized and the peak intensity increases. Furthermore, the amide nitrogen is also directed to the chlorine atom, which favors the increase in peak intensity. On the other hand, in the average structure spectrum it is possible to observe both a decrease in peak intensity and a shift to higher frequencies. This may be a consequence of a slight distortion of some structure dihedrals such as N12-C22-C13-C14 and those involving the carbon atom C27, which can assume more than one conformation as we show in previous sections. However, these minor distortions are predictable and completely acceptable and do not compromise the quality of the developed force field.

MD of the non-covalently bonded DNA-complex system

As mentioned earlier, the complex of this study has the potential to bind to the minor groove of DNA. This mechanism of interaction with DNA interferes with replication and transcription processes, this fact has already been elucidated for anticancer drugs that bind to the minor groove.⁶⁶ In spite of its great importance, surprisingly little detailed computational work on the action mechanism of this kind of drug has appeared.

To evaluate the structural deformations of the system during simulation, the RMSD of the complex and DNA were calculated. The RMSD of the DNA backbone and platinum (II) complex of the 100 ns of simulation were calculated taken as reference the final structure obtained after the heating step of the system, the results are shown in Figure 10. As can be seen, DNA oscillates considerably during the first 75 ns of simulation. During this time, the RMSD values range from $\sim 1\text{ \AA}$ to a maximum value of 3.82 \AA . In addition, some peaks in the RMSD of the complex can also be observed between 0 and 75 ns, indicating the presence of some different conformations from the equilibrium one. However, in the last 25 ns of simulation the whole system (platinum (II) + DNA complex) remains in equilibrium. For this reason, only the last 25 ns were

considered for the next analyses which require a good conformational stability of the DNA and the complex.

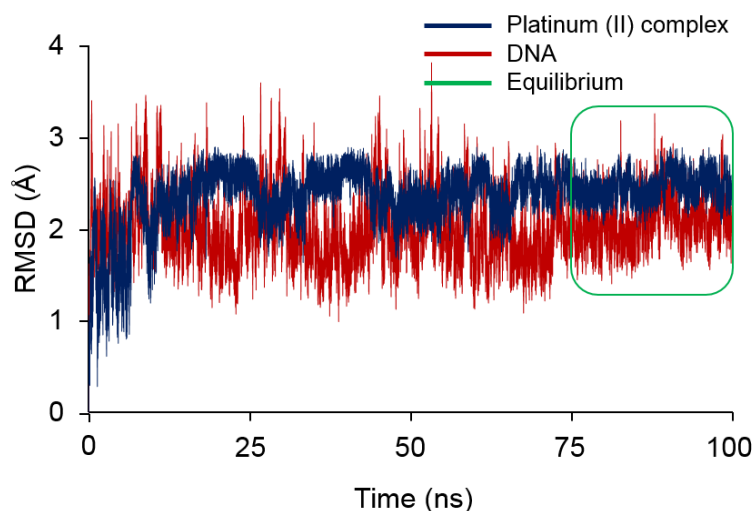


Figure 10. RMSD versus time graph calculated for platinum (II) complex (blue) and DNA (red) during 100 ns of the MD simulation of the non-covalently bonded DNA-complex system.

The average RMSD value of the complex and DNA were 2.43 Å and 2.05 Å, respectively (Supporting Information, Section S5 (Figure S5.1)). By the RMSD values, both the DNA and the complex presented a structural change in relation to the reference structure. For DNA, this average RMSD value can be a consequence of the complex presence in the minor groove. Moreover, it is plausible to consider that a conformational change of the complex is due to the chemical environment in which it is inserted. It is possible that the high affinity of the complex for the minor groove of the DNA have induced a conformational change that justifies the RMSD value. Therefore, we decided to analyze more deeply the modes of interaction responsible for the system equilibrium.

Hydrogen bonding analysis

The presence of hydrogen bonds (H-bonds) between the platinum (II) complex and the DNA bases were explored. This type of interaction seems to be the key to the stability of the complex in the minor groove of DNA. The VMD software was used to determine and quantify the complex and the DNA atoms involved in H-bonds. As a result, the analyzed MD simulation points that there are four acceptors (N12, O48, N23,

O26) and three H-bonds donors (O48-H49, N23-H24 and N30-H47 groups) in the complex structure. The maximum distance between H-bond donor and acceptor was 3.5 Å, while the maximum donor-hydrogen-receiver angle was 155°. ⁵⁹

All hydrogen bonds found during the last 25 ns of simulation can be seen in Figure 11. According to our findings, the complex acts mainly as a hydrogen bond donor. As shown in Figure 11 I), the N23-H24 group donates the proton for the O2 of the Thymine nucleotide. The N30-H47 group can interact with O4' (deoxyribose) in both DNA ribbons (Figure 11: I), II), III)). Finally, the O48-H49 group interacts with N3 (adenine), O2 (cytosine) and O4' (deoxyribose). These interactions are in agreement with those involving the minor groove ligands. ⁶⁷⁻⁶⁹ Among the possible hydrogen bonds that the complex can make as an acceptor, the only one observed between complex (atom N12) and DNA, is with the Guanine N2-H21 group.

Considering all simulation frames during the equilibrium, in 50.72% of the time is present the N23-H24...O2 (thymine) H-bond. Subsequently, the percentage of the simulated time that involves hydrogen bonds in the N30-H47 group was 14.07%. The O48-H49 was the hydrogen bond donor group which least interacted with DNA (9.12% of the time). The acceptor atom N12 makes H-bonds only in 0.02% of the frames. Of course, this is due to a possible intramolecular hydrogen bond between N12 and H49, which makes nitrogen less available to interact with DNA.

Because of these results, it is possible to realize that the interactions of the complex with nucleotides can contribute to the stability of the complex in the minor groove of DNA. It is visible, however, that the stability is mainly governed by interactions involving the N23-H24 donor group, which are the interactions most preserved during the simulation.

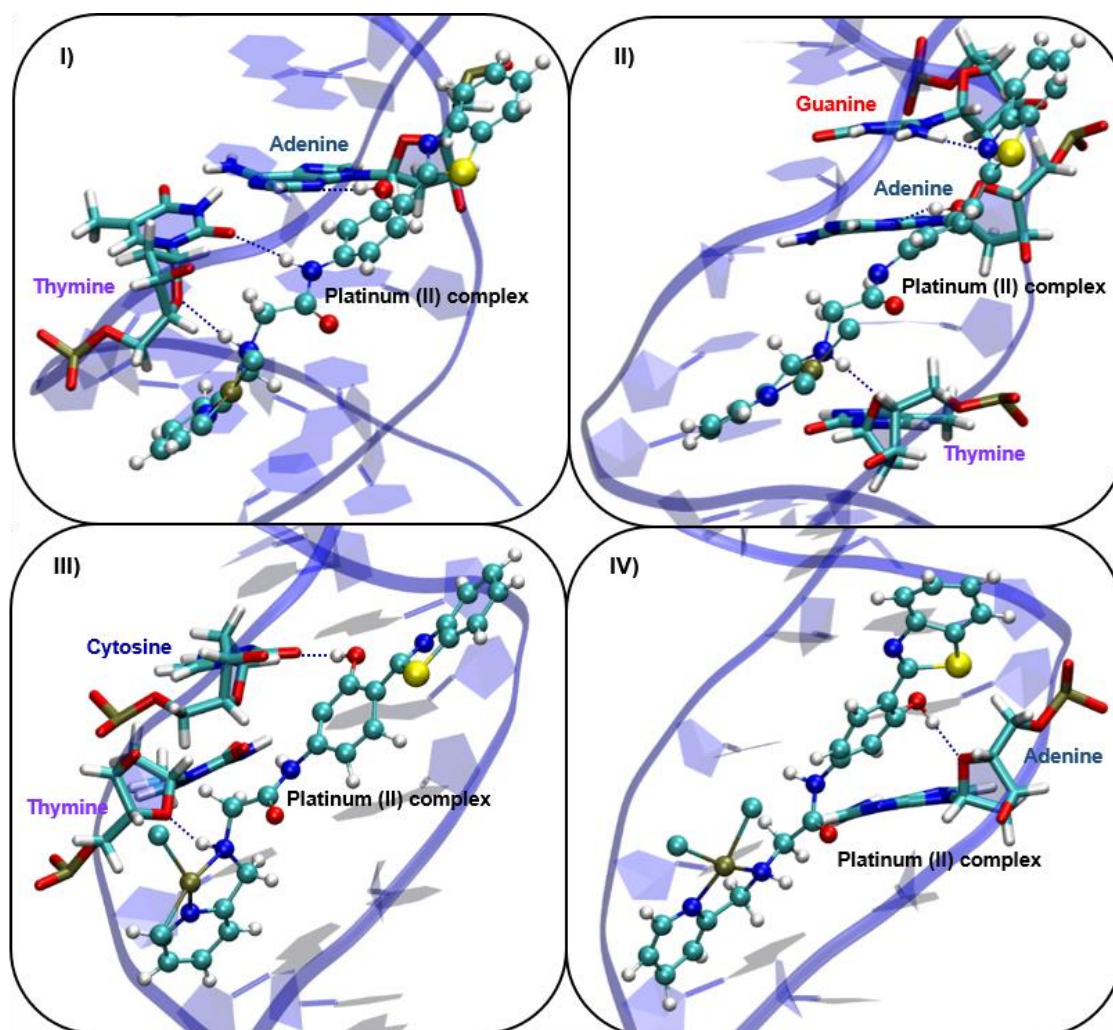


Figure 11. Hydrogen bonds between the platinum (II) complex and the nucleotides in the minor groove of DNA.

MM/PBSA calculations

In order to complement the discussion of the structural properties of the system of Figure S3.2, the free binding energy (ΔG_{bind}) of the complex in the minor groove of DNA was calculated using the MM/PBSA method.⁶¹ In thermodynamics, free energy can be used to indicate the direction in which a process occurs as well as the likelihood that the system will remain in a given state. Therefore, determining this thermodynamic property is of crucial importance in the study of biomolecular systems. The MM/PBSA method was chosen in this work to perform free energy calculations because it has good computational cost and accuracy agreement. Moreover, its accuracy has been corroborated previously in the determination of ligand-DNA free binding energy.^{47,67}

The absolute binding free energy of the platinum (II) complex in the minor DNA groove (ΔG_{bind}), as well as their contributions, are summarized in Table 1. It is important to mention that the term ΔE_{int} is null and is not shown in Table 1. This is because in the STP approach the internal energy is calculated from identical configurations, and the energy difference between the system (DNA-complex) and the individual components is the same.

As can be seen in Table 1, the other terms of ΔE_{MM} contribute positively to ΔG_{bind} . The value of van der Waals energy dominates electrostatic energy at 6.32 kcal mol⁻¹. On the other hand, the polar term of solvation free energy (G_{PB}) is unfavorable, while the non-polar term (G_{SA}) is slightly favorable for the value of ΔG_{bind} . Therefore, ΔG_{sol} has a positive value of 12.65 kcal mol⁻¹. Finally, a negative value for the entropic term was obtained. Although this value is unfavorable for ΔG_{bind} , it symbolizes that there is a reduction in the number of available microstates for the complex after its binding in the minor groove of DNA. In general, it is possible to say that the binding of the complex in the minor groove of DNA is favorable in water, with the value of ΔG_{bind} equal to -65.06 kcal mol⁻¹. This result is in line with previous predictions, which also indicate the link between the complex and the DNA.^{21,23,26,27}

Table 1. Binding free energy components (kcal mol⁻¹) for complex-DNA system.

Energy (kcal mol ⁻¹)	Δ_{vdW}	Δ_{elec}	Δ_{PB}	Δ_{SA}	T Δ S	ΔG_{bind}
Platinum (II) complex - DNA	-53.46 (3.75)	-47.17 (8.48)	16.34 (2.11)	-3.69 (0.22)	-22.92 (1.33)	-65.06

Standard deviations are reported in parentheses.

MD of the guanine-N7-linked complex

Again, to evaluate the structural deformations of the guanine-N7-linked complex, the RMSD graph was plotted (Figure 12). The geometry obtained after the heating step was adopted as a reference.

Approximately, in the first 10 ns of simulation, the complex tends to low RMSD values, while at the same time the DNA reaches values close to 4.0 Å. Over the next 53 ns, the complex keeps a conformational stability, despite reaching a minimum RMSD around 36 ns of simulation. However, the DNA structure continues to have high RMSD

values, reaching a maximum value of 4.6 Å. After approximately 63 ns of simulation, the complex appears to reach higher RMSD values. A maximum value of 3.70 Å can be observed around 93 ns of simulation. This analysis shows that the complex presents at least two clear different conformations along the MD simulation. When the complex is linked to DNA, its ligand is mostly in contact with the solvent. Thus, its structural deformations, even if less pronounced than DNA deformations, may be due to the rotations of the dihedrals that were previously predicted.

In parallel to the graph in Figure 10, the RMSD of Figure 12 shows that structural deformations after the formation of Pt-DNA adduct, especially to DNA, are much more severe.

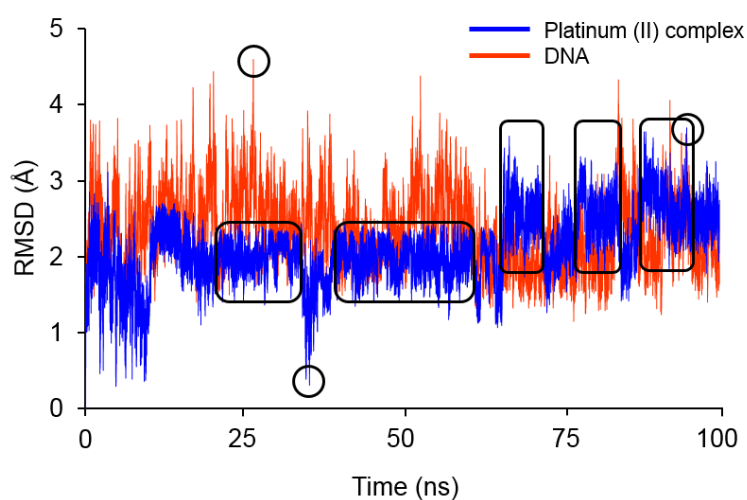


Figure 12. RMSD versus time graph calculated for platinum (II) complex (blue) and DNA (orange) during 100 ns of the MD simulation of the Platinum-DNA Intrastrand Adducts.

NMR spectroscopy

Previous studies with Pt complexes have shown that the metal presents different values of chemical shift in relation to the biological environment and the coordination sphere.⁷⁰ Given this result, the authors propose the application of the complex for the diagnosis of cancer. However, NMR parameters, such as the chemical shift of the metal centers, can also be a useful parameter for evaluating the possible preference of the complex for covalent bonding or interaction with the groove of DNA. This can be

confirmed by a time-dependent ^{195}Pt NMR spectra of the reaction between the complex and the DNA.

As a way of directing future research to further understand the behavior of the complex in the presence of DNA, Pt atom chemical shift calculations were performed. The calculations were made in gas phase under the following conditions: (i) N7 coordinated complex of the guanine bases of DNA; (ii) non-covalently interacting complex in the minor groove of DNA; (iii) complex in the absence of DNA. Details of NMR calculations can be found in Supporting Information, Section S6.

According to the results, the relative values of chemical shifts under conditions (i), (ii) and (iii) were 353.32 ppm, 26.71 ppm and 0 ppm, respectively. Clearly, the substitution of chlorine atoms with purine base nitrogen results in a higher chemical shift value than the others, indicating that the platinum atom is less shielded. In contrast, the chemical shift of the complex in the minor groove of DNA is slightly higher than in the absence of DNA.

Several factors that can influence the chemical shift of the platinum atom, such as temperature, concentration, chemical environment, among others.^{71,72} However, further studies are beyond the scope of this work. In any case, the NMR data presented are of considerable relevance for future research seeking to monitor and determine the predominance in coordination or interaction with the minor groove of the complex by NMR spectroscopy.

Conclusions and perspectives

In this work, we adopt a modern force field parameterization strategy, combining QM calculations with MD simulations, to derive parameters from a platinum (II) complex. Since the first published work with some parameters involving metal, little progress has been made in determining a complete and precise force field for modeling platinum complexes in MD simulations. Parameters for bonds, angles, dihedrals, and atomic charges have been developed and are available from Supporting Information. The results obtained using the new force field show that the structural properties are very well described and in agreement with the quantum geometry. These results are supported by the backbone RMSD analysis of the complex, connections involving the metallic center, dihedral distribution, BLA and IR spectrum. Also, BLA

analyses show that the binder is much better described with the developed force field parameters than with a widely used force field in the literature, the GAFF.

Given the quality of the developed force field, it was possible to perform long simulations of MD, which provide a better understanding of the interaction modes of the complex with DNA. The results support both the presence of the complex in the minor groove (adenine and thymine rich region), and coordinated to the N7 of the guanine bases of DNA. In the minor groove of DNA, the complex performs various hydrogen interactions with the nitrogenous bases and also with the sugars. In addition, the binding free energy value shows that the presence of the complex in the minor groove is thermodynamically favorable. Already the coordination of the metal leads to large deformations in the structure of DNA, which may indicate a possible new anti-cancer drug. Overall, the combined interaction effect of the proposed complex with DNA yields promising results and stimulates further research.

Finally, we show by NMR calculations that the chemical shift of the bound complex is considerably greater than when unbound to DNA. This result may be useful as a reference in future experimental determinations, using NMR spectroscopy, of the preference of the complex for these regions of the DNA.

Overall, this study presents new parameters for MD simulations of a platinum (II) complex with potential biological application. In addition, insights into the modes of interaction of the complex with DNA, which is the main target for platinum-based drugs, are provided. This stimulates future MD simulations of platinum (II) complexes, something little explored precisely because of the lack of parameters for the metal.

Acknowledgment

This work was also supported by Excellence project UHK. The authors thank the Brazilian agencies FAPEMIG, CAPES, and CNPq for the financial support of this research, and Federal University of Lavras - UFLA for infrastructure and encouragement in this work.

References

- (1) Rosenberg, B.; Van Camp, L.; Krigas, T. Inhibition of Cell Division in *Escherichia Coli* by Electrolysis Products from a Platinum Electrode. *Nature*

- 1965**, 205 (4972), 698.
- (2) Johnstone, T. C.; Suntharalingam, K.; Lippard, S. J. The next Generation of Platinum Drugs: Targeted Pt (II) Agents, Nanoparticle Delivery, and Pt (IV) Prodrugs. *Chem. Rev.* **2016**, 116 (5), 3436–3486.
 - (3) Kenny, R. G.; Marmion, C. J. Toward Multi-Targeted Platinum and Ruthenium Drugs—A New Paradigm in Cancer Drug Treatment Regimens? *Chem. Rev.* **2019**, 119 (2), 1058–1137.
 - (4) Dasari, S.; Tchounwou, P. B. Cisplatin in Cancer Therapy: Molecular Mechanisms of Action. *Eur. J. Pharmacol.* **2014**, 740, 364–378.
 - (5) Suntharalingam, K.; Mendoza, O.; Duarte, A. A.; Mann, D. J.; Vilar, R. A Platinum Complex That Binds Non-Covalently to DNA and Induces Cell Death via a Different Mechanism than Cisplatin. *Metallomics* **2013**, 5 (5), 514–523.
 - (6) Rosa, N. M. P.; Ferreira, F. H. D. C.; Farrell, N. P.; Costa, L. A. S. TriplatinNC and Biomolecules: Building Models Based on Non-Covalent Interactions. *Front. Chem.* **2019**, 7, 307.
 - (7) Hollingsworth, S. A.; Dror, R. O. Molecular Dynamics Simulation for All. *Neuron* **2018**, 99 (6), 1129–1143. <https://doi.org/10.1016/j.neuron.2018.08.011>.
 - (8) de Azevedo Santos, L.; Prandi, I. G.; Ramalho, T. C. Could Quantum Mechanical Properties Be Reflected on Classical Molecular Dynamics? The Case of Halogenated Organic Compounds of Biological Interest. *Front. Chem.* **2019**, 7.
 - (9) Norrby, P.; Liljefors, T. Automated Molecular Mechanics Parameterization with Simultaneous Utilization of Experimental and Quantum Mechanical Data. *J. Comput. Chem.* **1998**, 19 (10), 1146–1166.
 - (10) Seminario, J. M. Calculation of Intramolecular Force Fields from Second-derivative Tensors. *Int. J. Quantum Chem.* **1996**, 60 (7), 1271–1277.
 - (11) Stroet, M.; Caron, B.; Visscher, K. M.; Geerke, D. P.; Malde, A. K.; Mark, A. E. Automated Topology Builder Version 3.0: Prediction of Solvation Free Enthalpies in Water and Hexane. *J. Chem. Theory Comput.* **2018**, 14 (11), 5834–5845.
 - (12) Prandi, I. G.; Viani, L.; Andreussi, O.; Mennucci, B. Combining Classical Molecular Dynamics and Quantum Mechanical Methods for the Description of Electronic Excitations: The Case of Carotenoids. *J. Comput. Chem.* **2016**, 37 (11), 981–991.
 - (13) Yao, S.; Plastaras, J. P.; Marzilli, L. G. A Molecular Mechanics AMBER-Type

- Force Field for Modeling Platinum Complexes of Guanine Derivatives. *Inorg. Chem.* **1994**, *33* (26), 6061–6077.
- (14) Scheeff, E. D.; Briggs, J. M.; Howell, S. B. Molecular Modeling of the Intrastrand Guanine-Guanine DNA Adducts Produced by Cisplatin and Oxaliplatin. *Mol. Pharmacol.* **1999**, *56* (3), 633–643.
- (15) Yesylevskyy, S.; Cardey, B.; Kraszewski, S.; Foley, S.; Enescu, M.; Da Silva, A. M.; Dos Santos, H. F.; Ramseyer, C. Empirical Force Field for Cisplatin Based on Quantum Dynamics Data: Case Study of New Parameterization Scheme for Coordination Compounds. *J. Mol. Model.* **2015**, *21* (10), 268.
- (16) Jorgensen, W. L.; Maxwell, D. S.; Tirado-Rives, J. Development and Testing of the OPLS All-Atom Force Field on Conformational Energetics and Properties of Organic Liquids. *J. Am. Chem. Soc.* **1996**, *118* (45), 11225–11236.
- (17) Ponomarev, S. Y.; Kaminski, G. A. Polarizable Simulations with Second-Order Interaction Model (POSSIM) Force Field: Developing Parameters for Alanine Peptides and Protein Backbone. *J. Chem. Theory Comput.* **2011**, *7* (5), 1415–1427.
- (18) Cvitkovic, J. P.; Kaminski, G. A. Developing Multisite Empirical Force Field Models for Pt (II) and Cisplatin. *J. Comput. Chem.* **2017**, *38* (3), 161–168.
- (19) Rocha, E. P.; Ramalho, T. C. Probing the ESIPT Process in 2-Amino-1, 4-Naphthoquinone: Thermodynamics Properties, Solvent Effect and Chemometric Analysis. *Theor. Chem. Acc.* **2016**, *135* (2), 39.
- (20) Mancini, D. T.; Sen, K.; Barbatti, M.; Thiel, W.; Ramalho, T. C. Excited-State Proton Transfer Can Tune the Color of Protein Fluorescent Markers. *ChemPhysChem* **2015**, *16* (16), 3444–3449.
- (21) Mavroidi, B.; Sagnou, M.; Stamatakis, K.; Paravatou-Petsotas, M.; Pelecanou, M.; Methenitis, C. Palladium (II) and Platinum (II) Complexes of Derivatives of 2-(4'-Aminophenyl) Benzothiazole as Potential Anticancer Agents. *Inorganica Chim. Acta* **2016**, *444*, 63–75.
- (22) Tzanopoulou, S.; Sagnou, M.; Paravatou-Petsotas, M.; Gourni, E.; Loudos, G.; Xanthopoulos, S.; Lafkas, D.; Kiaris, H.; Varvarigou, A.; Pirmettis, I. C. Evaluation of Re and ^{99m}Tc Complexes of 2-(4'-Aminophenyl) Benzothiazole as Potential Breast Cancer Radiopharmaceuticals. *J. Med. Chem.* **2010**, *53* (12), 4633–4641.
- (23) Chen, Z.; Zhang, S.; Shen, L.; Zhu, Z.; Zhang, J. Fluorescence Imaging of a New

- Monofunctional Platinum (II) Complex Containing a Thioflavin-T (ThT)-Based Fluorophore. *New J. Chem.* **2015**, 39 (3), 1592–1596.
- (24) Rodriguez, R.; Zacharioudakis, E.; Kunaligam, L.; Bartoli, A.; Miller, K.; Agarwal, P. Visual Detection of Platinated Dna Lesions from a Clickable Cisplatin Probe Used as Diagnostic Tool or to Identify Synergistic Treatments. Google Patents December 13, 2018.
- (25) Schobert, R.; Biersack, B. Cis-Dichloroplatinum (II) Complexes with Aminomethylnicotinate and-Isonicotinate Ligands. *Inorganica Chim. Acta* **2005**, 358 (12), 3369–3376.
- (26) Mukherjee, S.; Mitra, I.; Misra, K.; Sengupta, P. S.; Linert, W.; Ghosh, G. K.; Moi, S. C. An Experimental and Theoretical Approach on the Kinetics and Mechanism for the Formation of a Four-Membered (S, S) Chelated Pt (II) Complex. *RSC Adv.* **2016**, 6 (22), 18288–18299.
- (27) Mukherjee, S.; Mitra, I.; Saha, R.; Dodda, S. R.; Linert, W.; Moi, S. C. In Vitro Model Reaction of Sulfur Containing Bio-Relevant Ligands with Pt (II) Complex: Kinetics, Mechanism, Bioactivity and Computational Studies. *RSC Adv.* **2015**, 5 (94), 76987–76999.
- (28) Spartan '14 V1. 1.4. Irvine (CA): Wavefunction; 2014.
- (29) Frisch, M. J.; Trucks, G. W.; Schlegel, H. B.; Scuseria, G. E.; Robb, M. A.; Cheeseman, J. R.; Scalmani, G.; Barone, V.; Mennucci, B.; Petersson, G. A.; Nakatsuji, H.; Caricato, M.; Li, X.; Hratchian, H. P.; Izmaylov, A. F.; Bloino, J.; Zheng, G.; Sonnenberg, J. L.; Hada, M.; Ehara, M.; Toyota, K.; Fukuda, R.; Hasegawa, J.; Ishida, M.; Nakajima, T.; Honda, Y.; Kitao, O.; Nakai, H.; Vreven, T.; Montgomery, J. A., Jr.; Peralta, J. E.; Ogliaro, F.; Bearpark, M.; Heyd, J. J.; Brothers, E.; Kudin, K. N.; Staroverov, V. N.; Kobayashi, R.; Normand, J.; Raghavachari, K.; Rendell, A.; Burant, J. C.; Iyengar, S. S.; Tomasi, J.; Cossi, M.; Rega, N.; Millam, N. J.; Klene, M.; Knox, J. E.; Cross, J. B.; Bakken, V.; Adamo, C.; Jaramillo, J.; Gomperts, R.; Stratmann, R. E.; Yazyev, O.; Austin, A. J.; Cammi, R.; Pomelli, C.; Ochterski, J. W.; Martin, R. L.; Morokuma, K.; Zakrzewski, V. G.; Voth, G. A.; Salvador, P.; Dannenberg, J. J.; Dapprich, S.; Daniels, A. D.; Farkas, Ö.; Foresman, J. B.; Ortiz, J. V.; Cioslowski, J.; Fox, D. J. Gaussian09, Revision A.1; Gaussian, Inc., Wallingford CT; 2009.
- (30) Weigend, F.; Ahlrichs, R. Balanced Basis Sets of Split Valence, Triple Zeta Valence and Quadruple Zeta Valence Quality for H to Rn: Design and

- Assessment of Accuracy. *Phys. Chem. Chem. Phys.* **2005**, *7* (18), 3297–3305.
- (31) Paschoal, D.; Marcial, B. L.; Lopes, J. F.; De Almeida, W. B.; Dos Santos, H. F. The Role of the Basis Set and the Level of Quantum Mechanical Theory in the Prediction of the Structure and Reactivity of Cisplatin. *J. Comput. Chem.* **2012**, *33* (29), 2292–2302.
- (32) Paschoal, D.; Guerra, C. F.; de Oliveira, M. A. L.; Ramalho, T. C.; Dos Santos, H. F. Predicting Pt-195 NMR Chemical Shift Using New Relativistic All-electron Basis Set. *J. Comput. Chem.* **2016**, *37* (26), 2360–2373.
- (33) Yang, Y.; Weaver, M. N.; Merz Jr, K. M. Assessment of the “6-31+ G**+ LANL2DZ” Mixed Basis Set Coupled with Density Functional Theory Methods and the Effective Core Potential: Prediction of Heats of Formation and Ionization Potentials for First-Row-Transition-Metal Complexes. *J. Phys. Chem. A* **2009**, *113* (36), 9843–9851.
- (34) Batista de Carvalho, A. L. M.; Parker, S. F.; Batista de Carvalho, L. A. E.; Marques, M. P. M. Novel Platinum-Based Anticancer Drug: A Complete Vibrational Study. *Acta Crystallogr. Sect. C Struct. Chem.* **2018**, *74* (5), 628–634.
- (35) Wang, J.; Wang, W.; Kollman, P. A.; Case, D. A. Automatic Atom Type and Bond Type Perception in Molecular Mechanical Calculations. *J. Mol. Graph. Model.* **2006**, *25* (2), 247–260.
- (36) Humphrey, W.; Dalke, A.; Schulten, K. VMD: Visual Molecular Dynamics. *J. Mol. Graph.* **1996**, *14* (1), 33–38.
- (37) Mayne, C. G.; Saam, J.; Schulten, K.; Tajkhorshid, E.; Gumbart, J. C. Rapid Parameterization of Small Molecules Using the Force Field Toolkit. *J. Comput. Chem.* **2013**, *34* (32), 2757–2770.
- (38) Cornell, W. D.; Cieplak, P.; Bayly, C. I.; Kollman, P. A. Application of RESP Charges to Calculate Conformational Energies, Hydrogen Bond Energies, and Free Energies of Solvation. *J. Am. Chem. Soc.* **2002**, *115* (21), 9620–9631.
- (39) Wang, J.; Wolf, R. M.; Caldwell, J. W.; Kollman, P. A.; Case, D. A. Development and Testing of a General Amber Force Field. *J. Comput. Chem.* **2004**, *25* (9), 1157–1174.
- (40) Lopes, J. F.; de A. Menezes, V. S.; Duarte, H. A.; Rocha, W. R.; De Almeida, W. B.; Dos Santos, H. F. Monte Carlo Simulation of Cisplatin Molecule in Aqueous Solution. *J. Phys. Chem. B* **2006**, *110* (24), 12047–12054.

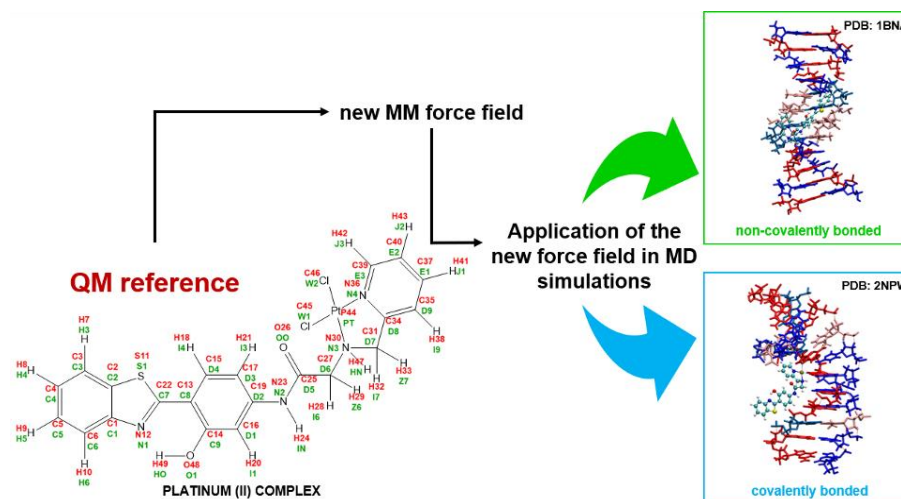
- (41) Case, D. A.; Darden, T. A.; Cheatham III, T. E.; Simmerling, C. L.; Wang, J.; Duke, R. E.; Luo, R.; Walker, R. C.; Zhang, W.; Merz, K. M. AMBER 12; University of California: San Francisco, 2012. *There is no Corresp. Rec. this Ref.* **2010**, 1–826.
- (42) Drew, H. R.; Wing, R. M.; Takano, T.; Broka, C.; Tanaka, S.; Itakura, K.; Dickerson, R. E. Structure of a B-DNA Dodecamer: Conformation and Dynamics. *Proc. Natl. Acad. Sci.* **1981**, 78 (4), 2179–2183.
- (43) Pjura, P. E.; Grzeskowiak, K.; Dickerson, R. E. Binding of Hoechst 33258 to the Minor Groove of B-DNA. *J. Mol. Biol.* **1987**, 197 (2), 257–271.
- (44) Wei, D.; Wilson, W. D.; Neidle, S. Small-Molecule Binding to the DNA Minor Groove Is Mediated by a Conserved Water Cluster. *J. Am. Chem. Soc.* **2013**, 135 (4), 1369–1377.
- (45) Brown, D. G.; Sanderson, M. R.; Skelly, J. V.; Jenkins, T. C.; Brown, T.; Garman, E.; Stuart, D. I.; Neidle, S. Crystal Structure of a Berenil-dodecanucleotide Complex: The Role of Water in Sequence-specific Ligand Binding. *EMBO J.* **1990**, 9 (4), 1329–1334.
- (46) Senerovic, L.; Zivkovic, M. D.; Veselinovic, A.; Pavic, A.; Djuran, M. I.; Rajkovic, S.; Nikodinovic-Runic, J. Synthesis and Evaluation of Series of Diazine-Bridged Dinuclear Platinum (II) Complexes through in Vitro Toxicity and Molecular Modeling: Correlation between Structure and Activity of Pt (II) Complexes. *J. Med. Chem.* **2015**, 58 (3), 1442–1451.
- (47) Kamal, A.; Reddy, K. S.; Khan, M. N. A.; Shetti, R. V.; Ramaiah, M. J.; Pushpavalli, S.; Srinivas, C.; Pal-Bhadra, M.; Chourasia, M.; Sastry, G. N. Synthesis, DNA-Binding Ability and Anticancer Activity of Benzothiazole/Benzoxazole–Pyrrolo [2, 1-c][1, 4] Benzodiazepine Conjugates. *Bioorg. Med. Chem.* **2010**, 18 (13), 4747–4761.
- (48) Yang, M.; Zhang, H.; Wang, W.; Wang, X. Design, Synthesis, and Evaluation of Bis-Benzothiazole Derivatives as DNA Minor Groove Binding Agents. *J. Heterocycl. Chem.* **2018**, 55 (1), 360–365.
- (49) Sun, Y.; Ji, F.; Liu, R.; Lin, J.; Xu, Q.; Gao, C. Interaction Mechanism of 2-Aminobenzothiazole with Herring Sperm DNA. *J. Lumin.* **2012**, 132 (2), 507–512.
- (50) Keene, F. R.; Smith, J. A.; Collins, J. G. Metal Complexes as Structure-Selective Binding Agents for Nucleic Acids. *Coord. Chem. Rev.* **2009**, 253 (15–16), 2021–

- 2035.
- (51) Bergamo, A.; Dyson, P. J.; Sava, G. The Mechanism of Tumour Cell Death by Metal-Based Anticancer Drugs Is Not Only a Matter of DNA Interactions. *Coord. Chem. Rev.* **2018**, *360*, 17–33.
- (52) Wu, Y.; Bhattacharyya, D.; King, C. L.; Baskerville-Abraham, I.; Huh, S.-H.; Boysen, G.; Swenberg, J. A.; Temple, B.; Campbell, S. L.; Chaney, S. G. Solution Structures of a DNA Dodecamer Duplex with and without a Cisplatin 1, 2-d (GG) Intrastrand Cross-Link: Comparison with the Same DNA Duplex Containing an Oxaliplatin 1, 2-d (GG) Intrastrand Cross-Link. *Biochemistry* **2007**, *46* (22), 6477–6487.
- (53) Ivani, I.; Dans, P. D.; Noy, A.; Pérez, A.; Faustino, I.; Hospital, A.; Walther, J.; Andrio, P.; Goñi, R.; Balaceanu, A. Parmbsc1: A Refined Force Field for DNA Simulations. *Nat. Methods* **2016**, *13* (1), 55.
- (54) Cheatham III, T. E.; Cieplak, P.; Kollman, P. A. A Modified Version of the Cornell et Al. Force Field with Improved Sugar Pucker Phases and Helical Repeat. *J. Biomol. Struct. Dyn.* **1999**, *16* (4), 845–862.
- (55) Darden, T.; York, D.; Pedersen, L. Particle Mesh Ewald: An $N \cdot \log(N)$ Method for Ewald Sums in Large Systems. *J. Chem. Phys.* **1993**, *98* (12), 10089–10092.
- (56) Kollman, P. A.; Massova, I.; Reyes, C.; Kuhn, B.; Huo, S.; Chong, L.; Lee, M.; Lee, T.; Duan, Y.; Wang, W. Calculating Structures and Free Energies of Complex Molecules: Combining Molecular Mechanics and Continuum Models. *Acc. Chem. Res.* **2000**, *33* (12), 889–897.
- (57) Špačková, N.; Cheatham, T. E.; Ryjáček, F.; Lankaš, F.; Van Meervelt, L.; Hobza, P.; Šponer, J. Molecular Dynamics Simulations and Thermodynamics Analysis of DNA– Drug Complexes. Minor Groove Binding between 4', 6-Diamidino-2-Phenylindole and DNA Duplexes in Solution. *J. Am. Chem. Soc.* **2003**, *125* (7), 1759–1769.
- (58) Hou, T.; Wang, J.; Li, Y.; Wang, W. Assessing the Performance of the MM/PBSA and MM/GBSA Methods. 1. The Accuracy of Binding Free Energy Calculations Based on Molecular Dynamics Simulations. *J. Chem. Inf. Model.* **2010**, *51* (1), 69–82.
- (59) Jawad, B.; Poudel, L.; Podgornik, R.; Steinmetz, N. F.; Ching, W.-Y. Molecular Mechanism and Binding Free Energy of Doxorubicin Intercalation in DNA. *Phys. Chem. Chem. Phys.* **2019**, *21* (7), 3877–3893.

- (60) Misra, V. K.; Honig, B. On the Magnitude of the Electrostatic Contribution to Ligand-DNA Interactions. *Proc. Natl. Acad. Sci.* **1995**, *92* (10), 4691–4695.
- (61) Miller III, B. R.; McGee Jr, T. D.; Swails, J. M.; Homeyer, N.; Gohlke, H.; Roitberg, A. E. MMPBSA. Py: An Efficient Program for End-State Free Energy Calculations. *J. Chem. Theory Comput.* **2012**, *8* (9), 3314–3321.
- (62) Sitkoff, D.; Sharp, K. A.; Honig, B. Accurate Calculation of Hydration Free Energies Using Macroscopic Solvent Models. *J. Phys. Chem.* **1994**, *98* (7), 1978–1988.
- (63) Gieseck, R. L.; Risko, C.; Bredas, J.-L. Distinguishing the Effects of Bond-Length Alternation versus Bond-Order Alternation on the Nonlinear Optical Properties of π -Conjugated Chromophores. *J. Phys. Chem. Lett.* **2015**, *6* (12), 2158–2162.
- (64) Wang, Y.; Liu, Q.; Qiu, L.; Wang, T.; Yuan, H.; Lin, J.; Luo, S. Molecular Structure, IR Spectra, and Chemical Reactivity of Cisplatin and Transplatin: DFT Studies, Basis Set Effect and Solvent Effect. *Spectrochim. Acta Part A Mol. Biomol. Spectrosc.* **2015**, *150*, 902–908.
- (65) Coates, J. Interpretation of Infrared Spectra, a Practical Approach. *Encycl. Anal. Chem. Appl. theory Instrum.* **2006**.
- (66) Goodsell, D.; Dickerson, R. E. Isohelical Analysis of DNA Groove-Binding Drugs. *J. Med. Chem.* **1986**, *29* (5), 727–733.
- (67) Jalili, S.; Maddah, M. Molecular Dynamics Simulation of the Sliding of Distamycin Anticancer Drug along DNA: Interactions and Sequence Selectivity. *J. Iran. Chem. Soc.* **2017**, *14* (3), 531–540.
- (68) Nair, M. S.; D’Mello, S.; Pant, R.; Poluri, K. M. Binding of Resveratrol to the Minor Groove of DNA Sequences with AATT and TTAA Segments Induces Differential Stability. *J. Photochem. Photobiol. B Biol.* **2017**, *170*, 217–224.
- (69) Nunn, C. M.; Garman, E.; Neidle, S. Crystal Structure of the DNA Decamer d(CGCAATTGCG) Complexed with the Minor Groove Binding Drug Netropsin. *Biochemistry* **1997**, *36* (16), 4792–4799.
- (70) Pereira, B. T. L.; Gonçalves, M. A.; Mancini, D. T.; Kuca, K.; Ramalho, T. C. First Attempts of the Use of ^{195}Pt NMR of Phenylbenzothiazole Complexes as Spectroscopic Technique for the Cancer Diagnosis. *Molecules* **2019**, *24* (21), 3970.
- (71) Still, B. M.; Kumar, P. G. A.; Aldrich-Wright, J. R.; Price, W. S. ^{195}Pt NMR—

- Theory and Application. *Chem. Soc. Rev.* **2007**, 36 (4), 665–686.
- (72) Priqueler, J. R. L.; Butler, I. S.; Rochon, F. D. An Overview of ^{195}Pt Nuclear Magnetic Resonance Spectroscopy. *Appl. Spectrosc. Rev.* **2006**, 41 (3), 185–226.

TABLE OF CONTENTS GRAPHIC



SUPPORTING INFORMATION

SECTION S1

QM calculations

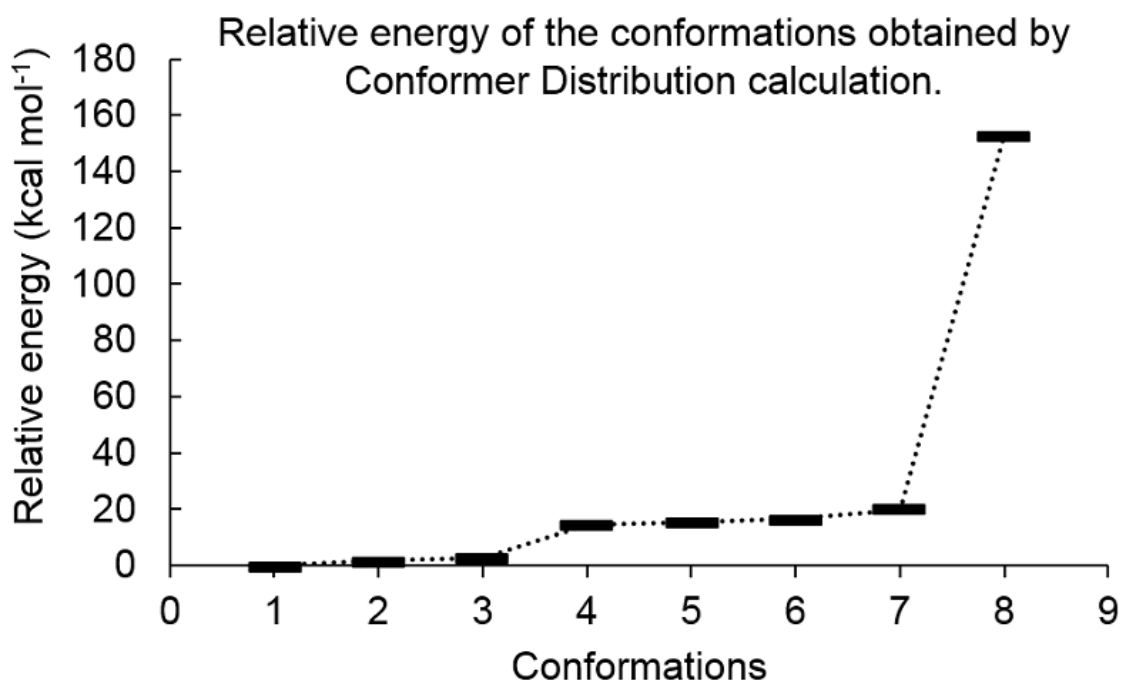


Figure S1.1. Energy of the conformations obtained after the conformational search of the platinum (II) complex.

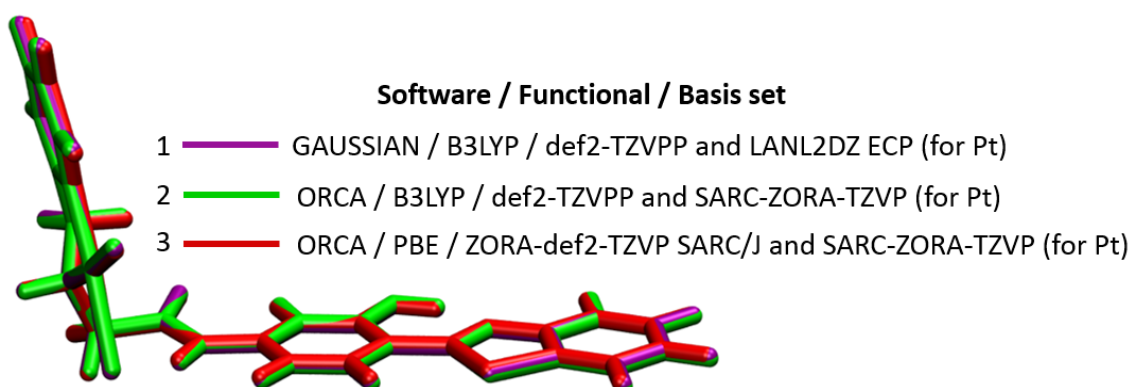


Figure S1.2. Structural projection of platinum (II) complex optimized with different levels of theory.

Table S1.1 Bond length (Å) and RMSD (Å) values for platinum (II) complex optimized at different levels of theory.

Structures	PT-W1 (Å)	PT-W2 (Å)	PT-N3 (Å)	PT-N4 (Å)	RMSD (Å)
1	2.336	2.315	2.127	2.044	0.0649
2	2.325	2.307	2.120	2.043	0.0827
3	2.292	2.274	2.085	2.010	0.0000

BLA Analysis

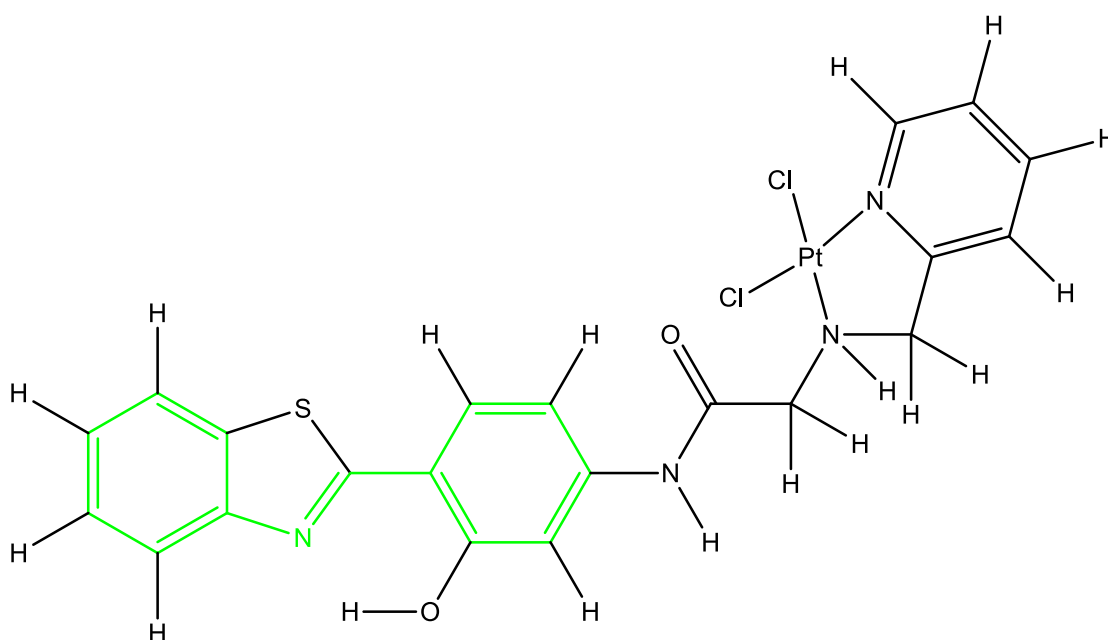


Figure S1.3. Part of the complex analyzed by BLA (green).

Table S1.2 Values of BLA (in Angstrom) for the platinum (II) complex computed on the DFT optimized structure and the MD average obtained with the new and the GAFF force fields.

Platinum (II) complex	BLA
GAUSSIAN / B3LYP / def2-TZVPP and LANL2DZ ECP (for Pt)	0.022
ORCA / B3LYP / def2-TZVPP and SARC-ZORA-TZVP (for Pt)	0.022
ORCA / PBE / ZORA-def2-TZVP SARC/J and SARC-ZORA-TZVP (for Pt)	0.024
New_FF	0.021 ± 0.007
GAFF	0.008 ± 0.006

SECTION S2

Parameters set for *cis*-dichloro(2-aminomethylpyridine)platinum (II) bonded to 2-(4'-amino2'-hydroxyphenyl)benzothiazole (AHBT)

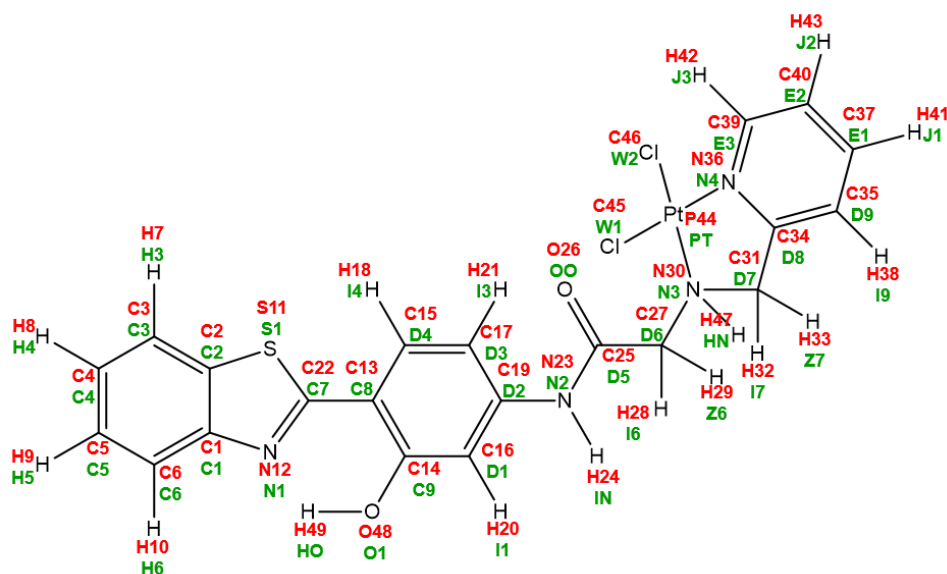


Figure S2.1. Atom names (in red) and atom types (in green).

MASS

W1	35.45	0.0
W2	35.45	0.0
C3	12.01	0.0
C1	12.01	0.0
C2	12.01	0.0
C4	12.01	0.0
C5	12.01	0.0
C6	12.01	0.0
H3	1.008	0.0
H4	1.008	0.0
H5	1.008	0.0
H6	1.008	0.0
S1	32.06	0.0
N1	14.01	0.0
C8	12.01	0.0
C9	12.01	0.0
D4	12.01	0.0
D1	12.01	0.0
D3	12.01	0.0
I4	1.008	0.0
D2	12.01	0.0
I1	1.008	0.0

I3 1.008 0.0
C7 12.01 0.0
N2 14.01 0.0
IN 1.008 0.0
D5 12.01 0.0
OO 15.99 0.0
D6 12.01 0.0
I6 1.008 0.0
N3 14.01 0.0
D7 12.01 0.0
I7 1.008 0.0
D8 12.01 0.0
D9 12.01 0.0
N4 14.01 0.0
E1 12.01 0.0
I9 1.008 0.0
E3 12.01 0.0
E2 12.01 0.0
J1 1.008 0.0
J3 1.008 0.0
J2 1.008 0.0
PT 195.1 0.0
HN 1.008 0.0
O1 15.99 0.0
HO 1.008 0.0
Z6 1.008 0.0
Z7 1.008 0.0

BOND

C1	C2	288.075	1.4099
C1	C6	394.616	1.3972
C1	N1	365.486	1.3769
C2	C3	400.195	1.3913
C2	S1	222.240	1.7395
C3	C4	413.375	1.3872
C3	H3	372.686	1.0812
C4	C5	383.286	1.4001
C4	H4	371.999	1.0816
C5	C6	420.111	1.3843
C5	H5	371.797	1.0816
C6	H6	373.735	1.0812
S1	C7	177.223	1.7678
N1	C7	481.430	1.3067
C8	C9	407.793	1.4178
C8	D4	386.411	1.4043
C8	C7	373.929	1.4487
C9	D1	399.282	1.3965
C9	O1	468.101	1.3398
D4	D3	444.483	1.3738
D4	I4	370.401	1.0822

D1	D2	414.876	1.3884
D1	I1	387.847	1.0763
D3	D2	382.668	1.4067
D3	I3	372.966	1.0813
D2	N2	397.897	1.4042
N2	IN	424.089	1.0193
N2	D5	472.298	1.3559
D5	OO	782.227	1.2221
D5	D6	269.930	1.5336
D6	I6	346.947	1.0908
D6	Z6	358.733	1.0863
D6	N3	298.778	1.4939
N3	D7	255.902	1.4875
N3	PT	122.185	2.1268
N3	HN	444.928	1.0168
D7	I7	350.953	1.0899
D7	Z7	344.141	1.0920
D7	D8	264.174	1.5007
D8	D9	410.149	1.3858
D8	N4	319.621	1.3501
D9	E1	414.665	1.3877
D9	I9	374.012	1.0810
N4	E3	432.064	1.3428
N4	PT	138.395	2.0443
E1	E2	413.404	1.3874
E1	J1	373.851	1.0813
E3	E2	414.863	1.3832
E3	J3	373.914	1.0806
E2	J2	376.682	1.0802
PT	W1	120.775	2.3357
PT	W2	133.317	2.3151
O1	HO	399.416	0.9876

ANGLE

C2	C1	C6	22.965	119.65
C2	C1	N1	27.048	114.58
C6	C1	N1	29.478	125.77
C1	C2	C3	22.159	121.36
C1	C2	S1	26.308	109.39
C3	C2	S1	26.568	129.24
C2	C3	C4	23.235	118.19
C2	C3	H3	23.465	121.11
C4	C3	H3	23.389	120.70
C3	C4	C5	23.816	120.91
C3	C4	H4	23.863	119.42
C5	C4	H4	23.838	119.67
C4	C5	C6	23.859	120.98
C4	C5	H5	23.902	119.44
C6	C5	H5	23.925	119.58
C1	C6	C5	23.599	118.91

C1	C6	H6	22.860	119.63
C5	C6	H6	22.796	121.46
C2	S1	C7	28.193	89.44
C1	N1	C7	34.757	112.65
C9	C8	D4	27.366	117.81
C9	C8	C7	76.672	120.30
D4	C8	C7	63.506	121.89
C8	C9	D1	27.259	120.45
C8	C9	O1	62.830	122.43
D1	C9	O1	54.516	117.13
C8	D4	D3	25.242	121.99
C8	D4	I4	24.689	119.32
D3	D4	I4	25.153	118.70
C9	D1	D2	24.877	120.08
C9	D1	I1	23.085	118.64
D2	D1	I1	23.193	121.28
D4	D3	D2	24.041	119.52
D4	D3	I3	24.278	120.56
D2	D3	I3	24.436	119.92
D1	D2	D3	25.923	120.15
D1	D2	N2	50.767	123.43
D3	D2	N2	48.831	116.41
S1	C7	N1	36.508	113.93
S1	C7	C8	46.554	122.50
N1	C7	C8	58.937	123.57
D2	N2	IN	35.039	115.28
D2	N2	D5	58.131	128.75
IN	N2	D5	39.006	115.46
N2	D5	OO	60.893	125.95
N2	D5	D6	65.285	114.54
OO	D5	D6	54.916	119.50
D5	D6	I6	15.961	106.28
D5	D6	Z6	15.985	112.03
D5	D6	N3	51.535	112.96
I6	D6	Z6	6.089	110.10
I6	D6	N3	19.447	109.05
Z6	D6	N3	19.875	106.42
D6	N3	D7	27.674	113.21
D6	N3	PT	21.469	119.46
D6	N3	HN	6.667	105.99
D7	N3	PT	12.073	107.73
D7	N3	HN	6.022	108.41
PT	N3	HN	4.543	100.89
N3	D7	I7	12.737	107.46
N3	D7	Z7	13.244	110.82
N3	D7	D8	17.553	111.18
I7	D7	Z7	5.364	106.91
I7	D7	D8	9.317	109.15
Z7	D7	D8	11.291	111.14
D7	D8	D9	27.927	122.27

D7	D8	N4	19.527	116.47
D9	D8	N4	24.785	121.20
D8	D9	E1	24.325	119.42
D8	D9	I9	23.939	119.53
E1	D9	I9	23.893	121.05
D8	N4	E3	24.113	119.65
D8	N4	PT	16.630	115.28
E3	N4	PT	26.072	124.94
D9	E1	E2	23.960	118.78
D9	E1	J1	23.727	120.39
E2	E1	J1	23.740	120.83
N4	E3	E2	25.787	121.65
N4	E3	J3	28.037	115.23
E2	E3	J3	24.409	123.11
E1	E2	E3	24.731	119.29
E1	E2	J2	23.603	121.45
E3	E2	J2	23.748	119.26
N3	PT	N4	8.942	81.08
N3	PT	W1	24.394	94.03
N4	PT	W2	22.570	94.38
W1	PT	W2	24.146	90.46
C9	O1	HO	81.325	108.15
N3	PT	W2	6.182	175.33
N4	PT	W1	6.629	177.73

DIHE

C6-C1-C2-C3	1	0.4486	180.00	2.000
C6-C1-C2-S1	1	0.3824	180.00	2.000
N1-C1-C2-C3	1	0.3650	180.00	2.000
N1-C1-C2-S1	1	0.5410	180.00	2.000
C2-C1-C6-C5	1	0.5612	180.00	2.000
C2-C1-C6-H6	1	0.5230	180.00	2.000
N1-C1-C6-C5	1	0.5746	180.00	2.000
N1-C1-C6-H6	1	0.6192	180.00	2.000
C2-C1-N1-C7	1	0.6165	180.00	2.000
C6-C1-N1-C7	1	0.4955	180.00	2.000
C1-C2-C3-C4	1	0.5466	180.00	2.000
C1-C2-C3-H3	1	0.5236	180.00	2.000
S1-C2-C3-C4	1	0.5703	180.00	2.000
S1-C2-C3-H3	1	0.5645	180.00	2.000
C1-C2-S1-C7	1	0.4593	180.00	2.000
C3-C2-S1-C7	1	0.3693	180.00	2.000
C2-C3-C4-C5	1	0.6637	180.00	2.000
C2-C3-C4-H4	1	0.6150	180.00	2.000
H3-C3-C4-C5	1	0.5707	180.00	2.000
H3-C3-C4-H4	1	0.6239	180.00	2.000
C3-C4-C5-C6	1	0.6819	180.00	2.000
C3-C4-C5-H5	1	0.6031	180.00	2.000
H4-C4-C5-C6	1	0.5946	180.00	2.000
H4-C4-C5-H5	1	0.6267	180.00	2.000

C4-C5-C6-C1	1	0.6696	180.00	2.000
C4-C5-C6-H6	1	0.5773	180.00	2.000
H5-C5-C6-C1	1	0.6324	180.00	2.000
H5-C5-C6-H6	1	0.6432	180.00	2.000
C2-S1-C7-N1	1	0.6427	180.00	2.000
C2-S1-C7-C8	1	0.7702	180.00	2.000
C1-N1-C7-S1	1	0.7855	180.00	2.000
C1-N1-C7-C8	1	0.8479	180.00	2.000
D4-C8-C9-D1	1	0.4867	180.00	2.000
D4-C8-C9-O1	1	0.7578	180.00	2.000
C7-C8-C9-D1	1	0.5836	180.00	2.000
C7-C8-C9-O1	1	0.9306	180.00	2.000
C9-C8-D4-D3	1	0.5575	180.00	2.000
C9-C8-D4-I4	1	0.4856	180.00	2.000
C7-C8-D4-D3	1	0.5991	180.00	2.000
C7-C8-D4-I4	1	0.5304	180.00	2.000
C9-C8-C7-S1	1	0.4970	180.00	2.000
C9-C8-C7-N1	1	0.7325	180.00	2.000
D4-C8-C7-S1	1	0.5392	180.00	2.000
D4-C8-C7-N1	1	0.9427	180.00	2.000
C8-C9-D1-D2	1	0.5196	180.00	2.000
C8-C9-D1-I1	1	0.5175	180.00	2.000
O1-C9-D1-D2	1	0.7148	180.00	2.000
O1-C9-D1-I1	1	0.7352	180.00	2.000
C8-C9-O1-HO	1	1.3779	180.00	2.000
D1-C9-O1-HO	1	1.8486	180.00	2.000
C8-D4-D3-D2	1	0.6173	180.00	2.000
C8-D4-D3-I3	1	0.5958	180.00	2.000
I4-D4-D3-D2	1	0.5854	180.00	2.000
I4-D4-D3-I3	1	0.6200	180.00	2.000
C9-D1-D2-D3	1	0.4900	180.00	2.000
C9-D1-D2-N2	1	0.5860	180.00	2.000
I1-D1-D2-D3	1	0.5503	180.00	2.000
I1-D1-D2-N2	1	0.6174	180.00	2.000
D4-D3-D2-D1	1	0.5170	180.00	2.000
D4-D3-D2-N2	1	0.5299	180.00	2.000
I3-D3-D2-D1	1	0.4718	180.00	2.000
I3-D3-D2-N2	1	0.5525	180.00	2.000
D1-D2-N2-IN	1	0.3962	180.00	2.000
D1-D2-N2-D5	1	0.3200	180.00	2.000
D3-D2-N2-IN	1	0.4011	180.00	2.000
D3-D2-N2-D5	1	0.4073	180.00	2.000
D2-N2-D5-OO	1	0.7371	180.00	2.000
D2-N2-D5-D6	1	0.7688	180.00	2.000
IN-N2-D5-OO	1	1.1007	180.00	2.000
IN-N2-D5-D6	1	0.8725	180.00	2.000
N2-D5-D6-I6	1	0.1375	0.00	6.000
N2-D5-D6-Z6	1	0.1372	0.00	6.000
N2-D5-D6-N3	1	0.1891	0.00	6.000
OO-D5-D6-I6	1	0.1455	0.00	6.000

OO-D5-D6-Z6	1	0.1333	0.00	6.000
OO-D5-D6-N3	1	0.1771	0.00	6.000
D5-D6-N3-D7	1	0.7232	0.00	3.000
D5-D6-N3-PT	1	0.7527	110.19	3.000
D5-D6-N3-HN	1	0.9061	0.00	3.000
I6-D6-N3-D7	1	0.4027	0.00	3.000
I6-D6-N3-PT	1	0.4423	0.00	3.000
I6-D6-N3-HN	1	0.4339	0.00	3.000
Z6-D6-N3-D7	1	0.4283	0.00	3.000
Z6-D6-N3-PT	1	0.4042	0.00	3.000
Z6-D6-N3-HN	1	0.4288	0.00	3.000
D6-N3-D7-I7	1	0.5808	134.27	3.000
D6-N3-D7-Z7	1	0.5785	250.75	3.000
D6-N3-D7-D8	1	0.6891	14.89	3.000
PT-N3-D7-I7	1	0.5444	268.60	3.000
PT-N3-D7-Z7	1	0.4989	25.08	3.000
PT-N3-D7-D8	1	0.2957	149.22	3.000
HN-N3-D7-I7	1	0.4241	16.98	3.000
HN-N3-D7-Z7	1	0.4068	133.46	3.000
HN-N3-D7-D8	1	0.3752	257.59	3.000
D6-N3-PT-N4	1	1.0368	332.45	3.000
D6-N3-PT-W1	1	1.3583	150.44	3.000
D7-N3-PT-N4	1	0.3112	201.48	3.000
D7-N3-PT-W1	1	0.8134	19.47	3.000
HN-N3-PT-N4	1	0.5397	87.96	3.000
HN-N3-PT-W1	1	0.7426	265.95	3.000
N3-D7-D8-D9	1	0.0549	23.65	6.000
N3-D7-D8-N4	1	0.0541	0.00	6.000
I7-D7-D8-D9	1	0.1452	265.27	6.000
I7-D7-D8-N4	1	0.1568	0.00	6.000
Z7-D7-D8-D9	1	0.1278	0.00	6.000
Z7-D7-D8-N4	1	0.1391	0.00	6.000
D7-D8-D9-E1	1	0.4803	180.00	2.000
D7-D8-D9-I9	1	0.5323	180.00	2.000
N4-D8-D9-E1	1	0.5131	180.00	2.000
N4-D8-D9-I9	1	0.5174	180.00	2.000
D7-D8-N4-E3	1	0.3897	180.00	2.000
D7-D8-N4-PT	1	0.4043	180.00	2.000
D9-D8-N4-E3	1	0.3973	180.00	2.000
D9-D8-N4-PT	1	0.3560	180.00	2.000
D8-D9-E1-E2	1	0.6408	180.00	2.000
D8-D9-E1-J1	1	0.5972	180.00	2.000
I9-D9-E1-E2	1	0.6033	180.00	2.000
I9-D9-E1-J1	1	0.6731	180.00	2.000
D8-N4-E3-E2	1	0.5245	180.00	2.000
D8-N4-E3-J3	1	0.5800	180.00	2.000
PT-N4-E3-E2	1	0.4788	180.00	2.000
PT-N4-E3-J3	1	0.5730	180.00	2.000
D8-N4-PT-N3	1	0.0375	171.73	6.000
D8-N4-PT-W2	1	0.1175	352.82	6.000

E3-N4-PT-N3	1	0.0475	347.57	6.000
E3-N4-PT-W2	1	0.1084	168.65	6.000
D9-E1-E2-E3	1	0.6701	180.00	2.000
D9-E1-E2-J2	1	0.6455	180.00	2.000
J1-E1-E2-E3	1	0.5937	180.00	2.000
J1-E1-E2-J2	1	0.6853	180.00	2.000
N4-E3-E2-E1	1	0.6710	180.00	2.000
N4-E3-E2-J2	1	0.6393	180.00	2.000
J3-E3-E2-E1	1	0.6474	180.00	2.000
J3-E3-E2-J2	1	0.7208	180.00	2.000
D6-N3-PT-W2	1	1.3583	345.85	3.000
D7-N3-PT-W2	1	0.8134	214.88	3.000
D8-N4-PT-W1	1	0.1175	149.38	6.000
W2-PT-N3-HN	1	0.7426	101.36	3.000
E3-N4-PT-W1	1	0.1084	325.22	6.000

NONBON

C1	1.9080	0.0860	!
C2	1.9080	0.0860	!
C3	1.9080	0.0860	!
C4	1.9080	0.0860	!
C5	1.9080	0.0860	!
C6	1.9080	0.0860	!
H6	1.4590	0.0150	!
S1	2.0000	0.2500	!
N1	1.8240	0.1700	!
C8	1.9080	0.0860	!
C9	1.9080	0.0860	!
D4	1.9080	0.0860	!
D1	1.9080	0.0860	!
D3	1.9080	0.0860	!
I4	1.4590	0.0150	!
D2	1.9080	0.0860	!
I1	1.4590	0.0150	!
I3	1.4590	0.0150	!
C7	1.9080	0.0860	!
N2	1.8240	0.1700	!
IN	0.6000	0.0157	!
D5	1.9080	0.0860	!
OO	1.6612	0.2100	!
D6	1.9080	0.0860	!
I6	1.3870	0.0157	!
Z6	1.3870	0.0157	!
N3	1.8240	0.1700	!
D7	1.9080	0.0860	!
I7	1.3870	0.0157	!
Z7	1.3870	0.0157	!
D8	1.9080	0.0860	!
D9	1.9080	0.0860	!
N4	1.8240	0.1700	!

```

E1      1.9080  0.0860  !
I9      1.4590  0.0150  !
E3      1.9080  0.0860  !
E2      1.9080  0.0860  !
J1      1.4590  0.0150  !
J3      1.4590  0.0150  !
J2      1.4590  0.0150  !
PT      2.0735  1.0550  !
W1      1.9480  0.2650  !
W2      1.9480  0.2650  !
O1      1.7210  0.2104  !
H3      1.4590  0.0150  !
H4      1.4590  0.0150  !
H5      1.4590  0.0150  !
HO      0.0000  0.0000  !
HN      0.6000  0.0157  !
END

```

Table S2.1 Atomic charges (RESP) for platinum (II) complex.

Atom Types	q / e^-
C1	0.26922494
C2	0.15135017
C3	-0.25530844
C4	-0.15877563
C5	-0.07476197
C6	-0.26217407
H6	0.16119514
S1	-0.12994961
N1	-0.39877076
C8	-0.16104897
C9	0.47552757
D4	-0.10186023
D1	-0.48459717
D3	-0.40603759
I4	0.17990829
D2	0.51934629
I1	0.24266736

I3	0.17311046
C7	0.22853780
N2	-0.70713730
IN	0.36117404
D5	0.80563809
OO	-0.53456657
D6	-0.43615790
I6	0.16565574
Z6	0.16208379
N3	0.06976426
D7	-0.31149842
I7	0.12463467
Z7	0.15675010
D8	0.41201126
D9	-0.34837936
N4	-0.08185593
E1	0.007656262
I9	0.17664619
E3	0.15793931
E2	-0.26215821
J1	0.13326028
J3	0.08529343
J2	0.16953478
PT	-0.16955026
W1	-0.30887077
W2	-0.29910268
O1	-0.52879841
H3	0.19396777
H4	0.13460882
H5	0.12102157

HO	0.35143015
HN	0.23142173

SECTION S3

Case of study: MD simulations of the platinum (II) complex with DNA

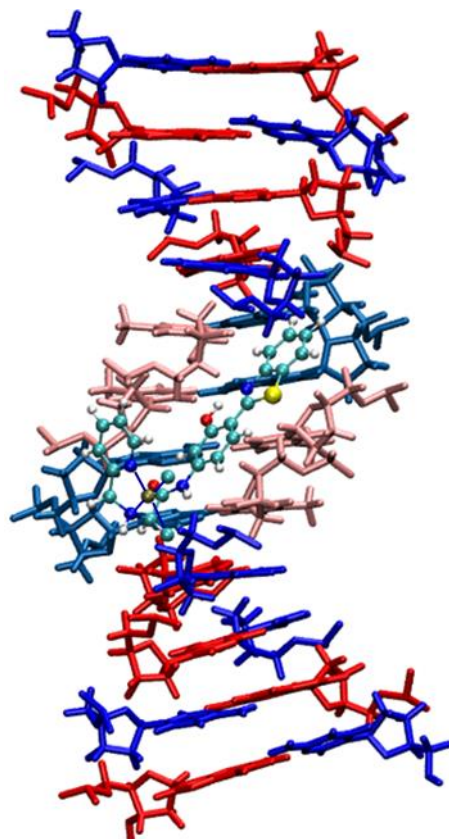


Figure S3.1. Platinum (II) complex in the minor groove of DNA (sequence 5'-CGCGAATTCGCG-3', PDB ID: 1BNA).¹ Cytosine (C) in blue, Guanine (G) in red, Adenine (A) in light blue, Thymine (T) pink.

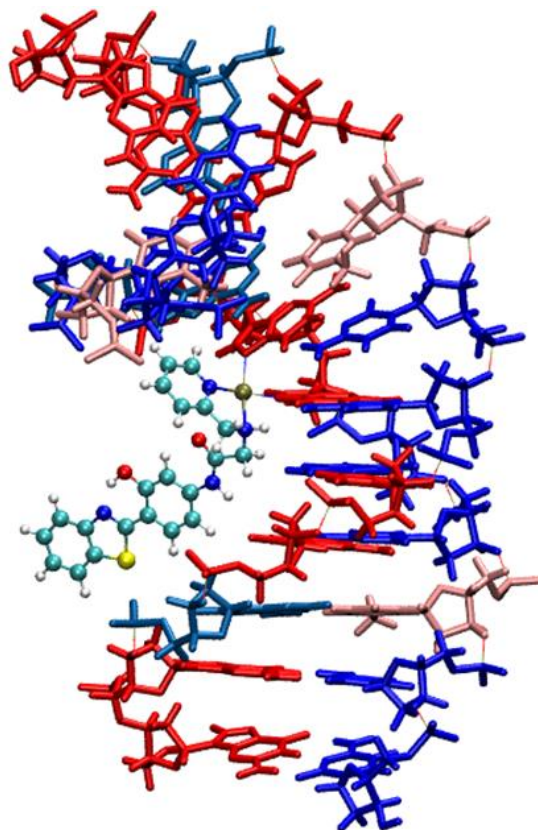


Figure S3.2. Platinum (II) complex bonded in the DNA (sequence 5'-CCTCAG*G*CCTCC-3', PDB ID: 2NPW).² Cytosine (C) in blue, Guanine (G) in red, Adenine (A) in light blue, Thymine (T) in pink.

SECTION S4

Complex coordinated with DNA

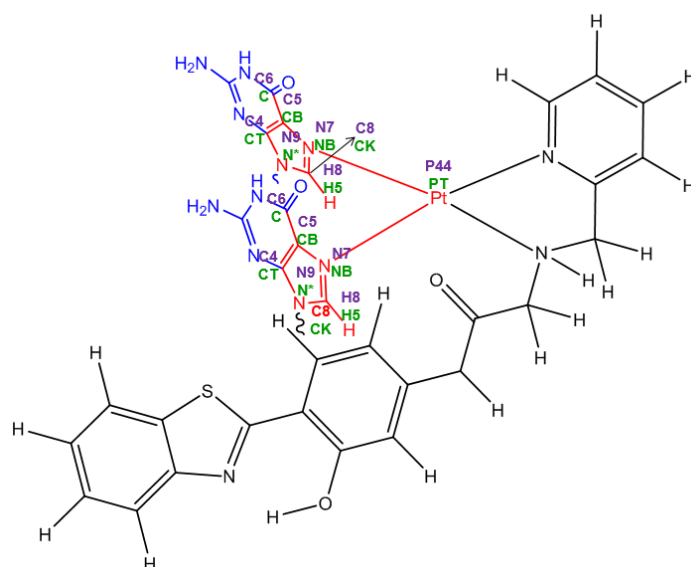


Figure S4.1. Atom names (in purple) and atom types (in green).

BOND

NB PT 143.892 2.0651

ANGLE

NB PT N4 7.000 177.74
 NB PT N3 9.000 171.69
 N3 PT N4 9.693 82.42
 CK NB PT 35.446 125.92
 CB NB PT 39.420 127.86

DIHE

N*-CK-NB-PT 1 0.5132 180.00 2.000
 H5-CK-NB-PT 1 0.3534 180.00 2.000
 PT-NB-CB-C 1 0.2570 180.00 2.000
 PT-NB-CB-CT 1 0.4184 180.00 2.000
 CK-NB-PT-NB 1 0.2450 180.00 6.000
 CB-NB-PT-NB 1 0.2450 180.00 6.000
 CB-NB-PT-N4 1 0.5120 180.00 6.000
 CK-NB-PT-N4 1 0.0512 180.00 6.000
 CK-NB-PT-N3 1 0.0512 180.00 6.000
 CB-NB-PT-N3 1 0.0512 180.00 6.000

Table 2. Atomic charges (RESP) for platinum (II) complex bound to DNA.

Atom Types	q/e^-
C1	0.148910
C2	0.229962
C3	-0.300241
C4	-0.020318
C5	-0.051394
C6	-0.194160
H3	0.249174
H4	0.181979
I5	0.162436
H6	0.190062
S1	-0.010667
N1	-0.148759
C8	0.213187
C9	0.225000
D4	-0.250053

D1	-0.075300
D3	-0.143342
I4	0.232120
D2	0.088505
I1	0.133615
I3	0.193286
C7	0.028426
N2	-0.289468
IN	0.276979
D5	0.380658
OO	-0.372727
D6	0.586505
I6	-0.030197
Z6	-0.030197
N3	-1.158553
D7	0.113566
I7	0.152998
Z7	0.152998
D8	-0.066084
D9	-0.152177
N4	0.261669
E1	0.023893
I9	0.154933
E3	-0.328418
E2	-0.116882
J1	0.167783
J3	0.369097
J2	0.163972
PT	0.584448
HN	0.510384

O1	-0.423530
HO	0.303465

SECTION S5

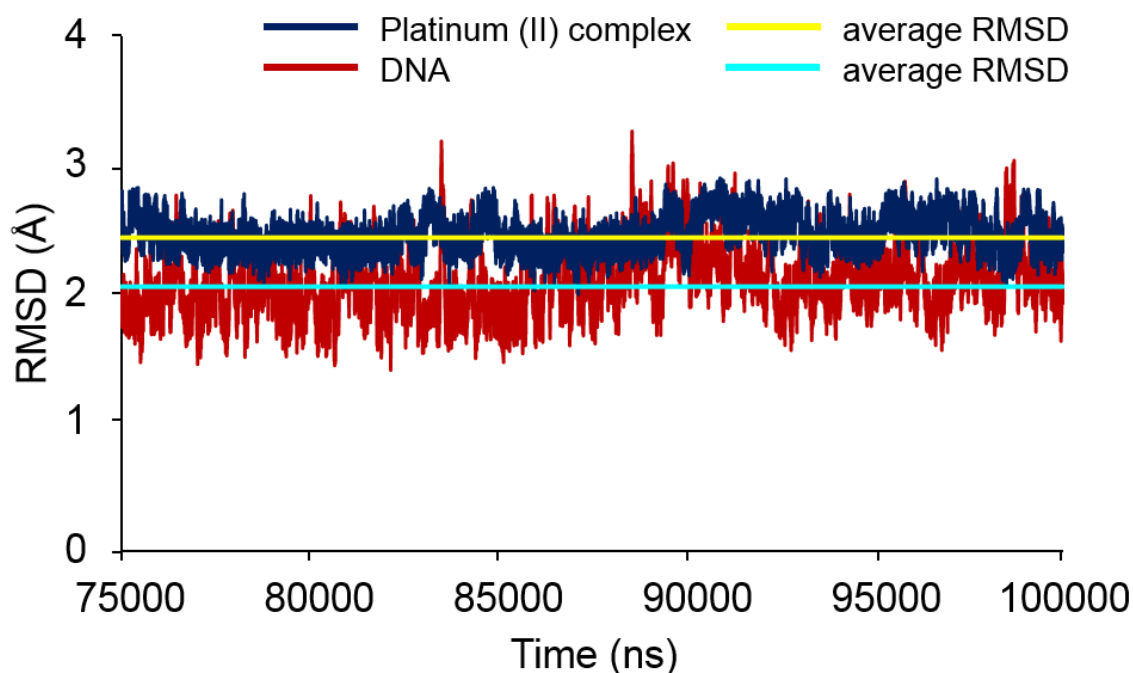


Figure S5.1 RMSD versus time graph calculated for platinum (II) complex (green) and DNA (blue) during 25 ns of the MD simulation.

SECTION S6

The ^{195}Pt -chemical shift parameters were performed in gas phase with the gauge-including atomic orbitals (GIAO)–DFT method. The functional PBEPBE and DHK basis set were used. This base set has been developed for several atoms, especially for calculations of NMR properties, including the platinum atom.³

The calculations were made under the following conditions: (i) N7 coordinated complex of the guanine bases of DNA; (ii) non-covalently interacting complex in the minor groove of DNA; and (iii) complex in the absence of DNA. For (i) and (ii), the average geometries obtained after equilibrium conditions were adopted (last 25 and 25 ns of bound and unbound MD simulation, respectively). The systems (i) and (ii) were cut, given the high computational demand, if larger systems to those used were adopted.

In (i), the complex coordinated with two guanine bases was adopted, while that in (ii), the complex with the two nucleobases closer to the metal was adopted.

References

- (1) Drew, H. R.; Wing, R. M.; Takano, T.; Broka, C.; Tanaka, S.; Itakura, K.; Dickerson, R. E. Structure of a B-DNA Dodecamer: Conformation and Dynamics. *Proc. Natl. Acad. Sci.* **1981**, 78 (4), 2179–2183.
- (2) Wu, Y.; Bhattacharyya, D.; King, C. L.; Baskerville-Abraham, I.; Huh, S.-H.; Boysen, G.; Swenberg, J. A.; Temple, B.; Campbell, S. L.; Chaney, S. G. Solution Structures of a DNA Dodecamer Duplex with and without a Cisplatin 1, 2-d (GG) Intrastrand Cross-Link: Comparison with the Same DNA Duplex Containing an Oxaliplatin 1, 2-d (GG) Intrastrand Cross-Link. *Biochemistry* **2007**, 46 (22), 6477–6487.
- (3) Paschoal, D.; Guerra, C. F.; de Oliveira, M. A. L.; Ramalho, T. C.; Dos Santos, H. F. Predicting Pt-195 NMR Chemical Shift Using New Relativistic All-electron Basis Set. *J. Comput. Chem.* **2016**, 37 (26), 2360–2373.

ANEXO I – Trabalhos desenvolvidos

Letters in Drug Design & Discovery vol. 13, 360-371 (2016)

Send Orders for Reprints to reprints@benthamscience.ae

Letters in Drug Design & Discovery, 2016, 13, 000-000

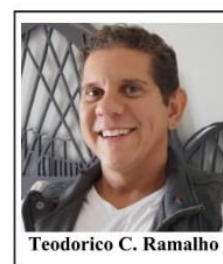
1

Flexibility in the Molecular Design of Acetylcholinesterase Reactivators: Probing Representative Conformations by Chemometric Techniques and Docking/QM Calculations

Willian E.A. de Lima¹, Ander F. Pereira¹, Alexandre A. de Castro¹, Elaine F.F. da Cunha¹ and Teodorico C. Ramalho^{1,2*}

¹Laboratory of Molecular Modeling, Chemistry Department, Federal University of Lavras, Lavras, MG, 37200-000, Brazil

²Center for Basic and Applied Research, University Hradec Kralove, Hradec Kralove, Czech Republic



Teodorico C. Ramalho

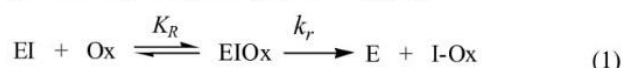
Abstract: Neurotoxic organophosphate compounds (OP) are toxic and acetylcholinesterase (AChE) inhibitors widely used as insecticides and pesticides in agriculture. This is a key enzyme in the search for new strategies for poisoning treatment by means of pesticides and insecticides. The standard OP intoxication treatment involves the administration of an anticholinergic to reduce spasms and convulsion as well as a cationic oxime capable of removing the OP compounds inside the AChE active site to reactivate the enzyme. In this paper, a theoretical strategy combining docking(MM), chemometric analysis and QM calculations was employed to check out the association and kinetic reactivation coefficients associated to oximes, confronting *in vitro* the data found in the literature before. The docking results were selected by means of the principal components analysis and submitted to QM calculations. The calculated thermodynamics and kinetics parameters revealed a good correspondence between the calculated intermolecular energy values of the oximes and experimental results, reinforcing the theoretical findings and confirming the theoretical strategy used as a suitable tool for the prediction of kinetic and thermodynamics parameters, which would be able to collaborate with the design of new oximes more effective.

Keywords: Acetylcholinesterase, oximes, docking, reaction mechanism, organophosphate, chemometrics.

1. INTRODUCTION

The action of neurotoxic organophosphorous (OP), as toxic compounds and Acetylcholinesterase (AChE) inhibitors is very popular [1]. In fact, those compounds are able to stop the cleavage of the neurotransmitter acetylcholine (Ach), which can drive to the irreversible inhibition of AChE (aged), thus causing the cholinergic syndrome. Recently, the growing population has led to the increase of world food production and consequently there is the employment of intense use of OP compounds as insecticides and pesticides in the agricultural activity [2]. In this line, with the use of those compounds in agriculture as well as potential use as chemical warfare agents, there is a concern from the scientific community to design effective antidotes for the intoxication caused by those agents [3]. This outlook has been aggravated, after episodes like the anthrax incident after September 11th in the USA or the use of chemical weapons in the Syrian civil war [4, 5]. Thus, it became quite clear that chemical and biological agents are the first choice weapons for terrorist groups worldwide because of their low cost and ease of use.



This certainly raises the need for continuous research on the development of new acetylcholinesterase reactivators [6, 7]. An important class of OP is the nerve agents, which are correlated in terms of structural properties and activity in biological systems. Other examples are the organophosphorus pesticides and insecticides, which are widely used in agriculture [8]. Currently, one of the most used strategies to circumvent the AChE inhibition by OP compounds is the use of acetylcholinesterase reactivators, which are usually pyridinium oximes. Actually, oximes work as antidotes, because they can reactivate the enzyme as a result of the nucleophilic attack of their hydroxyl groups on the phosphorylated serine residue, removing the OP from the active site, reactivating the enzyme [8, 9]. Accordingly, the reactivation process consists of two steps: 1) there is the combination of the oxime to the inhibited enzyme (EIOx) and then the reactivation of it takes place by the (I-Ox) complex leaving the system (Equation 1) [10].



Where K_R is the dissociation coefficient, which represents the interaction between oxime and the inhibited AChE. k_r stands for the rate constant for the chemical reaction between oxime and OP inside the AChE active site [11].

*Address correspondence to this author at the Department of Federal University of Lavras, P.O. Box: 37200-000, Lavras, Brazil; Tel/Fax: +55-35-38291271, E-mail: teo@dqi.ufla.br

Mechanistic studies of new oximes reactivators of human butyryl cholinesterase inhibited by cyclosarin and sarin

Willian E. Amaral de Lima^a, Ander Francisco^a, Elaine F.F. da Cunha^a, Zoran Radic^b, Palmer Taylor^b,
 Tanos C.C. França^{c,d,e,*}  and Teodorico C. Ramalho^{a,c,*} 

^aLaboratory of Molecular Modeling, Chemistry Department, Federal University of Lavras, Lavras, MG 37200-000, Brazil; ^bSkaggs School of Pharmacy and Pharmaceutical Sciences, University of California at San Diego, San Diego, CA, USA; ^cLaboratory of Molecular Modeling Applied to the Chemical and Biological Defense (LMCBD), Military Institute of Engineering, Rio de Janeiro, RJ 22290-270, Brazil; ^dDepartment of Chemistry & Biochemistry, Concordia University, Montreal, QC, Canada; ^eFaculty of Informatics and Management, Center for Basic and Applied Research, University of Hradec Kralove, Hradec Kralove, Czech Republic

Communicated by Ramaswamy H. Sarma

(Received 14 February 2016; accepted 11 April 2016)

Butyryl cholinesterase (BChE) has been seen as a key enzyme in the search for new strategies in the treatment of poisoning by organophosphates (OPs), since human BChE (*Hss*BChE), complexed with the appropriate oxime, can be a suitable scavenger and deactivator for OPs in the blood stream. However, the efficacy of *Hss*BChE is limited by its strict stoichiometric scavenging, slow reactivation, and propensity for aging. The improvement of the reactivation rate by new and more efficient oximes could contribute to mitigate this problem and increase the *Hss*BChE efficiency as scavenger. Several oximes have been synthesized and tested with this goal, some with promising results, but the mechanistic aspects of the reactivation reaction are not fully understood yet. In order to better investigate this mechanism, docking and mixed quantum and molecular mechanics combined with principal components analysis were performed here to evaluate the capacity of reactivation and determine the preferred route for the reactivation reaction of two new oximes on *Hss*BChE inhibited by the neurotoxic agents cyclosarin and sarin. Plots of potential energies were calculated and all the transition states of the reactional mechanism were determined. Our results showed a good correlation with experimental data and pointed to the most efficient oxime with both OPs. The protocol used could be a suitable tool for a preliminary evaluation of the *Hss*BChE reactivation rates by new oximes.

Keywords: neurotoxic agents; oximes; butyrylcholinesterase; docking; mechanistic studies and chemometrics

1. Introduction

Intoxication with organophosphates (OPs) is still a thoughtful problem with great implications in chemical defense. Some of these compounds are powerful chemical warfare agents that target the enzymes acetylcholinesterase (AChE) and butyrylcholinesterase (BChE), causing the cholinergic syndrome and death by cardiovascular complications and respiratory compromise. Current therapy to combat OP poisoning involves a cationic oxime reactivator (2-PAM, obidoxime, TMB4, or HI-6) combined with atropine and on occasion an anticonvulsant, but this strategy presents some limitations (Raveh, Grauer, Grunwald, Cohen, & Ashani, 1997; Raveh et al., 1993; Wolfe et al., 1992) like: (1) the incapacity of cationic oximes to penetrate the blood–brain barrier (BBB) and reactivate cholinesterases inside the central and peripheral nervous systems (CNS and PNS); (2) the inexistence of other molecular classes than oximes able to effectively reactivate cholinesterases and (3) the inexistence of an universal oxime, able to reactivate

cholinesterases inhibited by any OP. Some approaches reported in literature to transpose the limitations are commented below.

Koning and co-workers have proposed new oximes with long aliphatic tails able to both bind to the peripheral site of AChE (known for having a great number of hydrophobic residues) in order to increase the affinities for cholinesterases, and also penetrate the BBB (Almeida et al., 2016; Koning, Joosen, Noort, van Zuylen, & Tromp, 2011; Koning, van Grol, & Noort, 2011). These oximes presented promising experimental results. In a different strategy to penetrate the BBB, Sit and coworkers (2011) and Radic and coworkers (2012) have synthesized a series of oximes containing tertiary amine or imidazole protonable functional groups which equilibria between the neutral and protonated species, enables these oximes to cross the BBB and reactivate cholinesterases inside the CNS.

Delfino and Figueroa-Villar (2009) performed a molecular modeling study on other molecular classes as potential cholinesterase reactivators and have proposed

*Corresponding authors. Email: tanos@ime.eb.br (T.C.C. França); teo@dqi.ufla.br (T.C. Ramalho)

Insights into the Drug Repositioning Applied to the Alzheimer's Disease Treatment and Future Perspectives

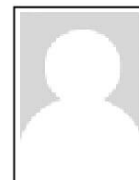
Alexandre A. de Castro^a, Teodorico C. Ramalho^{*a,b}, Elaine F. F. da Cunha^a, Ander F. Pereira^a, Flávia V. Soares^a, Daniel H. S. Leal^{a,c}, and Kamil Kuca^{b,d}

^aLaboratory of Molecular Modeling, Department of Chemistry, Federal University of Lavras, Lavras/MG, 37200-000, Brazil.

^bCenter for Basic and Applied research, University Hradec Kralove, Hradec Kralove, Czech Republic.

^cDepartment of Health Sciences, Federal University of Espírito Santo, São Mateus/ES, 29932-540, Brazil.

^dBiomedical Research Center, University Hospital Hradec Kralove, Hradec Kralove, Czech Republic.



Abstract: Alzheimer's disease is known to be a chronic disease, with an estimated prevalence of about 10–30%, considering the population over 60 years of age. Most patients with this disorder (> 95%) present the sporadic form, being characterized by a late onset (80–90 years of age), and it is the consequence of the failure to clear the amyloid- β ($A\beta$) peptide from the interstices of the brain. Significant numbers of genetic risk factors for the sporadic disease have been researched. Some existing drugs for Alzheimer's disease provide symptomatic benefit for up to 12 months, but there are no approved disease-modifying therapies. In this line, a complementary strategy based on repositioning drugs which are approved for the treatment of other disorders could be interesting. It is noteworthy the fact that some clinical trials indicate that several classes of drugs own potent and beneficial effects on the Alzheimer's disease treatment. In this present work, we present the details and evaluation of these alternative treatments. It is highlighted several compounds with relevant evidence for this purpose, which deserve further investigation to clarify an optimal treatment conditions in the clinical trials of patients with Alzheimer's disease.

Keywords: Alzheimer's disease; neurodegeneration; drug repositioning; tau protein; amyloid- β peptide; pharmacophores.

1. Introduction

Degenerative disorders of the Central Nervous System (CNS) are characterized by an irreversible and progressive loss of neurons located in specific regions of the brain. One of such disturbances is the Alzheimer's Disease (AD), characterized by neuronal losses in hippocampus and cortex causing cognitive malfunctions and memory deficits. It is estimated that AD affects about 10% of the population in the age above 65 years. Although it might occur in any decade of adulthood, it is the most common cause of dementia in elderly people. Over the age of 70, approximately 10% of people show significant memory loss, AD being responsible for more than 50% of these cases [1, 2].

1.1. Alzheimer's disease

Pathophysiologically, AD is marked by the extracellular accumulation of amyloid- β protein ($A\beta$) in amyloid plaques and by the formation of neurofibrillary tangles resulting from the hyperphosphorylation of the protein tau associated with cellular microtubules (Figure 1). The gradual accumulation of these components results in neuronal dysfunction and cell death. Both these biomolecules can be used as biomarkers for AD. The lipid carrier protein known as apoE (apolipoprotein E) also appears to be associated with an increased risk of developing AD (Figure 1) [1, 3].

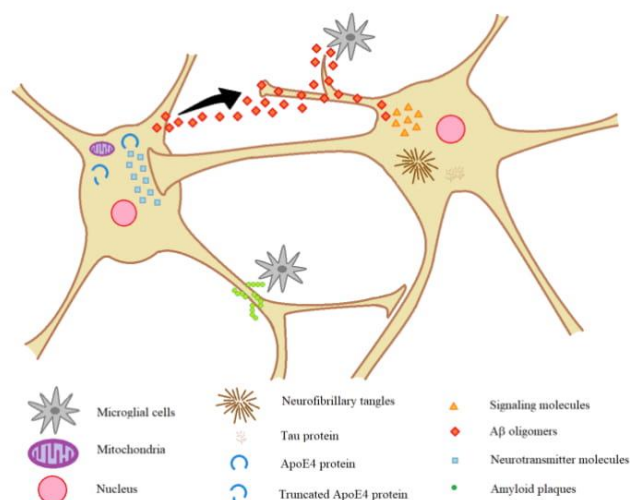


Figure 1. General cell aspects and events of the development of AD (adapted from [4]).



Several neurotransmitter systems are affected by AD, the most striking of which is the lack of neurotransmission by acetylcholine (ACh) (1, Figure 2). The currently available treatments for AD attenuate the symptoms of the disease, but do not affect the evolution of the neurodegenerative process, and are considered as much less effective than, for example, current drugs in use for treatment of other neurodegenerative disorders such as Parkinson's Disease [1, 5].

*Address correspondence: Department of Chemistry, Federal University of Lavras, Lavras/MG, 37200-000, Brazil. Fax: 55 35 3829-1271; Tel: 55 35 3829-1522; E-mail: teo@dqf.ufla.br



Article

Theoretical Studies Applied to the Evaluation of the DFPase Bioremediation Potential against Chemical Warfare Agents Intoxication

Flávia V. Soares¹, Alexandre A. de Castro¹, Ander F. Pereira¹, Daniel H. S. Leal^{1,2},
Daiana T. Mancini¹, Ondrej Krejcar³ , Teodorico C. Ramalho^{1,3} , Elaine F. F. da Cunha¹
and Kamil Kuca^{3,*}

¹ Laboratory of Molecular Modeling, Chemistry Department, Federal University of Lavras, 37200-000 Lavras, MG, Brazil; flaviavillela09@yahoo.com.br (F.V.S.); alexandre.a.castro@hotmail.com (A.A.d.C.); ander.francisco@hotmail.com (A.F.P.); daniel.leal@ufes.br (D.H.S.L.); daianateixeira60@yahoo.com.br (D.T.M.); teo@dqi.ufla.br (T.C.R.); elaine_cunha@dqi.ufla.br (E.F.F.d.C.)

² Department of Health Sciences, Federal University of Espírito Santo, 29932-540 São Mateus, ES, Brazil

³ Center for Basic and Applied Research, Faculty of Informatics and Management, University Hradec Kralove, 50003 Hradec Kralove, Czech Republic; ondrej.krejcar@uhk.cz

* Correspondence: kamil.kuca@uhk.cz; Tel.: +420-495-833-447

Received: 24 March 2018; Accepted: 19 April 2018; Published: 23 April 2018



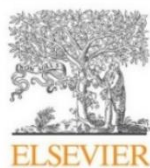
Abstract: Organophosphorus compounds (OP) are part of a group of compounds that may be hazardous to health. They are called neurotoxic agents because of their action on the nervous system, inhibiting the acetylcholinesterase (AChE) enzyme and resulting in a cholinergic crisis. Their high toxicity and rapid action lead to irreversible damage to the nervous system, drawing attention to developing new treatment methods. The diisopropyl fluorophosphatase (DFPase) enzyme has been considered as a potent biocatalyst for the hydrolysis of toxic OP and has potential for bioremediation of this kind of intoxication. In order to investigate the degradation process of the nerve agents Tabun, Cyclosarin and Soman through the wild-type DFPase, and taking into account their stereochemistry, theoretical studies were carried out. The intermolecular interaction energy and other parameters obtained from the molecular docking calculations were used to construct a data matrix, which were posteriorly treated by statistical analyzes of chemometrics, using the PCA (Principal Components Analysis) multivariate analysis. The analyzed parameters seem to be quite important for the reaction mechanisms simulation (QM/MM). Our findings showed that the wild-type DFPase enzyme is stereoselective in hydrolysis, showing promising results for the catalytic degradation of the neurotoxic agents under study, with the degradation mechanism performed through two proposed pathways.

Keywords: organophosphorus compounds; DFPase; tabun; cyclosarin; soman; molecular docking; PCA; QM/MM

1. Introduction

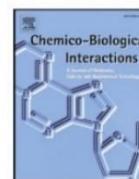
The use of chemical substances in wars was boosted in the 1930s with the discovery of the toxic properties of organophosphorus compounds (OP). Since then, the interest in the synthesis of substances that present toxicity intensified, and more potent compounds were developed, such as the neurotoxic agents, which later came to be used as chemical weapons [1].

These OP agents present structural characteristics which cause them have different activities, being employed as insecticides, herbicides, plant growth regulators, therapeutic agents and chemical weapons [2–4]. The members of this family, called nerve agents or neurotoxic agents, are the most lethal [5], due to their high toxicity. Given these characteristics, they have potential for use as chemical



Contents lists available at ScienceDirect

Chemico-Biological Interactions

journal homepage: www.elsevier.com/locate/chembioint

Development of technologies applied to the biodegradation of warfare nerve agents: Theoretical evidence for asymmetric homogeneous catalysis



Ander Francisco Pereira^a, Alexandre A. de Castro^a, Flavia Villela Soares^a,
Daniel Henriques Soares Leal^{a,c}, Elaine F.F. da Cunha^a, Daiana Teixeira Mancini^a,
Teodorico C. Ramalho^{a,b,*}

^a Laboratory of Molecular Modeling, Department of Chemistry, Federal University of Lavras, Lavras, MG, 37200-000, Brazil

^b Department of Chemistry, Faculty of Science, University of Hradec Kralove, Hradec Kralove, Czech Republic

^c Department of Health Sciences, Federal University of Espírito Santo, São Mateus, ES, 29932-540, Brazil

ARTICLE INFO

Keywords:

OpdA enzyme
Warfare nerve agents
Docking
QM/MM
AIM
FERMO

ABSTRACT

Organophosphorus compounds have been widely employed to the development of warfare nerve agents and pesticides, resulting in a huge number of people intoxicated annually, being a serious problem of public health. Efforts worldwide have been done in order to design new technologies that are capable of combating or even reversing the poisoning caused by these OP nerve agents. In this line, the bioremediation arises as a promising and efficient alternative for this purpose. As an example of degrading enzymes, there is the organophosphate-degrading (OpdA) enzyme from *Agrobacterium radiobacter*, which has been quite investigated experimentally due to its high performance in the degradation of neurotoxic nerve agents. This work aims to look into the structural and electronic details that govern the interaction modes of these compounds in the OpdA active site, with the posterior hydrolysis reaction prediction. Our findings have brought about data about the OpdA performance towards different nerve agents, and among them, we may realize that the degradation efficiency strongly depends on the nerve agent structure and its stereochemistry, being in this case the compound Tabun the one more effectively hydrolyzed. By means of the chemical bonds (AIM) and orbitals (FERMO) analysis, it is suggested that the initial reactivity of the OP nerve agents in the OpdA active site does not necessarily dictate the reactivity and interaction modes over the reaction coordinate.

1. Introduction

High exposures to organophosphorus (OP) pesticides have been a worldwide problem, resulting in the deaths of thousands of people. According to the World Health Organization (WHO), about 3.000.000 people are poisoned by pesticides annually in underdeveloped countries, most of them by OP pesticides, resulting in more than 250.000 deaths [1,2]. Another OP compounds class capable of mass destruction in a quick and efficient manner, is defined as chemical warfare weapons, such as Sarin (GB), Soman (GD) and Tabun (GA) (Fig. 1) [3]. Not so far, Sarin has been used in terrorist attacks in Syria, with more than 3.600 victims [4].

OP compounds are capable of irreversibly inhibiting the Acetylcholinesterase (AChE) enzyme by binding to Ser203 amino acid residue present at its active site [5,6]. The human AChE is an enzyme

belonging to the cholinesterase family, being responsible for the finalization of the transmission of nerve impulses in the cholinergic synapses by the hydrolysis of the acetylcholine (ACh) neurotransmitter; its active site contains the catalytic triad Ser203-His447-Glu334 [7]. The reaction between OP neurotoxic agents and AChE interrupts the hydrolysis of the ACh, resulting in a cholinergic syndrome as a consequence of the accumulation of ACh in its receptors [8]. It is known that the spontaneous reactivation process of the enzyme is inefficient due to the strong covalent bond formed between the atoms of phosphorus (from the OP) and oxygen (from the Ser203 residue); however, this process can be sped up by the administration of a strong nucleophile, such as pyridine aldoximes, which are capable of removing the phosphate group bonded to Ser203 and reactivating the inhibited enzyme [9]. However, the efficacy of these antidotes is limited because an oxime can be extremely effective in reactivating the AChE inhibited by

Abbreviations: ACh, acetylcholine; AChE, acetylcholinesterase; OP, organophosphorus; OpdA, organophosphate-degrading enzyme; OPH, organophosphorus hydrolase enzyme; PLP, piecewise linear potential; R_P and S_P , R and S enantiomers assigned over the phosphorus atom, respectively; TS, transition state

* Corresponding author. Department of Chemistry, University Town, Federal University of Lavras, P. O. Box 3037, Lavras, MG, 37200-000, Brazil.

E-mail address: teo@ufla.br (T.C. Ramalho).

<https://doi.org/10.1016/j.cbi.2019.06.007>

Received 15 January 2019; Received in revised form 21 April 2019; Accepted 3 June 2019

Available online 04 June 2019

0009-2797/ © 2019 Published by Elsevier B.V.

Asymmetric biodegradation of the nerve agents Sarin and VX by human dUTPase: Chemometrics, Molecular Docking and Hybrid QM/MM calculations

Alexandre A. de Castro^a, Flávia Villela Soares^a, Ander Francisco Pereira^a, Telles Cardoso Silva^a, Daniela Rodrigues Silva^a, Daiana Teixeira Mancini^a, Melissa Soares Caetano^c, Elaine F. F. da Cunha^a, Teodorico C. Ramalho^{a,b†}

^a Laboratory of Molecular Modeling, Chemistry Department, Federal University of Lavras, Lavras/MG, 37200-000, Brazil.

^b Center for Basic and Applied research, University Hradec Kralove, Hradec Kralove, Czech Republic.

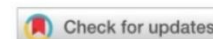
^c Institute of Exact and Biological Sciences, Federal University of Ouro Preto, University Campus, Ouro Preto/MG, 35400-000, Brazil.

Corresponding author: Teodorico C. Ramalho

e-mail: †teo@dqi.ufla.br

Fax: 55 35 3829-1271

www.nucleoestudo.ufla.br/gqc



Publisher: Taylor & Francis

Journal: *Expert Review of Neurotherapeutics*

DOI: 10.1080/14737175.2019.1608823

Non-conventional compounds with potential therapeutic effects against Alzheimer's disease

Alexandre A. de Castro¹, Flávia V. Soares¹, Ander F. Pereira¹, Daniel A. Polisel¹, Melissa S. Caetano², Daniel H. S. Leal^{1,3}, Elaine F. F. da Cunha¹, Eugenie Nepovimova,⁴ Kamil Kuca^{4†} and Teodorico C. Ramalho^{1,5†}

¹Laboratory of Molecular Modeling, Department of Chemistry, Federal University of Lavras, Lavras/MG, 37200-000, Brazil.

²Institute of Exact and Biological Sciences, Federal University of Ouro Preto, University Campus, Ouro Preto/MG, 35400-000, Brazil.

³Department of Health Sciences, Federal University of Espírito Santo, São Mateus/ES, 29932-540, Brazil.

⁴Department of Chemistry, Faculty of Science, University of Hradec Kralove, Hradec Kralove, Czech Republic.

⁵Center for Basic and Applied Science, Faculty of Informatics and Management, University of Hradec Kralove, Hradec Kralove, Czech Republic.

†These authors have contributed equally to this work

***Corresponding authors:**

Kamil Kuca

Email: kamil.kuca@uhk.cz

Telephone: +420 603 289 166

Teodorico C. Ramalho

Email: teo@ufla.br

Telephone: +55 35 38291155